A STABLE ISOTOPE INVESTIGATION INTO FLUID-ROCK INTERACTION DURING REGIONAL METAMORPHISM IN WESTERN DRONNING MAUD LAND, EAST ANTARCTICA

By

Warren Peter Johnstone

A dissertation submitted in fulfilment of the requirements for the degree of

MSc in Geology

University of Cape Town

2001

ABSTRACT

The Sverdrupfjella Group in western Dronning Maud Land forms part of a 1200 Ma to 900 Ma orogenic belt which experienced a thermal overprint at around 500 Ma. Although the degree of tectonic reworking during this later event remains uncertain, evidence for late fluid alteration is widespread. In this study, the high-grade metamorphic rocks which make up the Sverdrupfjella Group were sampled in the central Kirwanveggen area. The stable isotope and whole-rock composition of these rocks have been determined, in order to test whether zones of intense fluid-rock interaction can be used as evidence for Pan African overprinting of Grenvillian orogenesis in western Dronning Maud Land.

The Sistenup basalts have the lowest $\delta^{18}O$ values of any rock type sampled in western Dronning Maud Land ($\delta^{18}O$ as low as –1.3‰), but there is also evidence for significant fluid alteration in the central Kirwanveggen ($\delta^{18}O$ as low as 1.7‰). In this area, the presence of fluids is evidenced by hydrous retrograde mineral assemblages, low $\delta^{18}O$ values in calc silicate boudins, metasomatic calc silicate assemblages, silicic metasomatism and "rock-buffered" quartz vein precipitation. Investigation of these zones of alteration reveals that the source of the altering fluids is external and that the mechanism of infiltration is locally pervasive. Detailed sampling and stable isotope analysis indicate two distinct episodes of fluid-rock interaction in the Sverdrupfjella Group, resulting from early fluid activity during the Mesoproterozoic "Grenvillian" Orogeny and late fluid-rock interaction, probably associated with the Palaeozoic "Pan African" Orogeny. Palaeozoic reworking is also considered to be responsible for the intense ^{18}O depletion observed in the Sistenup basalts. Regional aeromagnetic anomalies provide further evidence for multiple stages of fluid-rock interaction and suggest that isolated zones of fluid alteration, such as those observed at Sistenup and in the central Kirwanveggen, may be part of the same regional metamorphic event.

ACKNOWLEDGEMENTS

My sincere appreciation to my supervisor and mentor Chris Harris who identified the remarkable ^{18}O depletion in the basalts at Sistenup, one of the coldest and most inhospitable places in western Dronning Maud Land, and who guided me through the world of stable isotope geochemistry. After my supervisor, the three most important people associated with this project are my 1997 - 1998 Field Assistant Paul Macey, my 1998 - 1999 Field Assistant, Howard Selfe (both of whom endured untold misery and sublime ecstasy on the ice) and Fayrooza Rawoot, the Stable Isotope Laboratory Assistant at the University of Cape Town.

Special thanks are due to my fellow researcher Chris Jackson who introduced me to the metamorphic rocks of the Sverdrupfjella Group and wasted no opportunity in reminding me how much I still had to (and have to) learn about ductile deformation in high-grade rocks. A major contributor to this study is Branko Corner, my thanks for long hours of processing and interpreting the aeromagnetic data presented in Chapter Seven. Other individuals who made significant scientific contributions to this study are also thanked, they are: Johan Krynauw, Geoff Grantham, Hartwig Frimmel, Warwick Board, Paul Macey, Howard Selfe, Mawson Croaker and Georg Kleinschmidt. I extend my appreciation to my colleagues in the Earth Science Working Group of the South African National Antarctic Programme (SANAP), especially Steve McCourt who directed South African Earth Science research in the Antarctic from 1996 to 2000. The SANAP is thanked for funding this research project and for arranging and providing the substantial logistical support demanded by Antarctic field work, my appreciation is also extended to the members of 22 Squadron of the South African Air Force (SAAF) for their efforts.

I would also like to thank Ian Cartwright and Marlen Yanni of Monash University for additional stable isotope analyses, as well as Andreas Späth and Fran Pocock at the University of Cape Town for ICP-MS and XRF analyses respectively. My appreciation to Ian Buick and Gregory Dipple for the opportunity to discuss the data presented here. Finally, my sincere thanks to Lauren, who has assisted me with the compilation and proof reading of this dissertation and Stephan who has had to put up with me this past year.

DECLARATION

This dissertation is my own unaided work, conducted under the supervision of Ass. Prof. Chris Harris. It is being submitted for the degree of MSc in Geology at the University of Cape Town, and has not been previously submitted for any degree or examination at any other university.

Signed by candidate

Warren Peter Johnstone

January 2001

CONTENTS

LIST OF FIGURES

Figure 3.4 Discordant pegmatite intruding granite gneiss at Tverreggtelen (Locality 36). The pegmatite cross-cuts both the S_1 and S_2 fabric of the granite gneiss host.

Figure 3.5 Photomicrograph of WJK 224. This coarse Feldspar-rich rock has interstices of recrystallized quartz. Plagioclase clasts are inclusion-rich and overprinted by epidote. Hornblende occurs as large (> 1mm) grains intergrown with biotite flakes, which are poorly orientated to define a cryptic fabric. FOV = 2.5mm.

Figure 3.6 High strain zone deflecting *Swartbandufsa Mafic Dykes* in the *Tverregga Banded Gneiss* at Tverregga. Retrograde mineral assemblages are defined by biotite, chlorite and epidote with lesser amounts of sericite, sphene and calcite.

Figure 3.7 Photomicrographs of WJK 152 showing the hydrous retrograde assemblage of quartz – chlorite - epidote – biotite with accessory sphene and late calcite. Photomicrograph a) cross polars, FOV = 3mm and b) cross polars, FOV = 1mm.

Figure 3.8 Photomicrograph of WJK 156 showing the hydrous retrograde assemblage of quartz – K-feldspar – plagioclase – sericite – chlorite with accessory epidote. Photomicrograph a) cross polars, FOV = 2.5mm and b) cross polars, FOV = 1mm.

Figure 3.9 Photomicrograph of WJK 155 showing the hydrous retrograde assemblage of quartz – epidote – muscovite – chlorite – calcite – sphene with accessory magnetite, apatite and allanite. Photomicrograph a) plane polars, FOV = 2.5mm and b) cross polars, FOV = 1mm.

Figure 3.10 Zoned calc silicate boudin at Tverregga hosted in retrogressed quartz – feldspar – hornblende – biotite gneiss (Locality 26). The core is calcite surrounded by diopside – actinolite – epidote, with a rim of quartz + feldspar.

Figure 3.11 Zone of scattered calc silicate boudins in the banded gneiss at Tverregga (Locality 26). Note how the leucocratic material "drowns out" the mafic cores.

Figure 3.12 Banded gneisses in the main face of Hallgrenskarvet. Note the alternating leucocratic and melanocratic units which define the regional S_3 fabric of the central Kirwanveggen. The circle indicates a man for scale.

Figure 3.13 Modified compositional layering in the banded gneisses at Hallgrenskarvet. Notice how leucocratic (competent) units thinner than ~ 30cm have been boudinaged and are encompassed by melanocratic (incompetent) schists.

Figure 3.14 Early amphibolite dykes within the banded gneiss package at Hallgrenskarvet. Note the locally discordant nature of the mafic units with respect to the regional S_3 fabric / compositional banding.

Figure 3.15 Geological map of the metasomatic calc silicate body at Tverreggtelen (Locality 41).

Figure 3.16 Photomicrograph of WJK 270 showing the make-up of the tremolite-rich zone of the metasomatic calc silicate body at Tverreggtelen. FOV = 2.5mm.

Figure 3.17 Peripheral zone of the metasomatic calc silicate body at Tverreggtelen.

Figure 3.18 The main face of Stignabben showing the homogenous nature of the *Kirwanveggen Megacrystic Orthogneiss Complex*. At Hallgrenskarvet homogenous megacrystic orthogneiss in the east becomes progressively more migmatized towards the west.

Figure 3.19 Distinctive augen texture of the *Kirwanveggen Megacrystic Orthogneiss Complex*. The mylonitic fabric is defined by the alignment of biotite and recrystallized tails of the K-feldspar porphyroclasts.

Figure 3.20 The Tverreggtelen Leucogranite suit in the north face of Tverreggtelen, this view looking south is down the plunge of the F_4 fold axes. Note the folded leucogneiss / banded gneiss contact and the S_3 parallel mafic dykes.

Figure 3.21 Finger-like apophyses of leucogranite intrude the host banded gneisses on the margins of the Tverreggtelen leucogranite at locality 39. The apophysy shown here has been termed the "Turquoise Dyke" by Jackson (1997) and cross-cuts a porphyritic granite dyke at this locality. The turquoise colouration is a result of large amazonite crystals which are characteristic of these dykes.

Figure 3.22 Silicic metasomatism in the Tverreggtelen Leucogranite at Tverreggtelen (Locality 44). Note the moderate to steep D_3 shear zone which affects the leucogneiss at this locality. Scale differs with perspective, but the cliff is ~ 60m high.

Figure 3.23 The Fuglefjellet Formation at Skarsnuten in the H. U. Sverdrupfjella. At this locality, a large body of undeformed pegmatite intrudes the layered carbonate, calc silicate and quartzofeldspathic gneiss sequence.

Figure 3.24 Zoned calc silicate boudin within a quartzofeldspathic gneiss host at Skarsnuten in the H. U. Sverdrupfjella. The pale green core comprises diopside – quartz – plagioclase, whereas the rims are feldspar + quartz with minor garnet and hornblende.

Figure 3.25 *Swartbandufsa Mafic Dykes* intruding gneisses of the *Kvervelnatten Granite Gneiss Complex* at Swartbandufsa in the central Kirwanveggen. The circle indicates a man for scale.

Figure 3.26 A Jurassic dolerite dyke intruding gneisses of the Sverdrupfjella Group at Hallgrenskarvet. The cliff is ~ 350m high for scale.

Figure 3.27 Photographs and corresponding field sketches showing the vein types of the central Kirwanveggen: a) synfolial, b) boudin-eye, and, c) discordant. Note that the sketches do not represent the exact locality of the photographs.

Figure 6.3 Theoretical $\delta^{18}O_A$ vs $\delta^{18}O_B$ plots for a) equilibrium and b) disequilibrium fractionations (after Buick 1998). Diagonal lines are isotherms for equilibrium fractionation between mineral phases A and B.

Figure 6.4 Stable isotope ratios for common geological materials, a) oxygen isotope values and b) carbon isotope values (after Hoefs 1997).

Figure 6.5 Plot of $\delta^{18}O$ vs Rock Type showing the range of $\delta^{18}O$ values for the metamorphic rock types of the Sverdrupfjella Group as well as syenite from the Sistefjell Complex and the Sistenup basalts. All $\delta^{18}O$ values are whole-rock determinations except for the metacarbonate samples, which indicate $\delta^{18}O$ values of calcite. The minimum, maximum and mean $\delta^{18}O$ value for each rock type is indicated by the 3 dots on each line.

Figure 6.6 Plot of whole-rock $\delta^{18}O$ vs the content of selected major elements: a) SiO_2, b) Al_2O_3, c) Fe_2O_3, and, d) CaO for the major metamorphic rock types of the Sverdrupfjella Group.

Figure 6.7 Plot of $\delta^{18}O$ vs δD for the basalts at Sistenup and granite gneisses from the central Kirwanveggen. The range of values for "normal" igneous rocks (after Taylor & Sheppard 1986) is also shown.

Figure 6.8 Stable isotope plots for calc silicate rocks from the central Kirwanveggen. Metacarbonate samples collected from Skarsnuten in the H. U. Sverdrupfjella are also plotted. Figure 6.8a is a plot of $\delta^{18}O$ vs $\delta^{13}C$, the field for unaltered limestone (Viezer & Hoefs 1976) is shown along with the theoretical curve for a precursor limestone undergoing Rayleigh decarbonation with a $\alpha_{CO_2\text{-rock}}$ for C of 1.002 and for O of 1.012. Figure 6.8b is a plot of $\delta^{18}O$ and $\delta^{13}C$ vs Wt%Cc.

Figure 6.9 Sampling diagram of WJK 145 at locality 26 with components, A: whole boudin ($\delta^{18}O$ = 11.2‰), B: core – periphery ($\delta^{18}O$ = 10.4‰), and, C: core ($\delta^{18}O$ = 12.8‰). A photograph of this boudin has been presented in Figure 3.10.

Figure 6.10 Photograph of the metasomatic calc silicate body at Tverreggtelen showing the heterogeneity of the calc silicate material reflected in sample WJK 274 at locality 41. A: host calcite – amphibole – talc ($\delta^{18}O$ = 13.4‰; $\delta^{13}C$ = 0.9‰), B: a coarse mafic layer of amphibole – talc ($\delta^{18}O$ = 14.4‰; $\delta^{13}C$ = 0.6‰), C: a calcite – amphibole – biotite layer ($\delta^{18}O$ = 13.5‰; $\delta^{13}C$ = 0.9‰), D: a calcite boudin ($\delta^{18}O$ = 13.9‰; $\delta^{13}C$ = 1.3‰), E: a coarse calcite pod ($\delta^{18}O$ = 14.9‰; $\delta^{13}C$ = 2.6‰), and, F: an amphibole porphyroblast ($\delta^{18}O$ = 14.5‰; $\delta^{13}C$ = 1.3‰). Note that components D and F are not shown in this photograph.

Figure 6.11 Augen gneiss at Stignabben a) field sketch of sampling locality 1 showing the sample traverse WJK 1 – WJK 6 across the D_5 shear zone, b) plot of $\delta^{18}O$ variation with distance from the shear zone.

Figure 6.12 Field sketch of sampling locality 5 showing the top contact of the Leucogneiss at Hallgrenskarvet and the sample positions for WJK 20 – WJK 25.

Figure 6.13 Field sketch of sampling locality 44 showing samples collected within and adjacent to the silicified D_3 shear zone at Tverreggtelen. See Figure 3.22.

Figure 6.14 Plot of quartz $\delta^{18}O$ (vein) vs whole-rock $\delta^{18}O$ (host) for quartz veins from the Sverdrupfjella Group in the central Kirwanveggen, a) all veins, b) veins in banded gneiss, c) veins in augen gneiss, and, d) veins in leucogneiss. Vein type (e.g. synfolial, boudin-eye or discordant) is distinguished by symbol. Quartz and calcite separate data from calcite-bearing quartz veins are shown in e).

Figure 6.15 Plot of $\delta^{18}O$ vs $\delta^{13}C$ for calcite in calcite-bearing quartz veins from the Sverdrupfjella Group. Note that vein type (e.g. synfolial, boudin-eye or discordant) is distinguished by symbol type.

Figure 6.16 Plot of $\delta^{18}O$ of quartz vs $\delta^{18}O$ of calcite in calcite-bearing quartz veins from the Sverdrupfjella Group. Diagonal lines are isotherms. Note that host rock type (e.g. banded gneiss or leucogneiss) is distinguished by symbol type.

Figure 6.17 Schematic diagram illustrating non-pervasive (channelized) infiltration of a low $\delta^{18}O$ fluid into a heterogeneous banded gneiss and the resulting pattern of $\delta^{18}O$ values. The oxygen isotope front highlights the permeability contrast between the melanocratic and leucocratic components of the banded gneiss.

LIST OF TABLES

CHAPTER ONE

1. INTRODUCTION

This dissertation forms part of *Study 6* of the 1996 – 2001 South African National Antarctic Programme (SANAP) 5-year Earth Science Sub-Programme entitled *Characterisation of Mesoproterozoic to Palaeozoic crustal evolution of western Dronning Maud Land.* The rationale behind *Study 6* is to test the hypothesis that zones of intense fluid-rock interaction can be used as evidence for Pan African overprinting of Grenvillian orogenesis in western Dronning Maud Land.

1.1 LOCATION OF THE STUDY AREA

Historically, Earth science research undertaken by SANAP has covered an area of western Dronning Maud Land extending from 70° S to 74° S and straddling the Greenwich Meridian from 6° W to 3° E (Fig. 1.1). This area was first explored in the late 1940s during the Norwegian-British-Swedish Antarctic Expedition (NBSA) and the majority of place names are Norwegian. The area encompasses the Ahlmannrygggen, Borgmassivet, Kirwanveggen and H. U. Sverdrupfjella mountain ranges. The physiography of the area is dominated by the Jutulstraumen - Pencksökket glacier system, which drains the East Antarctic ice cap and transports ice from the polar plateau northwards to the Fimbul ice shelf, a distance of almost 300km and an elevation difference of more than 2000m. The Pencksökket and Jutulstraumen glaciers separate the lower lying coastal Ahlmannrygggen and Borgmassivet ranges from the Kirwanveggen and H. U. Sverdrupfjella ranges which make up the polar escarpment in western Dronning Maud Land. The Kirwanveggen and H. U. Sverdrupfjella mountains are

bisected by the head of the Jutulstraumen glacier which, at this point, is more than 60km wide and displaces ice from an altitude of 2300m to 1900m over a distance of only 2km in a spectacular icefall.

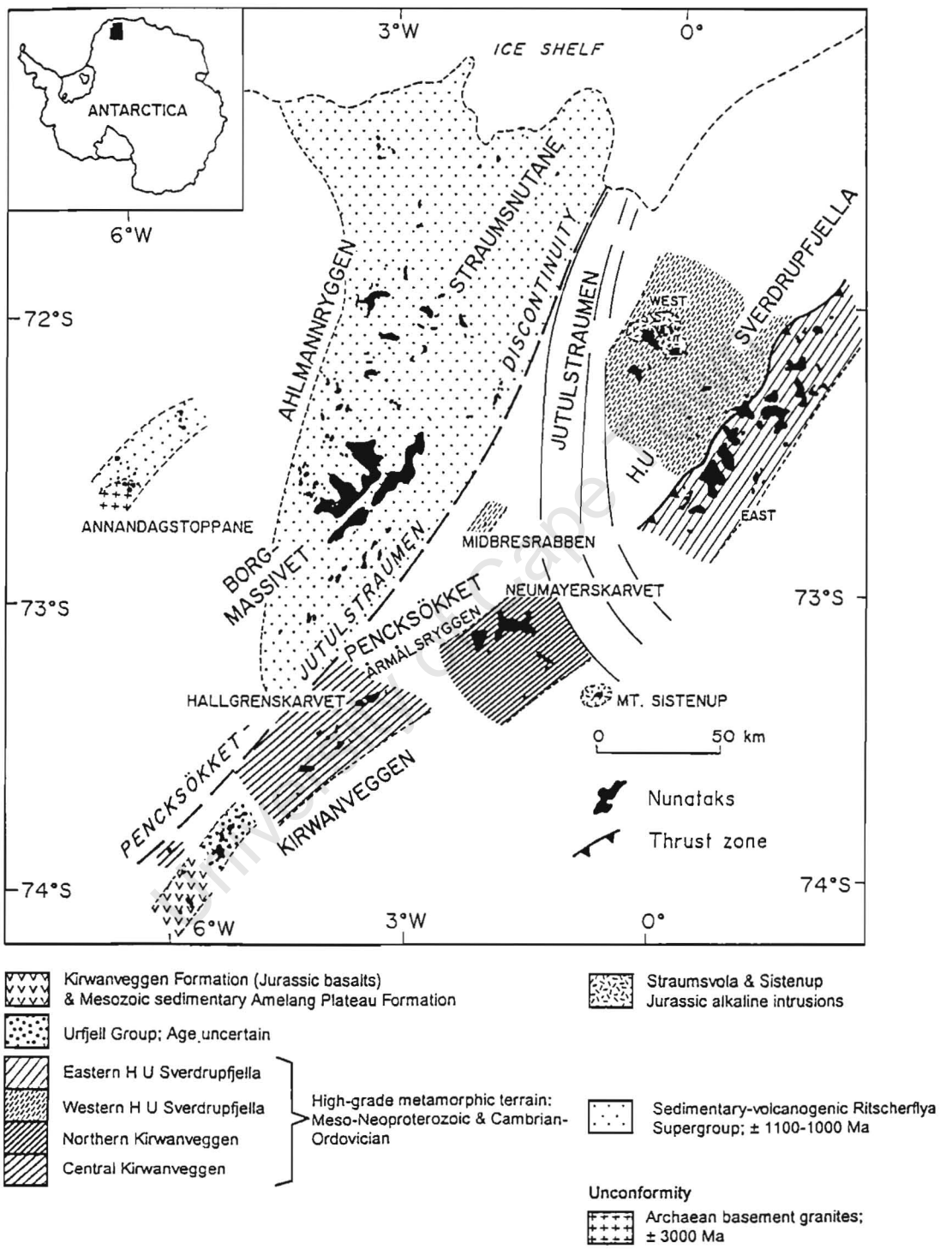

Figure 1.1 Geological map of western Dronning Maud Land (after Grantham *et al.* 1995*b*).

Samples relevant to this dissertation were collected from both the Kirwanveggen and H. U. Sverdrupfjella ranges and represent a transect of more than 200km. The majority of the field work was carried out in the central Kirwanveggen at the Hallgrenskarvet – Tverreggtelen – Tverregga group of nunataks located at 73°22 S and 03°26 W (Fig. 1.2). Sampling was also carried out at Stignabben, Kvervelnatten and Swartbandufsa in the central Kirwanveggen. Additional samples were collected in the H. U. Sverdrupfjella at Skarsnuten (Fig. 1.1).

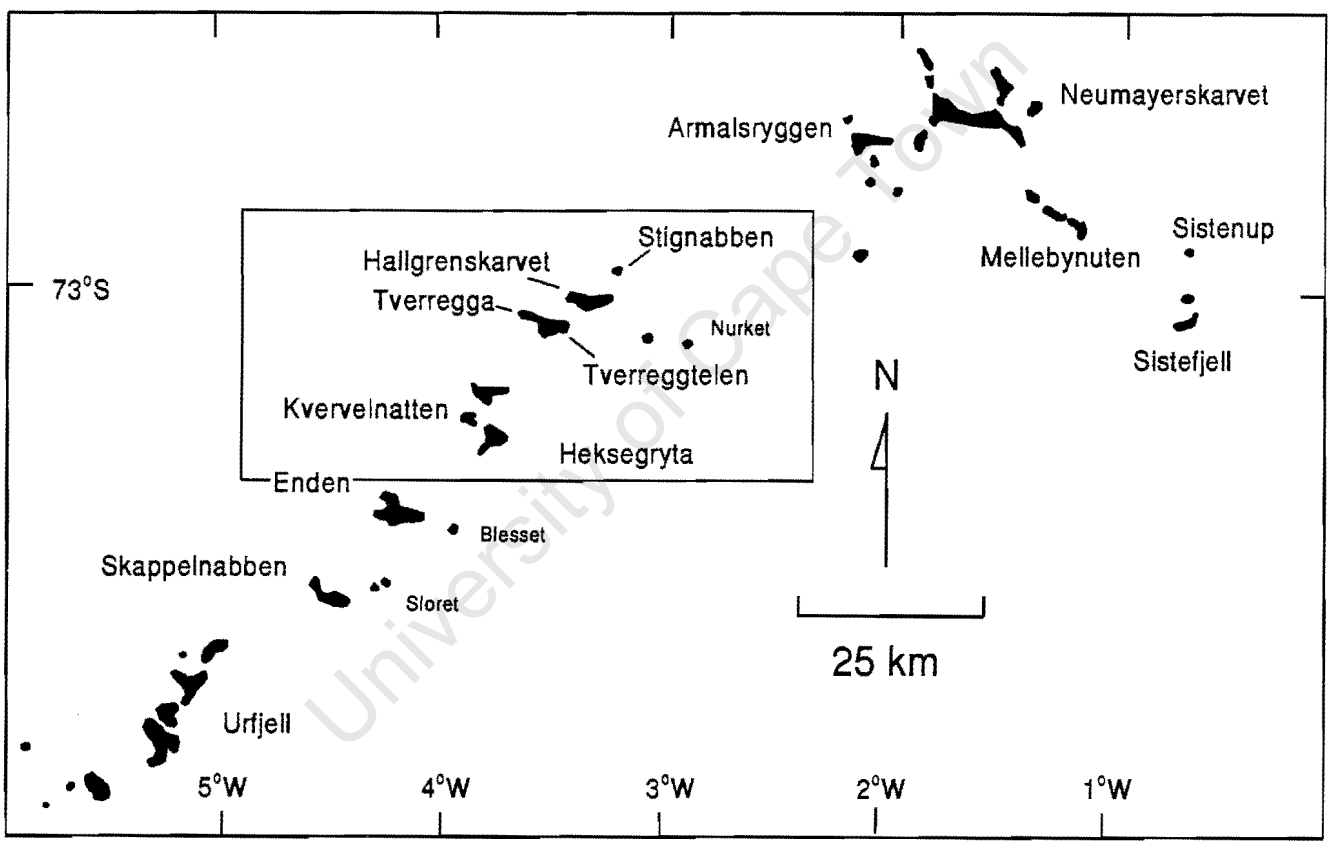

Figure 1.2 Map of the Kirwanveggen mountain range. The boundaries delineate the portion of the central Kirwanveggen relevant to this study.

1.2 PREVIOUS WORK

The first geological investigation of western Dronning Maud Land was carried out during the Norwegian-British-Swedish Antarctic Expedition (NBSA) between 1949 and 1952 by E. F. Roots who identified two distinct rock assemblages separated by the Pencksökket glacier (Roots 1953). He described a metamorphic complex comprising banded gneisses, amphibolites, schists and pegmatites to the south and east of the glacier, and a series of horizontal sediments, mostly siltstones, greywackes and conglomerates intruded by dioritic and gabbroic sills to the north and west of the glacier. Reconnaissance geological mapping in western Dronning Maud Land was carried out by Ravich & Soloviev (1969), followed by more detailed geological studies during the 1970s (Wolmarans & Kent 1982). Investigation of the Sverdrupfjella Group in the form of metamorphic, tectonic and geochronological studies has been ongoing since the late 1980s, focussing on the H. U. Sverdrupfjella mountain range (Grantham *et al.* 1988, 1991; Groenewald 1991; Groenewald & Hunter 1991; Groenewald *et al.* 1991; Grantham 1992; Groenewald 1993; Moyes *et al.* 1993*a, b*; Groenewald 1995). More recent work relating to the Sverdrupfjella Group has been concentrated in the Kirwanveggen mountain range as part of the 1991 - 1995 SANAP Earth Science 5-year programme. In the north eastern Kirwanveggen, Ferrar (1995) completed a metamorphic study of the Årmålsryggen, while C. Jackson mapped Neumayerskarvet and Moyes & Harris (1996) compiled a geochronological framework for the same area. Geological mapping of the central Kirwanveggen was initiated during the 1992 - 1993 field season and has continued through until the current 1996 - 2001 SANAP Earth Science 5-year Programme. During this time, Enden and Skappelnabben were mapped by M. Knoper, the Heksagryta area was mapped by P. D. Harris and J. R. Krynauw, and the Hallgrenskarvet - Tverreggtelen - Tverregga group of nunataks was mapped by C. Jackson (Antarctic Research Group 1995). The Urfjell Group

sedimentary rocks in the southern Kirwanveggen were mapped and studied by M. Croaker during the 1997 – 1998 season. The findings of these recent studies are reported by Jackson *et al.* (1993, 1994); Jackson (1995); Jackson & Jacobs (1995); Ferrar (1995); Moyes *et al.* (1995*a, b*); Harris & Krynauw (1995); Moyes & Harris (1996); Krynauw (1996). German Scientists have also participated in the recent geological investigations of the Kirwanveggen (Helferich & Kleinschmidt 1998, 1999). The first fluid alteration study was only very recently undertaken in western Dronning Maud Land, in order to establish the degree of fluid-rock interaction represented by the alteration of the Sistenup lavas (Harris & Johnstone 1999*b*). The data and findings reported in this dissertation form part of the first stable isotope investigation into fluid-rock interaction relating to high-grade metamorphic rocks in western Dronning Maud Land (Johnstone *et al.* 1998; Johnstone & Harris 1999*a, b*).

1.3 AIMS AND RATIONALE

The principal aim of the 1996 – 2001 SANAP Earth Science 5-year Programme was to identify and separate the Mesoproterozoic "Grenvillian" event from the Early Palaeozoic "Pan African" event in western Dronning Maud Land (Krynauw 1995). Reworking of the Mesoproterozoic Circum East Antarctic Mobile Belt (Yoshida 1994) during the Early Palaeozoic, from 550 – 500 Ma, has been identified in several areas such as Lützow-Holm Bay (Shiraishi *et al.* 1992) and the Larsemann Hills (Dirks *et al.* 1993). In western Dronning Maud Land, the Pan African regional metamorphic event has, until recently, only been recognized as a thermal event (Moyes & Groenewald 1996). This is partly due to the fact that separation of the two orogenic episodes on structural evidence has proved very difficult as a result of the coaxial nature of structures observed in the field (Grantham *et al.* 1995*b*). In order to solve this problem, the 1996 – 2001 SANAP Earth Science 5-year Programme

adopted a multi-disciplinary approach incorporating; structural mapping, metamorphic petrology, geophysics, protolith geochemistry, geochronology and stable isotope geochemistry. This dissertation reports on the fluid-rock interaction component of the Programme and is predominantly a stable isotope study of the high-grade metamorphic rocks, which make up the Sverdrupfjella Group (Hjelle 1974). The Sistenup lavas in the north eastern Kirwanveggen (Fig. 1.1) are highly altered and have been shown to have very low $\delta^{18}O$ values (> -1.3‰). This alteration must have occurred as a response to the infiltration of a high temperature fluid (> 400°C) at high fluid:rock ratios, probably during the Pan African regional metamorphic event. The rationale behind this project is to test the hypothesis that zones of intense fluid-rock interaction, such as that observed at Sistenup, result from 500 Ma overprinting of Grenvillian orogenesis in western Dronning Maud Land. The specific aims of this project are: a) to determine the presence and distribution of ^{18}O depletion in the Sverdrupfjella Group, b) to investigate the cause or causes of ^{18}O depletion, and, c) to consider the significance of ^{18}O depletion in the context of the tectonic and metamorphic history of western Dronning Maud Land (Fig. 1.3).

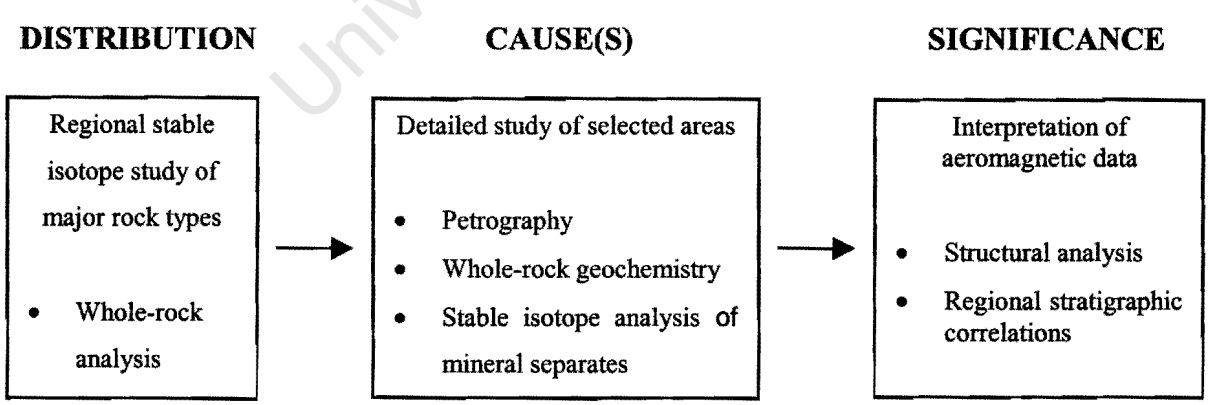

Figure 1.3 Flow diagram outlining the primary aims of this study, from identification / distribution to cause(s) and significance of ^{18}O depletion, and the procedure followed in order to achieve them.

1.3.1 Stable isotope geochemistry in regionally metamorphosed rocks

Stable isotope geochemistry is a powerful tool in the study of fluid-rock interaction during regional metamorphism (Valley 1986). Oxygen isotopes, for example, are well suited to fluid-rock interaction studies because oxygen isotope ratios are resistant to change as a result of metamorphism but are susceptible to fluid-assisted processes such as metasomatism. By using stable isotope geothermometers, which are independent of pressure, it is possible to construct temperature-time paths for metamorphic terranes. Furthermore, mass-transport processes such as diffusion, recrystallization, fluid infiltration and volatilization, which are active in regionally metamorphosed terranes, can be studied using stable isotope geochemistry. Stable isotopes are used to: a) identify fluid sources, b) characterize the nature of fluid flow e.g. pervasive or channelized, c) establish whether fluid flow occurred under equilibrium or disequilibrium conditions, and, d) quantify fluid:rock ratios. Furthermore, stable isotope studies allow a better understanding of the processes responsible for metasomatism, vein formation and fluid infiltration into shear zones. Metamorphic rocks are suited to fluid-rock interaction studies because the protolith compositions of metamorphosed rocks have very different stable isotope compositions compared to those of crustal fluids. For example, a meteoric fluid with a $\delta^{18}O$ value of ~ 0‰ would have a pronouced affect on a metacarbonate rock with a $\delta^{18}O$ value of ~ 20‰. In this study, an extensive regional stable isotope (O, D and C) database has been compiled (Chapter Six) for the majority of metamorphic rock types, which make up the Sverdrupfjella Group. A statistical reference value is calculated for each specific rock type against which anomalous values can be compared. In this way, several anomalous zones were identified and selected for more detailed sampling. Additional analyses constrain fluid-rock interaction in these areas and provide an insight into the relevance of fluid-rock interaction to the Grenvillian and, or Pan African events (Fig. 1.3).

1.3.2 Current stable isotope research

The application of stable isotope geochemistry to fluid-rock interaction in high-grade metamorphic terranes is the focus of many recent and current investigations. In East Antarctica, Buick *et al.* (1994) and Cartwright *et al.* (1997) have been working on granulite facies marbles and calc silicates from the Rauer Group. In North America, Valley *et al.* (1990) studied fluid flow in the Adirondacks, Pattison (1991) worked in the Grenville Province and Mora & Valley (1991) investigated the affect of fluid-rock interaction in calc silicate country rocks of the Idaho batholith. Fluid studies of the Southern Indian Craton have been carried out by Newton *et al.* (1980), Jiang *et al.* (1988) and Santosh *et al.* (1991). Some of the most active research has been conducted in the Reynolds and Harts ranges, which form part of the Palaeoproterozoic Arunta Inlier of central Australia. Numerous workers have carried out fluid related studies in these high-grade rocks (Buick *et al.* 1997; Buick & Cartwright 1996; Cartwright & Buick 1998, 1999; Cartwright *et al.* 1997; Williams *et al.* 1996; Vry *et al.* 1996; Vry & Cartwright 1998; Miller & Cartwright 1997; Read & Cartwright 1999). In the Mt. Isa Inlier of Australia, Oliver *et al.* (1990) have been investigating structural controls on metamorphic fluid flow and Perkins (1984) identified the link between metasomatism and the formation of ore deposits in the inlier. On King Island, Tasmania, Streit & Cox (1998) studied fluid infiltration during mid-crustal mylonitization. Mathematical modelling of fluid-rock interaction (Ferry & Dipple 1991; Streit & Cox 1998) has made it possible to determine the nature of fluid flow e.g. pervasive or channelized, as well as to establish the flow direction and volume of the fluid.

1.3.3 Other geochemical approaches to fluid studies

In addition to stable isotope geochemistry, fluid studies typically incorporate whole-rock geochemistry, fluid inclusion studies, metamorphic petrology and isotope geochronology. Whole-rock geochemistry is used to determine the protolith of metamorphosed rocks, and major element losses and gains can be used to quantify both the direction of fluid flow and the volume of fluid involved in fluid alteration (Cartwright & Buick 1999). Homogenization temperatures and the composition of fluids are determined by fluid inclusion microscopy, these data are useful in establishing the source of fluid. Fluid studies in metamorphic terranes rely on metamorphic petrology, which provides temperature and pressure information as well as mineral equilibria data. Sound geochronological data is essential in order to construct pressure-temperature-time paths for a particular metamorphic terrane. Some of the current techniques used to date thermal, deformational and fluid alteration events include Rb-Sr, Ar-Ar step-wise heating and U-Pb SHRIMP microprobe analysis of *in situ* minerals.

1.4 FIELD WORK

This study has predominantly been a sampling exercise as far as field work is concerned. In addition to sample collection, field work involved detailed site descriptions and sketches, in selected cases, large scale geological mapping of key outcrops was also carried out (Fig. 3.15). During the course of the 2 field seasons, numerous samples were collected from the Hallgrenskarvet – Tverreggtelen – Tverregga group of nunataks resulting in a highly representative distribution of samples for this area (See APPENDIX A). The sampling programme was pre-planned and each sample was collected and documented in a methodical fashion.

1.4.1 Sampling methodology

Fluid-rock interaction studies applied to Proterozoic high-grade metamorphic rocks is complicated by several factors including: a) *metamorphic effects* such as temperature and pressure conditions, mineral reactions and partial melting; b) *tectonic effects* such as exhumation and reactivation, and, c) *hydrological parameters* such as porosity, permeability, hydrostatic head and fluid flow. Very often these effects are combined to produce processes such as fluid-driven metamorphic reactions, deformation induced permeability, fluid focussing and seismic pumping. Many regionally metamorphosed terranes have been affected by multiple stages of orogenesis which reactivate structures acting as pathways to fluid flow, the result is often a complex mosaic of superimposed fluid events.

In addition to the above, metamorphic rocks are often intrinsically heterogeneous on an outcrop-scale which make them a difficult medium to sample (Fig. 3.13). Heterogeneities can take the form of compositional banding, migmatisation (leucosomes, segregations and melt patches), isoclinal folding, fabric intensification, boudinage, brecciation, veining and fluid alteration, to name only a few. As a consequence, it is absolutely essential to plan a sampling survey with a clear set of objectives. In this study, the primary objective was to identify areas of ^{18}O depletion and secondly, to investigate the cause(s) of ^{18}O depletion. In order to identify ^{18}O depletion, it is necessary to compare altered and unaltered rocks of the same type, to achieve this and at the same time, minimize the effect of the problems described above, the following procedure was observed when collecting a sample in the field:

- selection of fresh, unweathered samples (weathered surfaces removed if present),
- description of the sample e.g. mineral assemblage, texture, colour, and, if present; veins, inclusions and contamination,

- complete description of the site including surrounding lithology or lithologies, exotic material such as xenoliths and pods, structural readings etc. (a detailed sketch was made of every sample locality and a photograph taken if applicable), and,
- the stratigraphic position was recorded, as was any information which could have a bearing on the subsequent analytical procedure such as; degree of weathering and unavoidable contamination.

1.5 ANALYTICAL TECHNIQUES

Analytical techniques performed for this study include: a) whole-rock and mineral oxygen, carbon and hydrogen isotope analysis, b) major element determination by X-ray fluorescence spectroscopy (XRF), and, c) trace element (including rare earth element) analysis by inductively coupled mass spectrometry (ICP-MS). All of these techniques were applied "in-house" at the Department of Geological Sciences, University of Cape Town and a small number of oxygen isotope analyses were performed at Monash University. Sample preparation and analytical methods are described in Chapter Four.

CHAPTER TWO

2. GEOLOGY OF WESTERN DRONNING MAUD LAND

The East Antarctic Shield is exposed as a chain of metamorphic provinces extending for more than 5000km from the Heimefrontfjella in western Dronning Maud Land to the Bunger Hills at 100° E known as the Circum East Antarctic Mobile Belt (Yoshida 1994). These Mesoproterozoic mobile belts encompass Archaean nuclei such as the Grunehogna Craton, the Napier Complex, the Prince Charles Mountains, the Vestfold Hills (Dalziel 1992; Krynauw 1996) and the Rauer Group (Harley *et al.* 1995) and represent suturing of the older continental nuclei during Mesoproterozoic orogenesis (Tingey 1991).

Western Dronning Maud Land is characterized by two such geological entities, the Grunehogna Province (Krynauw *et al.* 1987) and the Maud Belt (Groenewald *et al.* 1995) (Fig. 1.1). The Jutulstraumen - Pencksöckket glacier system or Penck-Jutul Trough (Harris & Grantham 1993) which separates these two terranes, is a possible extension of the western limb of the East African rift system into Antarctica prior to the breakup of Gondwanaland (Grantham & Hunter 1991). Rifting probably exploited the pre-existing crustal discontinuity between the Grunehogna Craton and the Maud Belt (Krynauw *et al.* 1991) as early as the Jurassic and, at the same time as the southern end of the East African rift system began to develop (Wooley & Garson 1970).

2.1 THE GRUNEHOGNA PROVINCE

The Grunehogna Province is interpreted as being a fragment of the Kalahari Craton (Wolmarans & Kent 1982; Krynauw *et al.* 1991; Groenewald *et al.* 1991) and is termed the Grunehogna Craton by Groenewald *et al.* (1995). The Grunehogna Province comprises Archaean granitic basement at Annandagstoppane and an extensive sedimentary and volcanosedimentary sequence exposed in the Ahlmannryggen and Borgmassivet mountains; the Mesoproterozoic Ritscherflya Supergroup. Both the granite basement and sedimentary cover are intruded by the Borgmassivet Intrusives (Krynauw *et al.* 1991). No contact is preserved between the Annandagstoppane granite and the Richtersflya Supergroup making the relationship between basement and the cover sequence speculative. Interpretation of aeromagnetic and gravity data by Corner (1994) has outlined the extent of the Grunehogna Craton and indicates that most if not all of the Ritscherflya Supergroup is underlain by granitic basement.

2.1.1 The Annandagstoppane Granite

Undeformed granites are exposed in the Annandagstoppane group of nunataks at the western extent of the Grunehogna Province. The granites are intruded by Borgmassivet sills, but sediments of the Ritscherflya Supergroup are not present. Halpren (1970) determined a Rb-Sr model age of ~ 3000 Ma for the Annandagstoppane granite. This Archaean age was later confirmed by whole-rock Rb-Sr data, as well as Pb-Pb data (Barton *et al.* 1987). The granite has S-type characteristics and the geochemistry is distinct to that of the granites which make up the Kalahari Craton (Barton *et al.* 1987). However, certain granites in the Barberton area of South Africa have a similar chemistry (Krynauw 1996).

2.1.2 The Ritscherflya Supergroup

The Ritscherflya Supergroup covers the full extent of the Grunehogna Province and, along with the Borgmassivet Intrusives, is represented in almost all of the nunataks in the Ahlmannryggen and Borgmassivet mountain ranges of western Dronning Maud Land (Wolmarans & Kent 1982). Although the basal and upper contacts are not exposed, geophysical and geochemical evidence (Corner 1994; Krynauw *et al.* 1991) suggests that the Archaean Annandagstoppane granite forms the basement to the Ritscherflya Supergroup.

The Ritscherflya Supergroup is divided into a lower clastic sedimentary sequence, the Ahlmannryggen Group, and an upper volcanosedimentary sequence, the Jultulstraumen Group (Ferreira 1988). According to Ferreira, the Ahlmannryggen Group comprises basal greywackes with lesser arenites and siltstones overlain by a sequence of arenites, siltstones and mudstones with intraformational conglomerates, representing a progression from a marine bay setting to a tidal flat environment. A lateral facies variation to this upper sequence, in the form of conglomerates, greywackes and argillites indicates a braided to meandering river depositional environment. Conformably overlying this marine dominated sequence is a series of intra- and extra-formational conglomerates, quartz wackes and shales interpreted to be part of a braided stream complex. This progression from a marine to a braided river environment in the Ahlmannryggen Group is probably the result of a regressive depositional cycle (Ferreira 1988). The Jutulstraumen Group comprises basaltic and andesitic lavas known as the Straumsnuttane volcanics, with minor volcanoclastics and silicic horizons (Watters *et al.* 1991). In most cases, the lavas appear to have been extruded subaerially, however, there is evidence for substantial subaqueous extrusion. Evidence includes pillow lavas associated with hyaloclastite and tuffaceous beds, the latter containing ripple marks and desiccation

structures. These structures represent small, isolated bodies of water within the volcanics of the Jutulstraumen Group (Watters *et al.* 1991). In the eastern Ahlmannryggen, on the western boundary of the Jutulstraumen glacier, a series of sedimentary breccias and tuffs are overlain by arenites, tuffs and agglomerates, these sequences are interpreted as being the result of fault controlled alluvial fan deposition (Watters *et al.* 1991).

Extensive gabbroic sills have intruded the entire Ritscherflya Supergroup and are known as the Borgmassivet Intrusives. These intrusive rocks make up a large proportion of the Ahlmannryggen Group with individual sills measuring up to 400m (Krynauw *et al.*1988). The sills are generally conformable but are locally discordant, sediments adjacent to contacts are folded and small granitic segregations are sometimes observed. These observations have been cited as evidence that the sills intruded into the sediments while they were still wet and only partially consolidated (Krynauw *et al.* 1988), this interpretation implies that the intrusives are the same age as the sediments. The Borgmassivet intrusions are generally gabbroic with a range of compositions including lherzolite, pyroxenite, norite and quartz monzodiorite (Groenewald *et al.* 1995). The geochemistry of the intrusions has led several authors (Krynauw *et al.* 1991; Peters *et al.* 1991; Watters *et al.* 1991) to suggest that they are contemporaneous with the Straumsnuttane volcanics and that they have continental tholeiite characteristics similar to the Karoo lavas (Marsh & Eales 1984) and the Kirkpatrick basalts (Kyle *et al.* 1983). The Sistenup lavas, located more than 60km from the craton boundary (Fig. 1.1), are considered by Watters *et al.* (1991) to be correlatives of the Straumsnuttane volcanics.

The horizontal layering of the Ritscherflya Supergroup is largely undisturbed, except on, and near, the south eastern and eastern margins of the Grunehogna Province. Adjacent to the

Pencksökket glacier, sedimentary layering has been subjected to large-scale folding resulting in open synclinal structures, the fold axes of which trend east north east and north east. Further to the north east and adjacent to the western boundary of the Jutulstraumen glacier, the volcanic rocks of the Jutulstraumen Group steepen-up into near vertical north - south trending shear zones (Watters *et al.* 1991). The disruption of the margins of the Ritscherflya Supergroup adjacent to, and even at the position of the Grunehogna Craton boundary identified by Corner (1994), has led several authors to speculate on the nature and age of the deformation (Wolmarans & Kent 1982; Decleir & Van Autenboer 1982; Grantham *et al.* 1988; Grantham & Hunter 1991; Moyes & Harris 1996; Groenewald *et al.* 1995). Structural mapping of the Maud Belt indicates north west directed thrusting during continental collision against the boundary of the Grunehogna Craton, followed by multiple episodes of reactivation (Grantham *et al.* 1988; Grantham & Hunter 1991) which could have been responsible for the deformation of the Ritscherflya Supergroup. An alternative explanation is provided by Moyes & Harris (1996), who prescribe a foreland fold and thrust belt model which results from collision, followed by subduction of the Grunehogna Craton beneath the East Antarctic Craton.

Constraining the age of the Ritscherflya Supergroup has proved difficult because Rb-Sr techniques indicate a wide range of ages for the Borgmassivet Intrusives (Wolmarans & Kent 1982; Moyes & Barton 1990). More recent Rb-Sr dating indicates an age of ~ 1080 Ma for the Ritscherflya Supergroup and ~ 1000 Ma for the Borgmassivet Intrusives (Moyes *et al.* 1995*a*). Further constraints on the age of the sediments are provided by zircon separates from volcanoclastic material in the Ritscherflya Supergroup (Moyes & Harris 1996). An age of 1136 ± 2 Ma has been determined from U-Pb single zircon data using the zircon evaporation technique, which is interpreted as a maximum depositional age (Moyes & Harris 1996). In

summary, the deposition of the Ritscherflya Supergroup took place between ~ 1136 Ma and ~ 1080 Ma and was followed shortly thereafter by the intrusion of the Borgmassivet Intrusives at ~ 1000 Ma. Orogenesis in the adjacent Maud Belt was initiated at ~ 1135 Ma and continued through to ~ 990 Ma and could be responsible for both the deposition and deformation of the Ritscherflya Supergroup. The Ritscherflya Supergroup has been correlated with the Umkondo Group in Zimbabwe based on lithological, geochronological and palaeomagnetic evidence (Cahen *et al.* 1984).

2.2 THE MAUD BELT

The Maud Belt (Groenewald *et al.* 1995) of western Dronning Maud Land forms part of the Mesoproterozoic Circum East Antarctic Mobile Belt (Yoshida 1994). High-grade metamorphic rocks of the Maud Belt are exposed in the H. U. Sverdrupfjella, the Kirwanveggen and the Heimefrontfjella mountain ranges, where they make up the Sverdrupfjella Group (Hjelle 1974). There is an overall regional metamorphic trend along the length of the Maud Belt, which corresponds to an increase in metamorphic grade from south west to north east, Grantham pers. comm (1997). Two major orogenic episodes are identified in the Maud Belt, the Mesoproterozoic Maud Orogeny between 1200 Ma and 900 Ma, followed by the Palaeozoic '500 Ma event' (Groenewald *et al.* 1995). This later event has been correlated with the Pan African event of southern Africa and is further described by Grantham *et al.* (1995*a, b*) and Krynauw (1996).

2.2.1 The Sverdrupfjella Group

H. U. Sverdrupfjella

In the H. U. Sverdrupfjella, amphibolite facies calc-alkaline metavolcanics in the west are juxtaposed against granulites in the east comprising paragneisses and orthogneisses (Groenewald *et al.* 1995). In the west, the Jutulröra Formation comprises hornblende - biotite gneisses interpreted by Groenewald *et al.* (1995) as being part of a volcanic arc sequence close to a continental margin. In the east, the Rootshörga Formation is a package of paragneisses; pelites, meta-arenites and metagreywackes also interpreted by Groenewald *et al.* (1995) as having oceanic island arc precursors which developed close to an active continental margin. A series of metacarbonates and calc silicate gneisses belong to the Fuglefjellet Formation, which along with the Jutulröra Formation and the Rootshörga Formation, make up the supracrustal component of the Sverdrupfjella Group. Late intrusions include the A-type Brattskarvet batholith and associated bodies, all interpreted to be Pan African in age. Four episodes of metamorphism are described by Grantham *et al.* (1995*b*) and Groenewald *et al.* (1995). Early M_1 involved high-grade conditions (12 - 15 kbar, 750°C) during prograde metamorphism between 1200 Ma and 900 Ma in the eastern Sverdrupfjella followed by isothermal decompression (8 kbar, 850°C) during M_2. At around 500 Ma, medium-grade conditions (5 - 6 kbar, 600°C) prevailed during M_3. Finally, after ~ 180 Ma, hydrothermal alteration resulted in low-grade assemblages during M_4.

Kirwanveggen

The Kirwanveggen is different to the H. U. Sverdrupfjella in that the outcrop is dominated by orthogneisses with fewer paragneiss sequences. In the north east at Neumayerskarvet, granulite facies paragneisses and orthogneisses predominate and charnokite remnants are preserved. The

central Kirwanveggen comprises amphibolite facies orthogneisses which have been retrogressed to greenschist facies along discrete ductile shear zones. In the south west, the Urfjell range is underlain by upper amphibolite to greenschist facies schists which are in tectonic contact with the overlying Urfjell Group (Grantham *et al.* 1995*b*; Krynauw 1996). The metamorphic grade in the Kirwanveggen is altogether lower, although high-pressure amphibolite transitional into eclogite conditions (12 - 13 kbar, 650 - 700°C) have been identified by Ferrar (1995) in the north eastern Kirwanveggen. Further to the south west, in the central Kirwanveggen, amphibolite facies mineral assemblages record the peak metamorphic conditions. Hydrous retrograde assemblages characterized by biotite, chlorite and epidote are common in the central Kirwanveggen and occupy zones of high strain.

2.3 THE SISTENUP LAVAS

The Sistenup lavas are exposed at a single locality i.e. at Sistenup (Fig. 1.1), but nevertheless represent an important geological sequence in western Dronning Maud Land. Although no age has been determined for these lavas, Harris 'pers. comm' (2000) has suggested that they are correlatives of the Mesoproterozoic Straumsnuttane lavas on account of their composition. At Sistenup, the lavas are intruded by syenite of the Sistefjell Complex, which is exposed at Sisterabben and Sistefjell to the south. An intrusive age of 173 ± 2 Ma (Rb-Sr) has been established for the Sistefjell Complex (Harris & Johnstone 1999*b*) which is similar to the age of the Tvora and Straumsvola alkaline intrusions 150km to the north (Grantham *et al.* 1988). These basaltic lavas can be divided into aphyric and highly plagioclase-phyric varieties and are pervasively altered, with amphibole as the dominant groundmass mineral (Harris & Johnstone 1999*b*). The plagioclase-phyric texture of the rock is distinctive and is defined by numerous euhedral plagioclase laths randomly orientated in the amphibole matrix. The basalts

at Sistenup are overlain by a quartz porphyry, and the volcanic sequence is intruded by numerous late felsic dykes of syenitic and rhyolitic composition, presumably related to the Sistefjell intrusion. Late mafic dykes cut the lavas and the felsic dykes.

2.4 THE URFJELL GROUP

The Urfjell Group occurs as an isolated sequence of sedimentary rocks located in the south western Kirwanveggen. These sedimentary rocks tectonically overlie the Sverdrupfjella Group basement and are in turn unconformably overlain by sediments of the Permian Amelang Plateau Formation and the Kirwan Basalts (Aucamp *et al.* 1972). The Urfjell Group is treated separately here, because it is not considered to be part of the Grunehogna Province or part of the Maud Belt (Aucamp *et al.* 1972; Groenewald *et al.* 1995). The sedimentary sequence attains a maximum thickness of 1650m and is subdivided into three formations by Aucamp *et al.* (1972). These authors describe the lower Uven Formation as a 400m thick sequence of cross-bedded quartzites, which are overlain by the 1050m thick Tunga Formation comprising conglomerates and quartzites with interbeds of arkose and shale. The upper Urnosa Formation is a 200m thick sequence of quartzites, micaceous quartzites and mudstones. Detrital minerals such as quartz, orthoclase, plagioclase, garnet, muscovite and zircon indicate a granitic or gneissic source area which, according to palaeocurrent indicators, was located to the south south west. The large scale of cross-bedding and the poorly sorted nature of the conglomerates is interpreted to represent a high energy, near shore environment and points to a proximal source. The Urfjell Group has suffered moderate deformation prior to the deposition of the overlying Amelang Plateau Formation. The intensity of this deformation is greatest adjacent to the faulted contact between the Urfjell Group and basement gneisses in the south, Aucamp *et al.* (1972) describe north east trending thrust faults from this area which

have displacements in excess of 100m. Moyes & Harris (1996) have dated the Urfjell Group sediments by obtaining Rb–Sr data from whole-rock samples and detrital muscovite separates. The whole-rock data provides an age of 531 ± 25 Ma and the muscovite separate data suggest ages of 623 ± 18 Ma and 665 ± 22 Ma. The older ages are minimum ages for the detrital muscovite and represent the maximum age of deposition (Moyes & Harris 1996).

2.5 THE AMELANG PLATEAU FORMATION

Flat-lying sedimentary rocks of the Amelang Plateau Formation unconformably overlie both Sverdrupfjella Group gneisses and Urfjell Group sediments in the south western Kirwanveggen. The north eastern extent of the Amelang Plateau Formation is preserved at Tunga in the southern Urfjell where it is capped by the Kirwan Basalts. In this area, the sequence is at its thinnest (only ~ 100m thick) and rests unconformably on a well developed erosional surface. The Amelang Plateau Formation comprises sandstones and conglomerates and is characterized by numerous ferruginous concretions (15cm in diameter) which occur in the higher part of the sequence. A thin (20cm) carbonaceous shale horizon occurs just above the unconformity at Tunga and contains woody tissue of Permian age (Aucamp *et al.* 1972). Lithological similarities and the age of the Amelang Plateau Formation sedimentary rocks suggests that they are likely to be correlatives of Permo-Carboniferous sediments in the upper Beacon Supergroup of Victorialand, Antarctica (Juckes 1972).

2.6 GONDWANA FRAGMENTATION

Jurassic magmatism related to the break-up of Gondwanaland is widespread throughout western Dronning Maud Land. Alkaline intrusions and associated dykes have been described

by Harris & Grantham (1993), flood basalts have been studied by many workers (Juckes 1972; Hjelle & Wisnes 1972; Faure *et al.* 1979; Furnes *et al.* 1987; Harris *et al.* 1990; Luttinen & Siivola 1997) and regional dolerite dykes are described by Harris *et al.* (1991). Aspects such as the alignment of the alkaline intrusions, the chemistry of the flood basalts and the orientation of regional basics dykes tend to confirm the Gondwana reconstruction proposed by Martin & Hartnady (1986). The timing of break-up is difficult to constrain if only Jurassic magmatism is considered, this is because the ages of magmatic components are very similar e.g. ~ 170 Ma for the alkaline intrusions (Harris & Grantham 1993; Harris & Johnstone 1999*b*), 172 Ma for the flood basalts (Faure *et al.* 1979) and 170 – 200 Ma for the regional dykes (Grantham 1996). Grantham & Hunter (1991) have recorded faulting and jointing patterns parallel to the margins of the Pencksökket and Jutulstraumen glaciers and suggest that this glacier system was the site of continental-scale rifting. These structures cross-cut the alkaline intrusions on the eastern margin of the Jutulstraumen glacier indicating that actual rifting only occurred after the intrusion of these bodies at ~ 170 Ma.

2.6.1 Mesozoic alkaline intrusions

A series of Mesozoic alkaline intrusions exposed at Sistefjell, Straumsvola and Tvora are arranged in a roughly north - south orientation, parallel to, and on, the eastern boundary of the Jutulstraumen glacier (Fig. 1.1). The Straumsvola nepheline syenite is a 5km diameter pluton intruding high-grade metamorphic rocks of the Sverdrupfjella Group (Harris & Grantham 1993). The pluton consists of a massive outer zone and a layered inner zone, where the layering is defined by alternating mafic-rich and mafic-poor layers. Associated dykes have a variable chemistry and cover a range of ages, the earliest of which are cut by the syenite, whereas all other dykes intrude the syenite. Stable isotope studies of the Straumsvola

Complex indicate a mantle source for the magma and oxygen isotope analysis of the country rocks does not show evidence for extensive hydrothermal fluid circulation (Harris & Grantham 1993). At Sistenup, undeformed lavas are intruded by syenite of the Sistefjell Complex which has an intrusive age of 173 ± 2 Ma (Harris & Johnstone 1999*b*). The age of the lavas is not known and their relationship to the basement gneisses of the Sverdrupfjella Group is not clear. The Sistefjell pluton is interpreted to have a diameter of 10km on the basis of its aeromagnetic response (Corner 1994) and is associated with numerous felsic dykes of syenitic and rhyolitic composition, which intrude both the syenite itself and the surrounding lavas. Although the country rocks are highly altered ($\delta^{18}O$ as low as –1.3‰), Harris & Johnstone (1999*b*) maintain that fluid-rock interaction in the lavas occurred prior to the intrusion of the Sistefjell Complex and that, as at Straumsvola, there is no evidence for an extensive hydrothermal aureole associated with the intrusion.

2.6.2 The Kirwan Basalts

Jurassic age lavas are exposed in the south western Kirwanveggen, Heimefrontfjella and Vestfjella ranges of western Dronning Maud Land. Petrographic and geochemical studies have been carried out on the Kirwan basalts (Faure *et al.* 1979; Harris *et al.* 1990), the Heimefrontfjella basalts (Juckes 1972; Furnes *et al.* 1987) and the Vestfjella tholeiites (Furnes *et al.* 1987; Luttinen & Siivola 1997). The Kirwan Basalts comprise most of the outcrop in the Ladfjella and Lagfjella areas of the south western Kirwanveggen. In this area, the lavas rest conformably on the Permo-Triassic Amelang Plateau Formation, which in turn rests unconformably on Sverdrupfjella Group gneisses. The lavas attain a maximum thickness of 420m in the Lagfjella where the sequence comprises a total of 11 flows. Flow contacts dip very gently to the north east and the thickness of individual flows increases upwards to a

maximum of 90m. Some of the lower flows contain minor sandstone lenses (Harris *et al.* 1990). The age of the Kirwan Basalts has been determined by K-Ar dating to be 172 ± 10 Ma (Faure *et al.* 1979). According to Harris *et al.* (1990), contemporaneous magmatism is restricted to a few Jurassic dolerite dykes which intrude the Sverdrupfjella Group 50km to the north east. However, recent mapping by Helferich & Kleinschmidt (1999) reveals gabbros which intrude the Sverdrupfjella Group in close proximity to the Kirwan lavas and could be related to the extrusives. According to Harris *et al.* (1990), the geochemical characteristics of the Kirwan Basalts show an affinity to the nearby Heimefrontfjella basalts and even the Vestfjella tholeiites. These characteristics contrast with those of the Jurassic Kirkpatrick Basalts and Ferrar Dolerites of the Trans-Antarctic Mountains, which show a high degree of crustal contamination and a Sr-enriched source area (Hoefs *et al.* 1980; Kyle 1980). According to Harris *et al.* (1990) the Kirwan Basalts are most like the Sabie River Basalt Formation in the southern Lebombo area of the Karoo Basalt Province. Martin & Hartnady (1986) place these two areas adjacent to one another in their Gondwana reconstruction.

CHAPTER THREE

3. LITHOSTRATIGRAPHY

3.1 TECTONOSTRATIGRAPHY OF THE CENTRAL KIRWANVEGGEN

Recent detailed mapping of the central Kirwanveggen and, more specifically, the Hallgrenskarvet – Tverreggtelen - Tverregga group of nunataks (Fig. 1.2) has resulted in the construction of a tectonostratigraphic framework for this part of the Sverdrupfjella Group (Grantham *et al.* 1995*b*; Jackson 1997) (Table 3.1, APPENDIX B). A brief description of the main tectonostratigraphic units from oldest to youngest follows. All ages were determined by U-Pb SHRIMP dating of *in situ* minerals e.g. zircon, titanite (sphene) and monazite (Jackson 1997, 1999). All ages, unless otherwise stated, reflect primary magmatic crystallization.

The *Kvervelnatten Granite Gneiss Complex* (~ 1135 Ma) is exposed at Kvervelnatten and Tverreggtelen. This hornblende – biotite granite gneiss (Grantham *et al.* 1995*b*) preserves the oldest fabrics in this part of the Maud Belt and acts as a strain resistor to younger deformation (Jackson 1997).

The *Tverregga Banded Gneiss* (~ 1135 Ma and 992 ± 64 Ma) occurs only at the Tverregga nunatak. The scale and nature of the banding is similar to that of the *Mjöllföykje Banded Gneiss* which is described below, but the composition is distinct. This package comprises a sequence of gneisses including hornblende – biotite – plagioclase gneiss, hornblende amphibolite and quartz – feldspar – biotite ± hornblende granite gneiss interlayered with retrogressed gneisses such as diopside – epidote – plagioclase calc silicates, chlorite phyllite,

actinolite – epidote – chlorite – calcite schist and tremolite – serpentinite schist (Grantham *et al.* 1995*b*). The younger age reflects localized fluid-assisted recrystallization (Jackson, 1999).

The *Mjöllföykje Banded Gneiss* (1081 ± 4 Ma to 994 ± 22 Ma) is exposed at Mjöllföyke, Enden and in the main face of Hallgrenskarvet. This heterogeneous package of gneiss is characterized by metre-scale compositional banding and comprises alternating melanocratic (younger) and leucocratic (older) components. Grantham *et al.* (1995*b*) describe quartz – feldspar – biotite – garnet – hornblende gneiss with lenses of calc silicate and marble.

The *Kirwanveggen Megacrystic Orthogneiss Complex* (1074 ± 10 Ma) is the most voluminous rock unit in the central Kirwanveggen and occupies large portions of Enden, Mjöllföykje and Hallgrenskarvet. This orthogneiss occurs as large concordant tabular bodies, which intrude the *Mjöllföykje Banded Gneiss*. This quartz – feldspar – biotite ± garnet ± hornblende granite gneiss has a distinctive augen texture defined by K-feldspar porphyroclasts. The *Kirwanveggen Megacrystic Orthogneiss Complex* is known to contain charnokitic remnants and large amphibolite bodies, biotite-rich varieties are common and evidence for localized partial melting and migmatization is widespread.

The *Tverreggtelen Leucogranite Suite* (990 ± 12 Ma) occurs as thin (10 – 100m), tabular sheet-like bodies within the *Mjöllföykje Banded Gneiss* at Hallgrenskarvet, Tverreggtelen and Enden. Although the leucogneiss appears to intrude banded gneisses at Tverreggtelen, elsewhere leucogneiss sheets are incorporated within the fabric of the banded gneisses to the extent that they occur as detached boudins in some places. These quartz - K-feldspar – plagioclase – biotite – muscovite leucogneisses contain accessory flourite, ilmenite, magnetite and garnet.

Table 3.1 A summary of geochronological data from the tectonostratigraphic units of the central Kirwanveggen (after Jackson 1997).

Tectonostratigraphic unit	Age (Ma)	Method	Reference
Kvervelnatten Granite Gneiss Complex (KGGC)	1135	U-Pb SHRIMP	Jackson (1997)
Tverregga Banded Gneiss (TBG)	~ 1135 and 992 ± 64	U-Pb SHRIMP	Jackson (1997)
Mjöllföykje Banded Gneiss (MBG)	1081 ± 4 to 994 ± 22	U-Pb SHRIMP	Jackson (1997)
Kirwanveggen Megacrystic Orthogneiss Complex (KMOC)	1074 ± 10	U-Pb SHRIMP	Jackson (1997)
Tverreggtelen Leucogranite Suite (TLG)	990 ± 12	U-Pb SHRIMP	Jackson (1997)

Jackson (1997) has developed a deformational sequence for the central Kirwanveggen based on the field relationships of the tectonostratigraphic units described above and a series of cross-cutting dykes (Fig. 3.1). This 5-stage sequence has been refined by high precision U-Pb SHRIMP dating of the major units and cross-cutting dykes. The earliest episodes of deformation (D_n and D_{n+1}) formed S_n and S_{n+1} fabrics which are restricted to the *Kververlnatten Granite Gneiss Complex*. Subsequent deformation (D_{n+2}) formed the S_{n+2} fabric, which destroyed the earlier fabrics and formed the pervasive regional fabric of the central Kirwanveggen, the D_{n+2} event did not affect the early *Kververlnatten Granite Gneiss Complex*. Low intensity deformation (D_{n+3}) resulted in localized open folding of S_{n+2} fabrics,

such as those observed in the *Tverreggtelen Leucogranite Suite*. Late D_{n+4} deformation was then responsible for the development of discrete brittle-ductile shear zones which displace S_{n+2} fabrics along low angle thrusts. Finally, D_{n+5} brittle deformation produced joints and fractures related to the fragmentation of Gondwanaland. The sequence described here has been adopted for use in this study using simple D_1 through D_6 (S_1 through S_6) notation to represent episodes of deformation and corresponding fabrics, respectively.

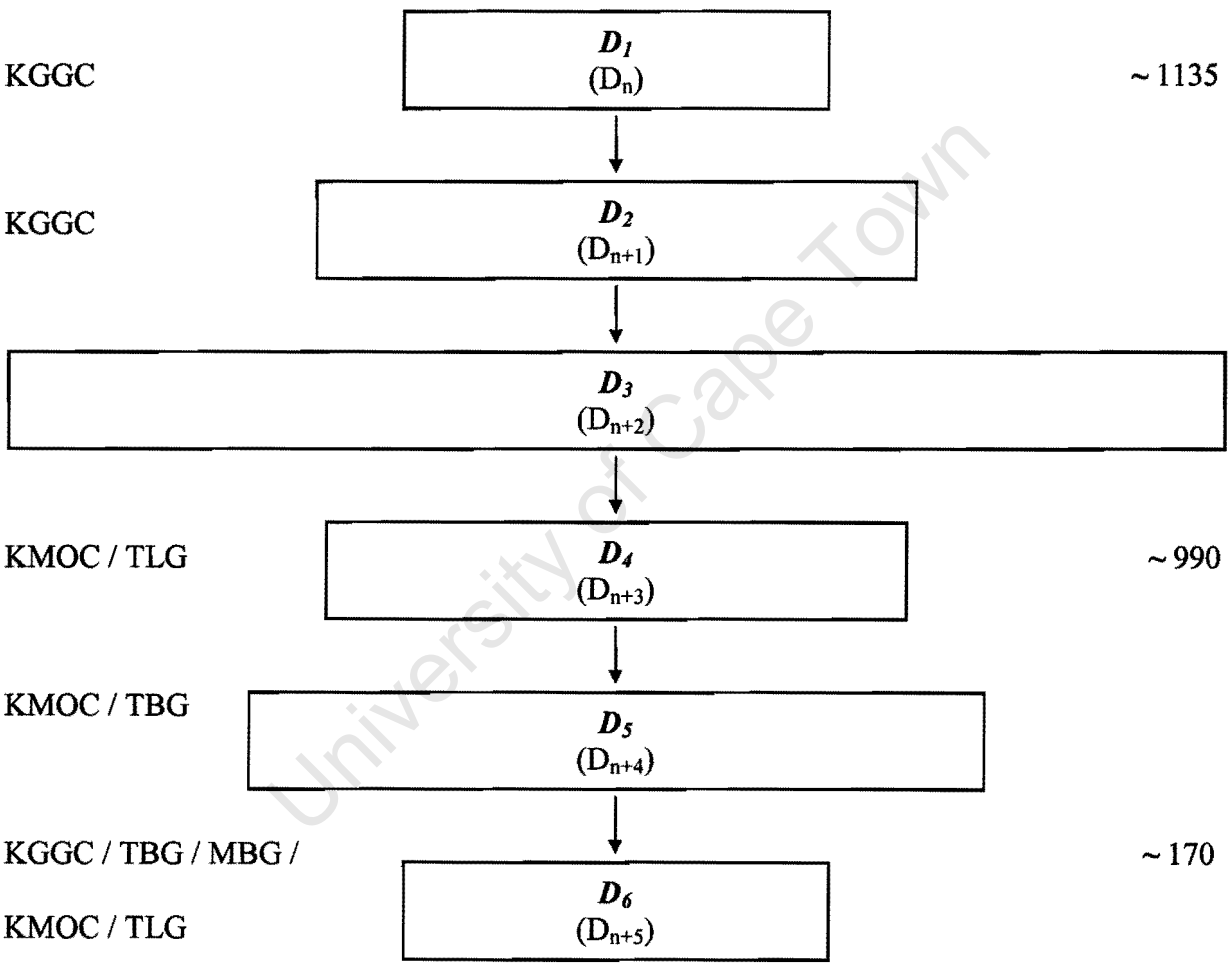

Figure 3.1 Deformational sequence for the central Kirwanveggen (after Jackson 1997). Width of boxes indicate the intensity and degree of influence of each event. The tectonostratigraphic units affected by each event are shown on the left and the corresponding age on the right. Note that D_3 affects all units excluding the KGGC.

3.2 ROCK TYPES

The majority of rock types described here belong to the Sverdrupfjella Group and most of the samples were collected in the central Kirwanveggen at the Hallgrenskarvet – Tverreggtelen – Tverregga - Stignabben group of nunataks (APPENDIX A). Fewer were collected from Heksagryta further to the south as well as limited sampling in the H. U. Sverdrupfjella. The rock types of the Sverdrupfjella Group are ordered according to the geochronological sequence established by Jackson (1999) and the tectonostratigraphic framework compiled by Grantham *et al.* 1995*b*. Metacarbonates of the Fuglefjellet Formation occur in the H. U. Sverdrupfjella and are described after the major rock types of the central Kirwanveggen. This is followed by a description of the different sets of dykes and veins in the central Kirwanveggen which span a large range of ages. The Sistenup lavas which are of unknown age are described first. Field photographs presented in this chapter are generic and petrographic descriptions of the different rock types are included in APPENDIX C.

According to Bucher & Frey (1994) there is not a single classification scheme for the naming of metamorphic rocks, although these authors recommend that the modal mineralogical composition and the mesoscopic structure of the rock be reflected in the name. In this dissertation the root name of the rock is generally used, e.g. gneiss or schist and the prefix usually contains the major minerals in order of modal abundance, e.g. quartz – feldspar – biotite gneiss. In some cases special names such as ultramylonite, greenschist, marble and calc silicate may be employed as a root name in order to describe the rock accurately. There are also cases where rock names used by previous workers have been adopted even if they are not considered to be the most accurate description of the rock, this is true for the metagabbro described in Section 3.2.4 which is more accurately described as an amphibolite.

3.2.1 Basalt & Syenite

Basalt, syenite and a variety of felsic intrusives are exposed at Sistenup in the north eastern Kirwanveggen. This isolated sequence of lavas has been described in some detail in Section 2.3, and is characterized by its restricted extent and distinctive texture. At Sistenup, the 200m-thick basalt sequence is roughly divided into a lower and upper unit overlain by a feldspar porphyry unit. The lower unit comprises alternating layers of aphyric and the distinctive plagioclase-phyric basalt shown in Figure 3.2. Syenite exposed at Sistenup intrudes the lavas and is considered to be part of the Sistefjell Complex. The syenite consists of alkali-feldspar phenocrysts with quartz and mafic minerals, predominantly amphibole, comprising the matrix.

3.2.2 Granite Gneiss

Granite gneiss is exposed at Tverreggtelen, Swartbandufsa and Kvervelnatten in the central Kirwanveggen where it makes up the *Kvervelnatten Granite Gneiss Complex* described by Grantham *et al.* (1995*b*). Typical fabric patterns showing earliest S_1 fabrics and S_1 leucosomes rotated about S_2 shear surfaces which also host leucosome development are characteristic of this rock type (Fig. 3.3). The granite gneiss is the only lithology that preserves the earliest fabrics in the central Kirwanveggen, an observation confirmed by U-Pb SHRIMP dating of S_1 and S_2 leucosomes, which provide an age of 1135 Ma (Jackson 1997). The preservation of early fabrics is considered to be a function of the granite gneiss acting as a strain resistor to subsequent deformation (Jackson 1997). The granite gneiss is dissected by several intrusive phases which cross-cut the early fabrics. These include discordant pegmatites (Fig. 3.4), porphyritic granite dykes, the *Swartbandufsa Mafic Dykes* (Figs. 3.6 and 3.25) and felsic dykes.

The granite gneiss comprises quartz – K-feldspar – hornblende – biotite with minor epidote, plagioclase, chlorite and accessory sphene. The early S_1-parallel leucosomes are thick (10cm to 1m) and can extend for several metres. The later S_2-parallel leucosomes have a lensoidal shape and are typically only 1cm thick and 10cm long. Both types of leucosome comprise quartz + K-feldspar and have a recrystallized migmatitic texture. Minor hornblende ± biotite is restricted to the early leucosomes which occasionally contain small slivers of host material. Petrographically, this is a coarse-grained feldspar-rich rock with interstices of recrystallized quartz. Plagioclase crystals are inclusion-rich and are overprinted by epidote. Hornblende occurs as large (> 1mm) grains intergrown with biotite flakes, the latter are poorly orientated to define a cryptic fabric (Fig. 3.5).

Figure 3.2 Plagioclase-phyric basalt at Sistenup. The groundmass is amphibole and the distinctive texture is defined by randomly orientated plagioclase phenocrysts.

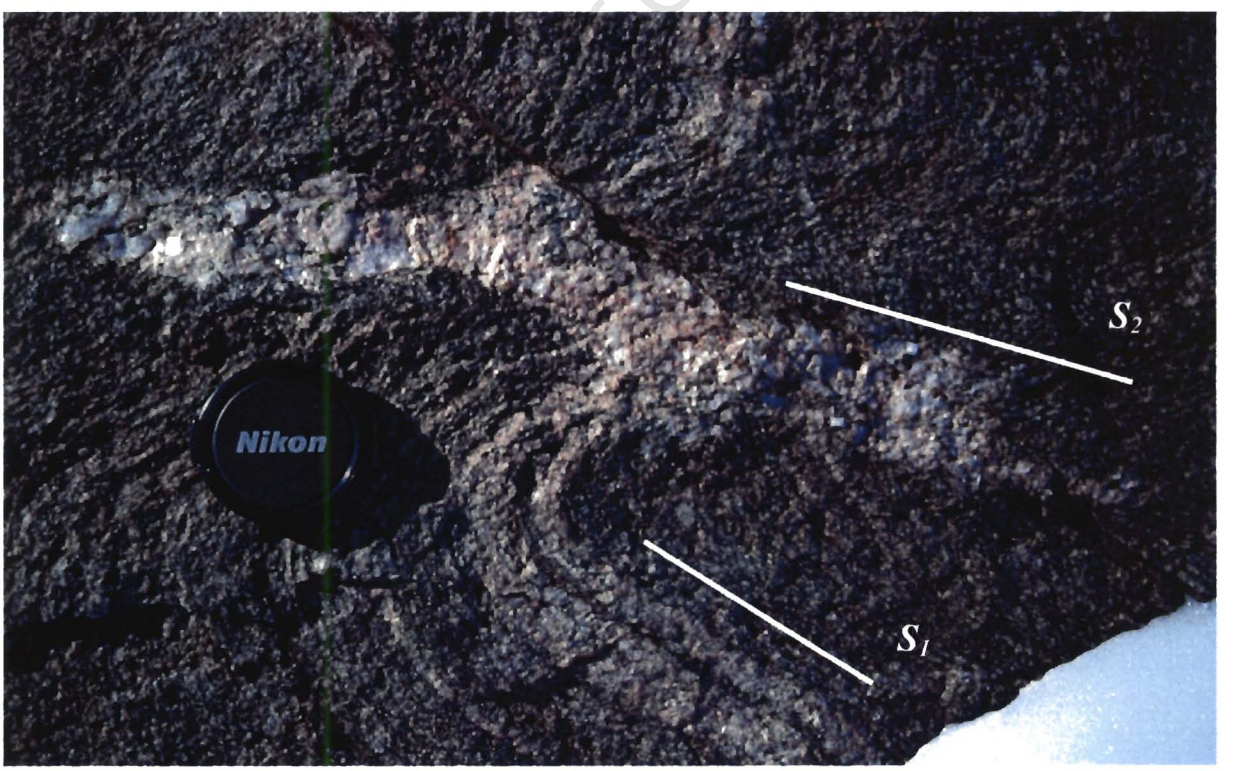

Figure 3.3 Granite gneiss at Tverreggtelen showing typical fabric pattern defined by S_1 fabrics folded about S_2 axial surfaces and associated leucosomes.

Figure 3.4 Discordant pegmatite intruding granite gneiss at Tverreggtelen (Locality 36). The pegmatite cross-cuts both the S_1 and S_2 fabric of the granite gneiss host.

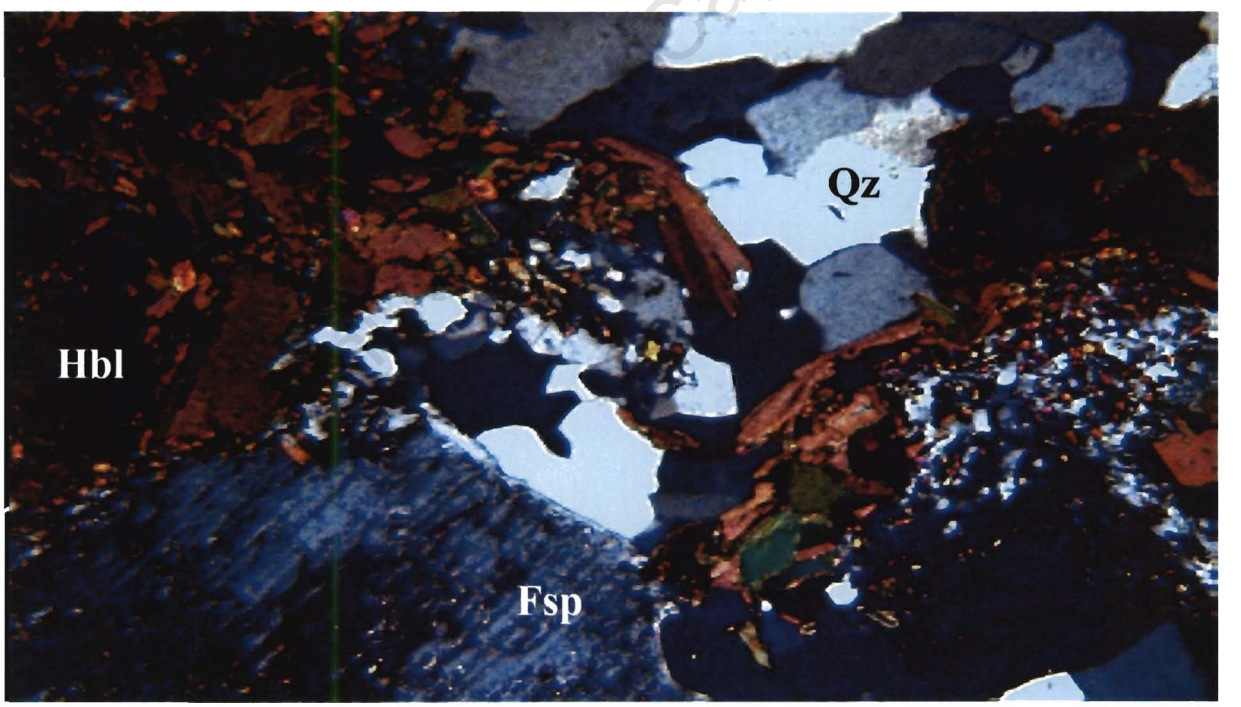

Figure 3.5 Photomicrograph of WJK 224. This coarse Feldspar-rich rock has interstices of recrystallized quartz. Plagioclase clasts are inclusion-rich and overprinted by epidote. Hornblende occurs as large (> 1mm) grains intergrown with biotite flakes, which are poorly orientated to define a cryptic fabric. FOV = 2.5mm.

3.2.3 Banded Gneiss (Retrograde assemblages)

A sequence of heterogeneous banded gneisses, very similar in appearance to the *Mjöllföykje Banded Gneiss* described in Section 3.2.4, is exposed at Tverregga and is termed the *Tverregga Banded Gneiss* (Grantham *et al.* 1995*b*). These gneisses and schists display a variable degree of hydrous retrogression, which is best developed within high strain domains (Fig. 3.6). The gneisses display mylonitic textures within the boundaries of the high strain zones, which define the moderately south east dipping S_3 regional planar fabric of the central Kirwanveggen. Mineral and stretching lineations within this fabric are generally down-dip, and field criteria such as porphyroblasts, shear bands and fabric re-orientation indicate a "top to the north west" sense of shear. U-Pb SHRIMP dating of monazite from an ultramylonite within one of these high strain zones yields ages of ~ 1135 Ma for monazite cores and 992 ± 64 Ma for recrystallized rims (Jackson 1999). Although more localized, similar assemblages are also observed around the margins of the intrusive leucogranite at Tverreggtelen, and within the banded gneisses which make up the central portion of the Hallgrenskarvet escarpment. Rare calc silicate boudins are an important feature of these retrogressed paragneisses.

Retrograde mineral assemblages are defined by biotite, chlorite and epidote with lesser amounts of sericite, sphene and calcite. The *Tverregga Banded Gneiss* consists of three distinctive lithological components, namely; quartz – chlorite - epidote – biotite schist (Fig. 3.7), quartz – K-feldspar – plagioclase – sericite – chlorite schist (Fig. 3.8), and quartz – epidote – muscovite – chlorite – calcite – sphene schist (Fig. 3.9). Quartzofeldspathic gneisses in these zones have epidote and biotite as major phases while magnetite is a major accessory phase in most of the samples from Tverregga. Calc silicate assemblages comprise quartz – plagioclase – diopside – actinolite – sphene with minor epidote + tremolite and accessory biotite + chlorite.

Calc silicate boudins

Scattered calc silicate boudins (Fig. 3.10) conform to the early regional fabric and are hosted in retrogressed quartz – biotite - chlorite banded gneisses making up an extensive horizon more than 20m thick which forms part of the *Tverregga Banded Gneiss* described by Grantham *et al.* (1995*b*). Individual boudins range from 5 – 20cm in diameter, and are ellipsoidal in shape with their long axis parallel to the mineral stretching lineation within the plane of the foliation. Most show a distinct mineral zonation from core to periphery. Cores are relatively rich in mafic minerals and comprise quartz – K-feldspar – plagioclase - diopside – hornblende with minor calcite and sphene whereas the more felsic periphery comprises plagioclase – quartz – K-feldspar + minor calcite. Mineral zonation is most often poorly developed with the surrounding felsic component "drowning out" the mafic cores (Fig. 3.11).

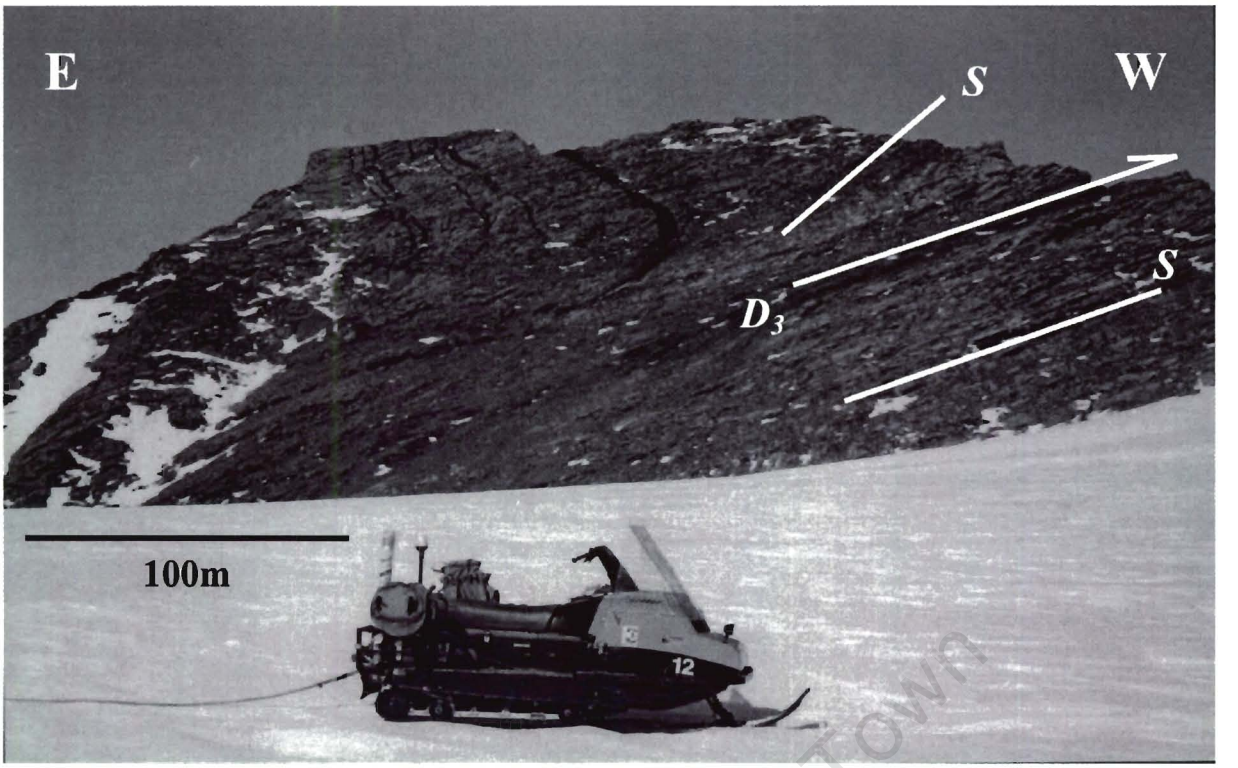

Figure 3.6 High strain zone deflecting *Swartbandufsa Mafic Dykes* in the *Tverregga Banded Gneiss* at Tverregga. Retrograde mineral assemblages are defined by biotite, chlorite and epidote with lesser amounts of sericite, sphene and calcite.

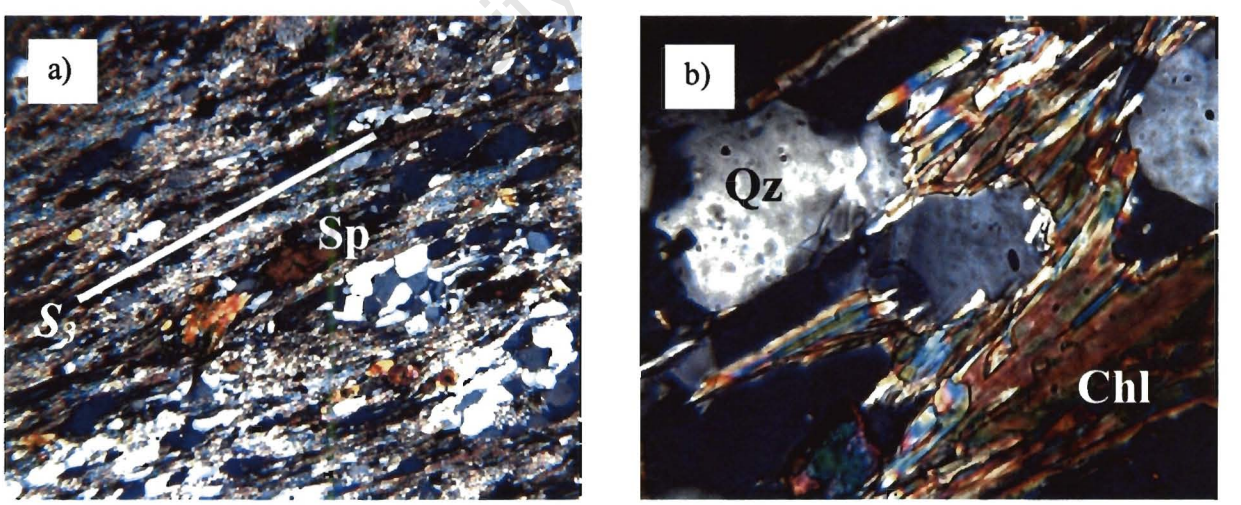

Figure 3.7 Photomicrographs of WJK 152 showing the hydrous retrograde assemblage of quartz – chlorite - epidote – biotite with accessory sphene and late calcite. Photomicrograph a) cross polars, FOV = 3mm and b) cross polars, FOV = 1mm.

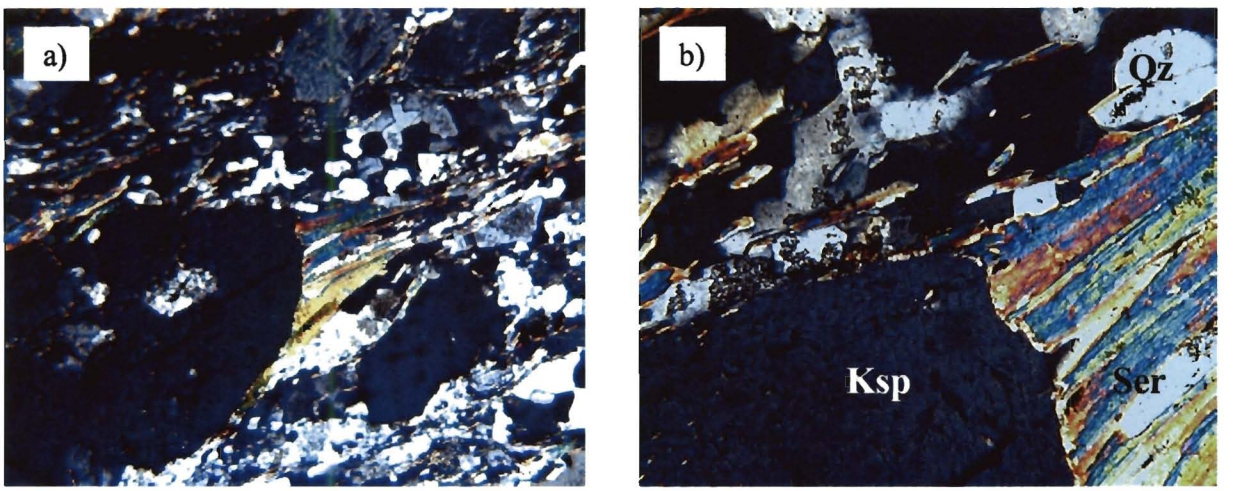

Figure 3.8 Photomicrograph of WJK 156 showing the hydrous retrograde assemblage of quartz – K-feldspar – plagioclase – sericite – chlorite with accessory epidote. Photomicrograph a) cross polars, FOV = 2.5mm and b) cross polars, FOV = 1mm.

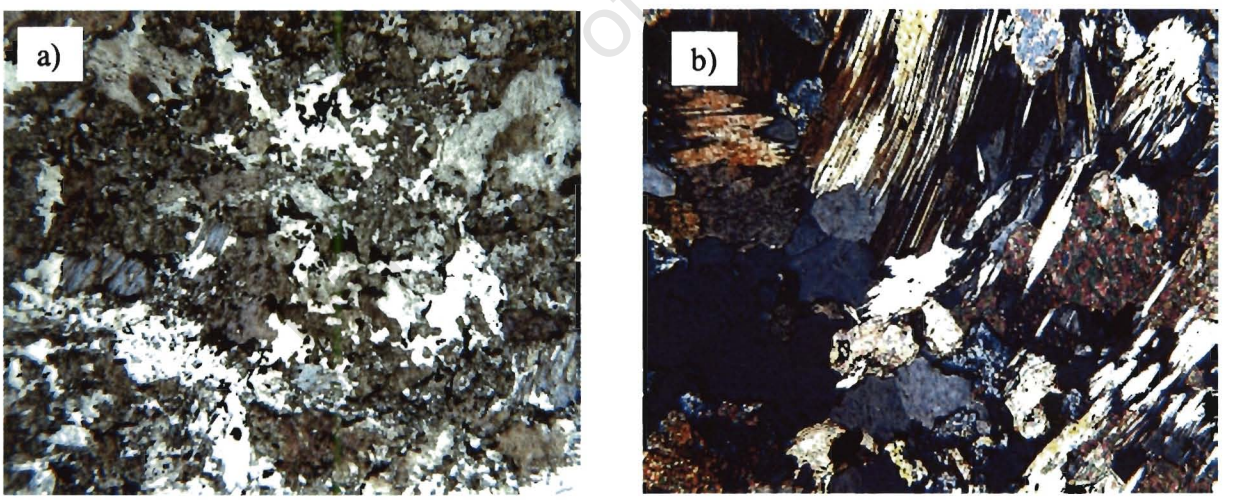

Figure 3.9 Photomicrograph of WJK 155 showing the hydrous retrograde assemblage of quartz – epidote – muscovite – chlorite – calcite – sphene with accessory magnetite, apatite and allanite. Photomicrograph a) plane polars, FOV = 2.5mm and b) cross polars, FOV = 1mm.

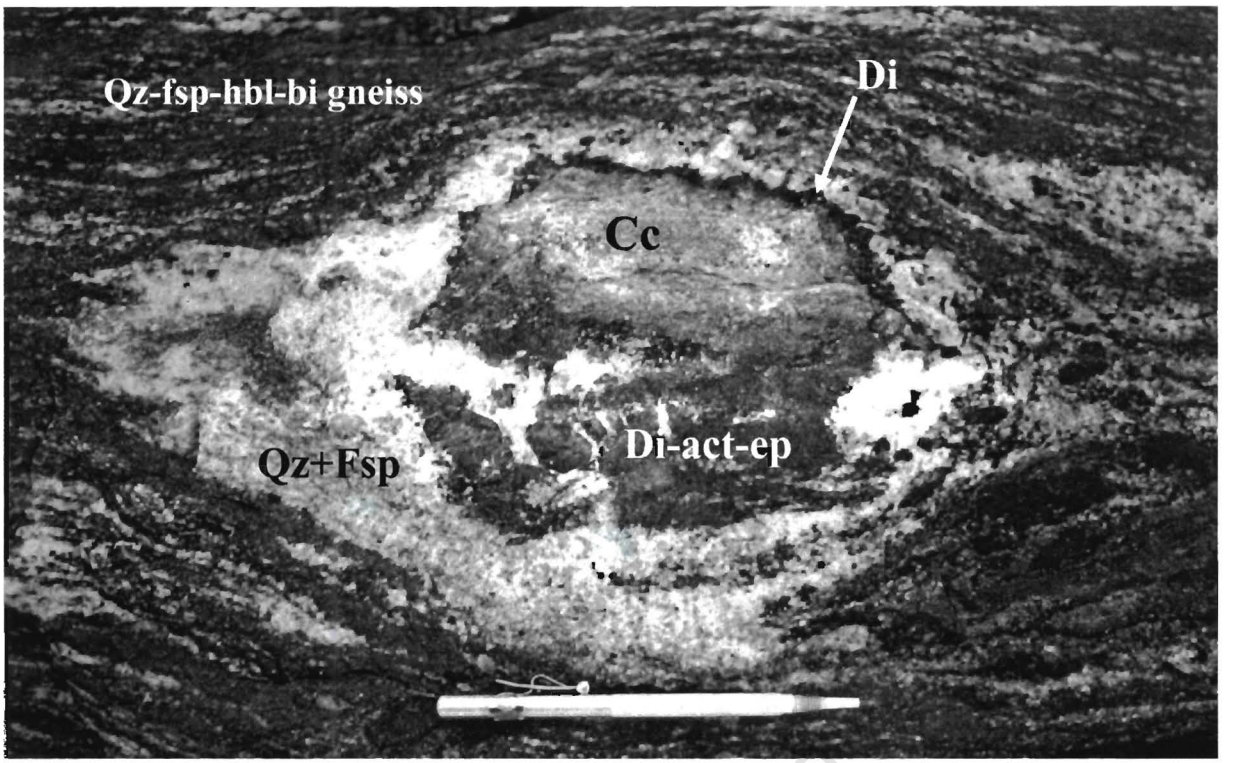

Figure 3.10 Zoned calc silicate boudin at Tverregga hosted in retrogressed quartz – feldspar – hornblende – biotite gneiss (Locality 26). The core is calcite surrounded by diopside – actinolite – epidote, with a rim of quartz + feldspar.

Figure 3.11 Zone of scattered calc silicate boudins in the banded gneiss at Tverregga (Locality 26). Note how the leucocratic material "drowns out" the mafic cores.

3.2.4 Banded Gneiss

This heterogeneous package of gneiss is characterized by metre-scale compositional banding of alternating leucocratic and melanocratic units (Fig. 3.12). The banded gneiss is exposed in the main face of Hallgrenskarvet, at Tverreggtelen and at Mjöllföykje and is collectively termed the *Mjöllföykje Banded Gneiss* (Grantham *et al.* 1995*b*). U-Pb SHRIMP dating of zircons from the leucocratic component of this unit provides an age of 1084 ± 4 Ma and zircons from the melanocratic component an age of 994 ± 22 Ma (Jackson 1999). The metamorphic banding which characterizes this gneiss defines the regionally consistent S_3 fabric of the central Kirwanveggen. The south east dipping planar fabric is penetrative and overprints earlier fabrics in all rock types of the central Kirwanveggen apart from the granite gneiss of the *Kvervelnatten Granite Gneiss Complex*. The planar compositional banding of these gneisses is modified by the competency difference between the leucocratic and melanocratic components. Competent leucocratic gneiss layers thinner than 30cm frequently occur as trains of boudins within the less competent melanocratic schists (Fig. 3.13). Chloritised biotite- and amphibole-rich units are interspersed throughout the sequence and are considered to be early dykes on account of their locally discordant nature (Fig. 3.14). The biotite- and amphibole-rich schists are very dark in colour and generally have a well developed crenulation cleavage. Apart from leucocratic gneisses and melanocratic schists, the banded gneiss package incorporates migmatite leuco-boudins, a metasomatic calc silicate body and an amphibolitic body described as a metagabbro. Dolerite dykes assumed to be Jurassic in age, and related to the Karoo Province cross-cut the gneisses at a high angle (Figs. 3.14 and 3.26).

The melanocratic component of the banded gneiss package is a quartz – K-feldspar – plagioclase – biotite ± hornblende ± chlorite ± epidote schist with accessory sphene and apatite. The leucocratic component of the banded gneiss package is a quartz – plagioclase - K-feldspar ± muscovite ± biotite gneiss with accessory hornblende, sphene, apatite and oxides. Migmatite leuco-boudins comprise coarse-grained quartz + K-feldspar with minor plagioclase + muscovite and accessory chlorite + sphene. The amphibolite, described by the Antarctic Research Group (1995) as a metagabbro, is a homogeneous quartz – K-feldspar – hornblende – biotite – sphene rock with minor plagioclase and accessory apatite + epidote.

Metasomatic calc silicates

Calc silicate mineral assemblages are rare in the central Kirwanveggen where they occur as scattered boudins, which are described above, and as a pervasive metasomatic body hosted in amphibole-rich banded gneisses of the *Mjöllföykje Banded Gneiss* sequence. The metasomatic alteration body at Tverreggtelen occurs as a pervasive lens extending for at least 150m along strike and hosted within a D_3 shear zone (Fig. 3.15) which extends into the adjacent leucogneiss where it is associated with silicification (Section 3.2.6). The metasomatic assemblage comprises calcite - diopside with variable amounts of hornblende - actinolite ± chlorite ± serpentinite ± tremolite ± talc ± epidote. The Tverreggtelen calc silicate body is distinctly zoned with a hornblende- and diopside-rich mafic core surrounded by a voluminous tremolite-rich central zone comprising calcite - quartz - diopside - tremolite - talc and sphene (Fig. 3.16), the periphery of the body is a friable mass of quartz - calcite - hornblende - talc - serpentinite - actinolite and diopside (Fig. 3.17).

Figure 3.12 Banded gneisses in the main face of Hallgrenskarvet. Note the alternating leucocratic and melanocratic units which define the regional S_3 fabric of the central Kirwanveggen. The circle indicates a man for scale.

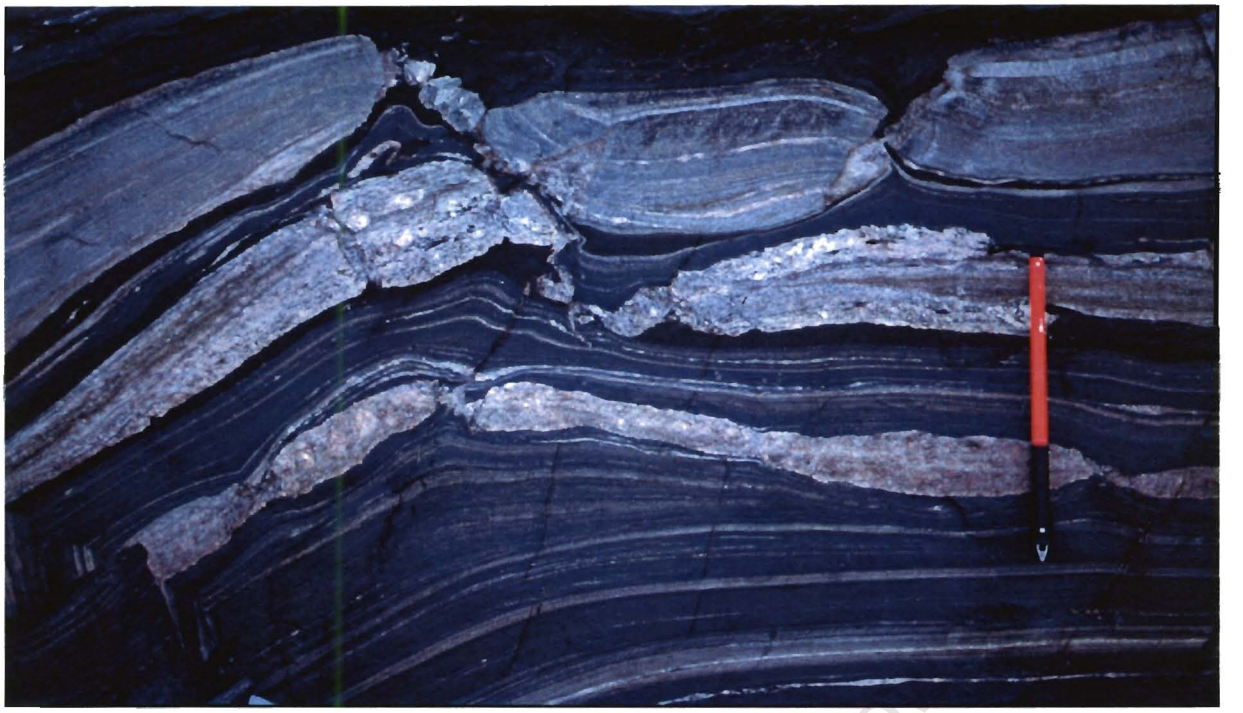

Figure 3.13 Modified compositional layering in the banded gneisses at Hallgrenskarvet. Notice how leucocratic (competent) units thinner than ~ 30cm have been boudinaged and are encompassed by melanocratic (incompetent) schists.

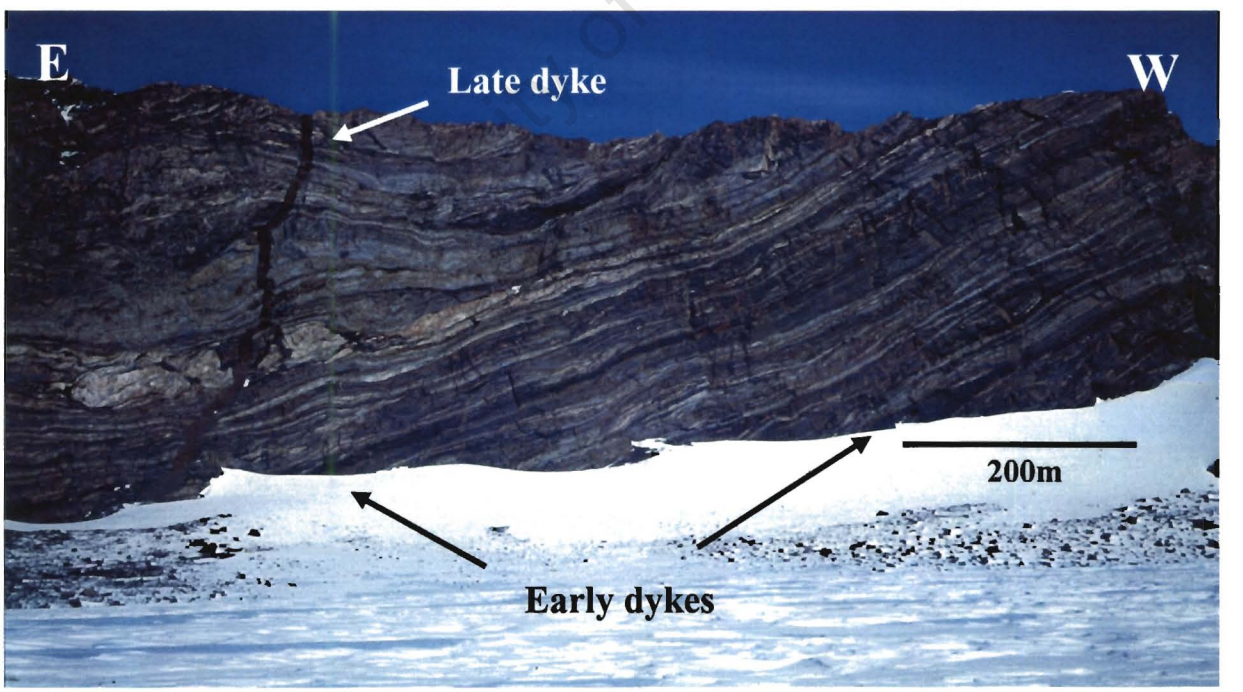

Figure 3.14 Early amphibolite dykes within the banded gneiss package at Hallgrenskarvet. Note the locally discordant nature of the mafic units with respect to the regional S_3 fabric / compositional banding.

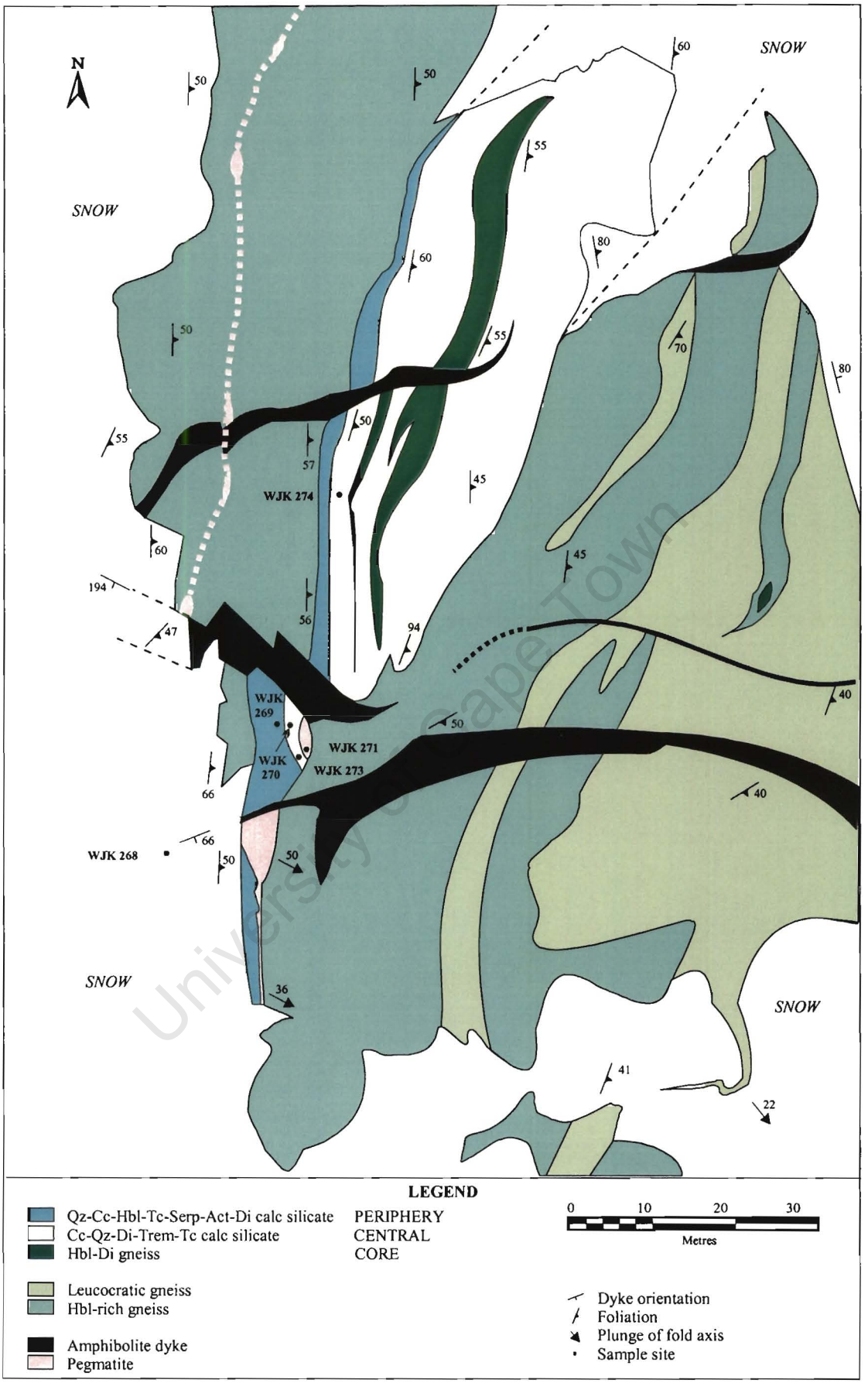

Figure 3.15 Geological map of the metasomatic calc silicate body at Tverreggtelen (Locality 41).

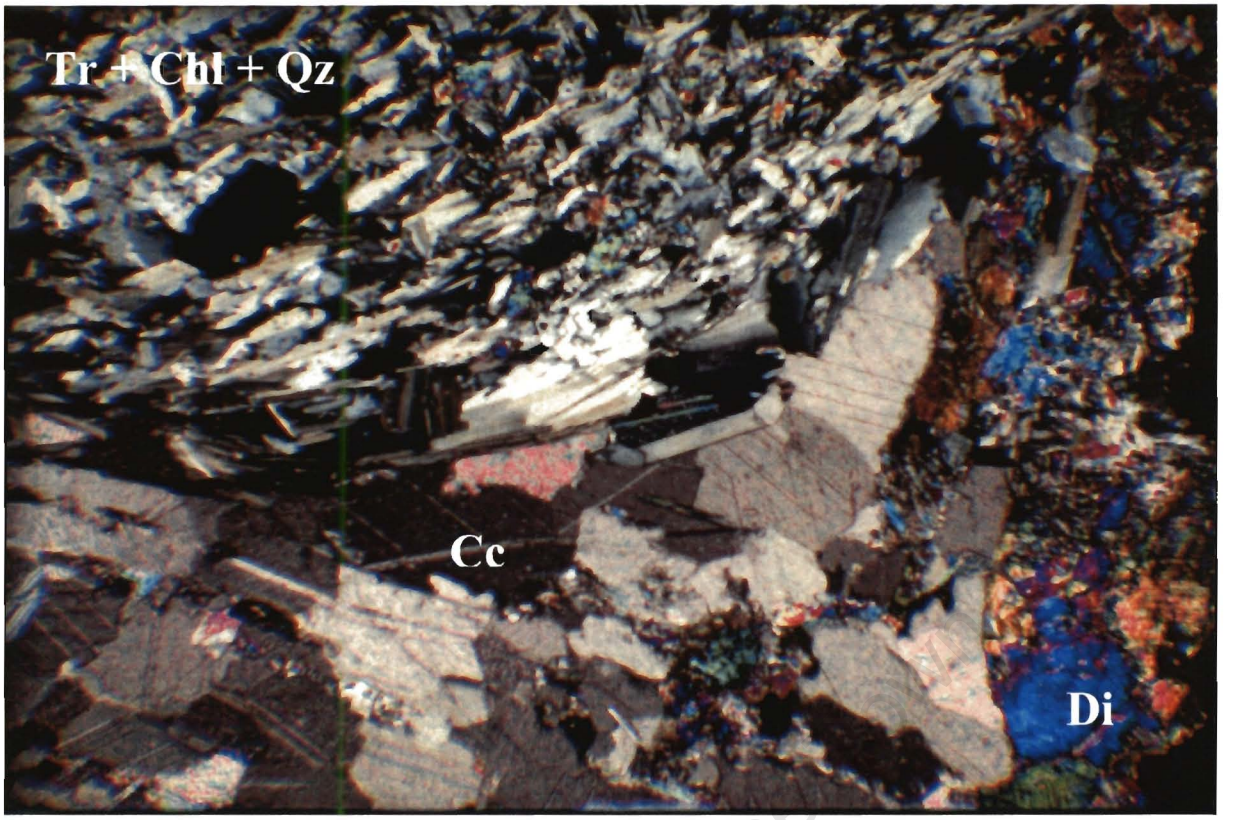

Figure 3.16 Photomicrograph of WJK 270 showing the make-up of the tremolite-rich zone of the metasomatic calc silicate body at Tverreggtelen. FOV = 2.5mm.

Figure 3.17 Peripheral zone of the metasomatic calc silicate body at Tverreggtelen.

3.2.5 Augen Gneiss

Augen textured orthogneiss is the most voluminous rock type in the central Kirwanveggen and makes up the bulk of the escarpment at Mjöllföyke and Hallgrenskarvet where it is known as the *Kirwanveggen Megacrystic Orthogneiss Complex* (Grantham *et al.* 1995*b*). Jackson (1999) determined a U-Pb SHRIMP crystallization age for the *Kirwanveggen Megacrystic Orthogneiss Complex* of 1074 ± 10 Ma. The augen gneiss is regionally homogenous (Fig. 3.18), although, biotite-rich varieties, large amphibolite bodies, localized migmatization and partial melting are common. A variably developed mylonitic fabric is ubiquitous and corresponds to the regional S_3 fabric of the central Kirwanveggen. On an outcrop-scale, the homogeneous augen gneiss is dissected by numerous late aplite dykes and contains amphibolite schlieren aligned parallel to the dominant fabric direction. The amphibolite bodies range in size from small (cm-scale) to large (4m × 0.5m) and are interpreted to be deformed xenoliths. Contacts between the augen gneiss and banded gneisses have generally been deformed by subsequent fabric development but intrusive contacts are preserved locally. Late discrete ductile shear zones contain S_5 ultramylonites, which cut the S_3 fabric of the augen gneiss at a high angle (Fig. 3.18).

The distinctive augen texture (Fig. 3.19) of this megacrystic gneiss is dominated by large (± 2cm) K-feldspar porphyroclasts within a medium-grained quartz – plagioclase – K-feldspar – biotite ± hornblende matrix. The coarse mylonitic fabric is defined by the alignment of biotite grains and recrystallized tails of K-feldspar porphyroclasts.

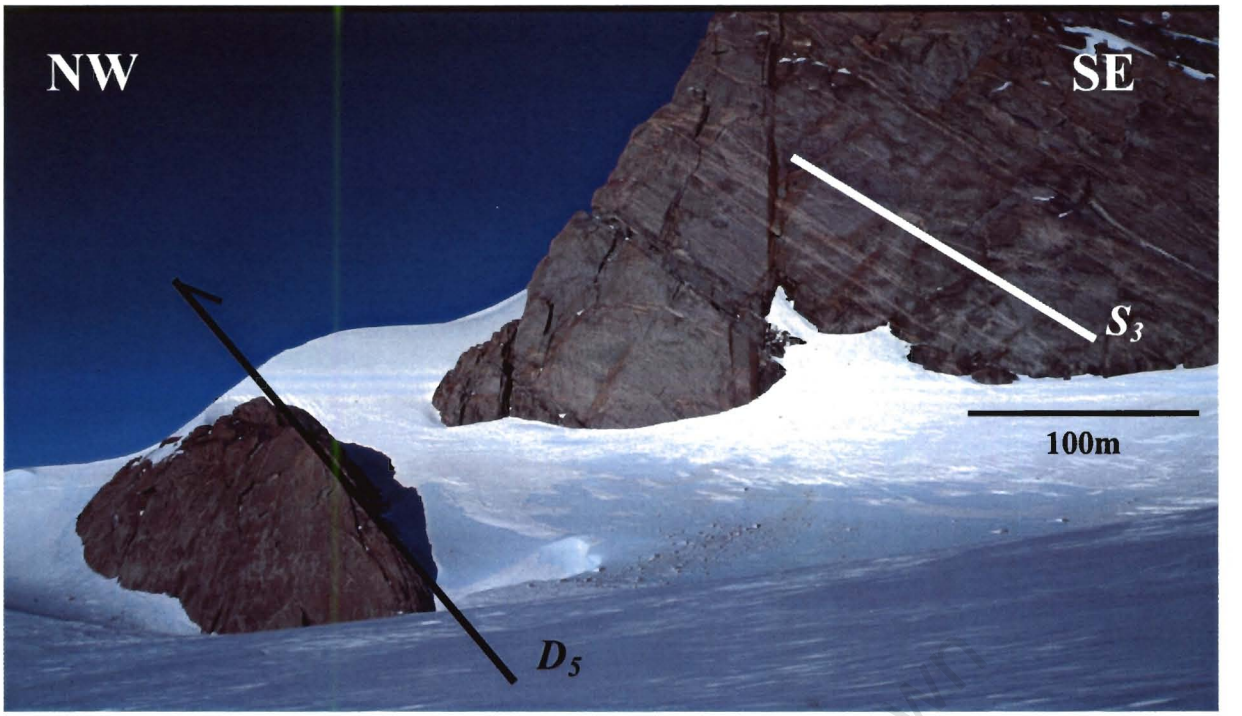

Figure 3.18 The main face of Stignabben showing the homogenous nature of the *Kirwanveggen Megacrystic Orthogneiss Complex*. At Hallgrenskarvet homogenous megacrystic orthogneiss in the east becomes progressively more migmatized towards the west.

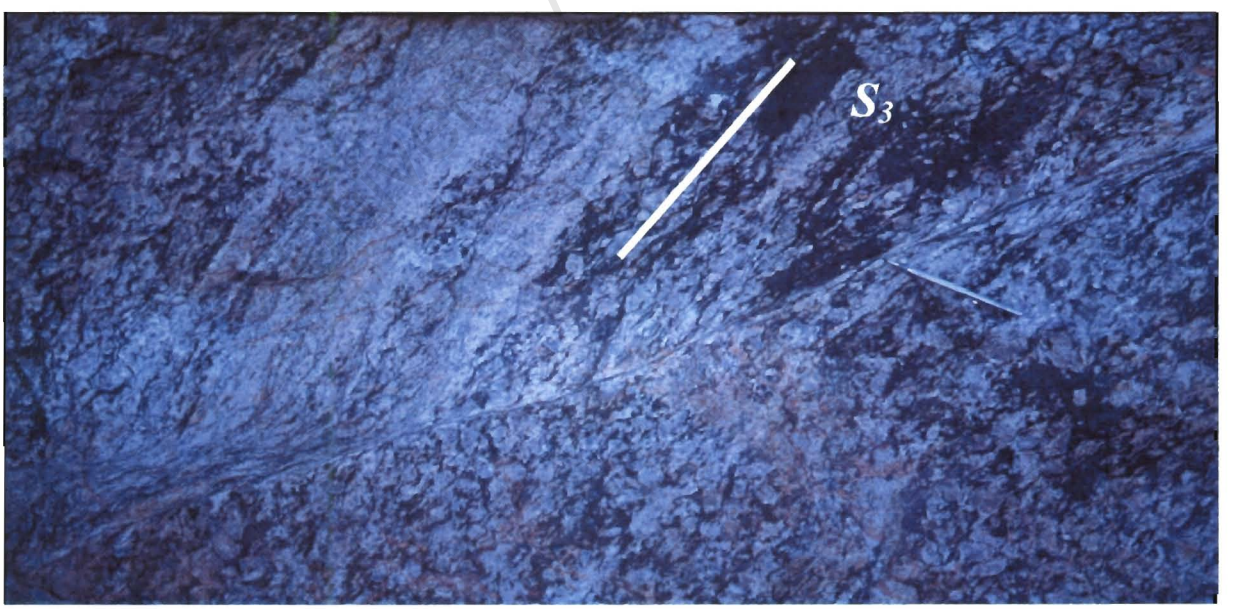

Figure 3.19 Distinctive augen texture of the *Kirwanveggen Megacrystic Orthogneiss Complex*. The mylonitic fabric is defined by the alignment of biotite and recrystallized tails of the K-feldspar porphyroclasts.

3.2.6 Leucogneiss

Homogeneous medium- to fine-grained felsic gneiss, the *Tverreggtelen Leucogranite Suite* (Jackson 1999) intrudes banded gneisses of the *Mjöllföykje Banded Gneiss* at Hallgrenskarvet, Tverreggtelen and Enden in the central Kirwanveggen. Jackson (1997) established an intrusive age of ~ 990 Ma for the leucogranite by U-Pb SHRIMP dating of zircon. The leucogneiss occurs as tabular sheet-like bodies, which contain and conform to the regional S_3 fabric of the central Kirwanveggen (Fig. 3.20). At Tverreggtelen, the S_3 fabric is folded about macro-scale F_4 fold axial surfaces and finger-like apophyses of leucogranite intrude the host banded gneisses extending for up to several hundred metres away from the main body (Fig. 3.21), one such apophysy has been termed a "Turquoise Dyke" by Jackson (1997). A single shear zone at Tverreggtelen is characterized by pervasive silicic metasomatism parallel to the S_3 fabric of the leucogneiss (Fig. 3.22). This D_3 shear zone is less discrete than the younger D_5 shear zones because the silicification is several metres thick and discolouration penetrates the leucogneiss wall-rock for up to 10m away from the shear zone. Large (4m × 2m) brittle quartz veins occur within the leucogneiss adjacent to the shear zone where they cross-cut the S_3 internal fabric. Along strike, this shear zone cross-cuts the adjacent amphibole-rich banded gneisses and is associated with pervasive calc silicate metasomatism (Section 3.2.4).

The leucogneiss is a quartz – K-feldspar – muscovite – biotite – plagioclase – fluorite gneiss with accessory sphene and apatite. The coarse texture comprises quartz + K-feldspar + plagioclase with lesser amounts of muscovite + biotite (occasionally altered to chlorite + hornblende). Mica grains define a weak fabric whereas irregular fluorite grains are intergrown with quartz + feldspar grains in the matrix.

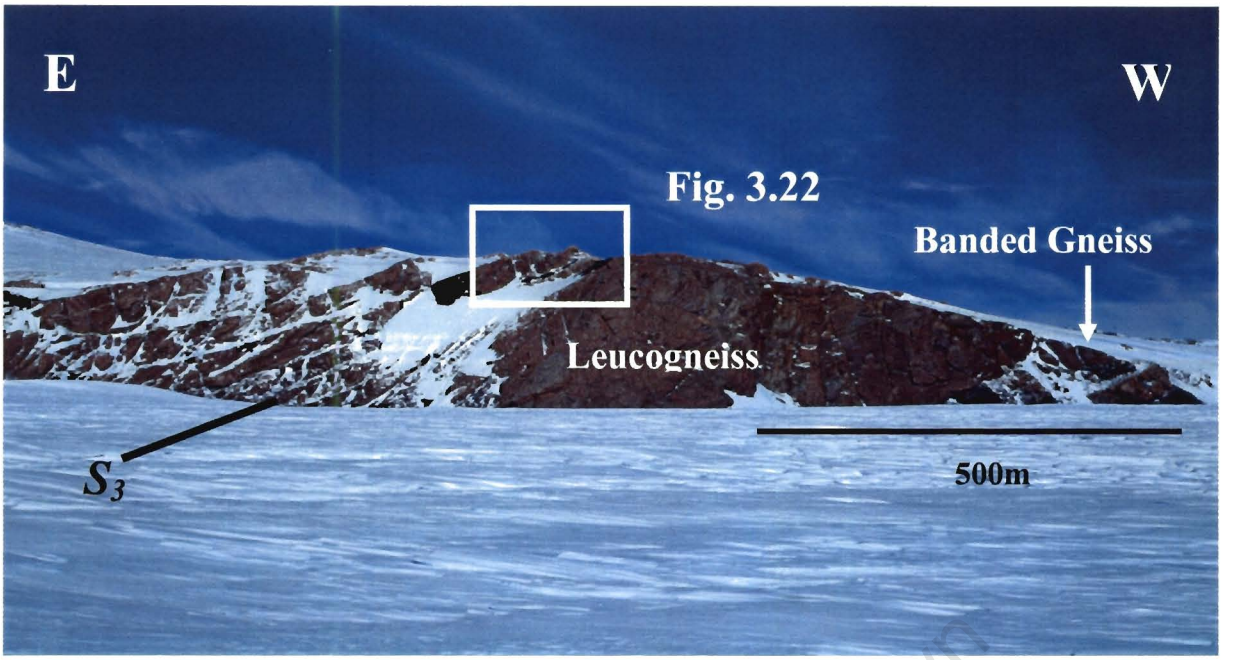

Figure 3.20 The *Tverreggtelen Leucogranite Suite* in the north face of Tverreggtelen, this view looking south is down the plunge of the F_4 fold axes. Note the folded leucogneiss / banded gneiss contact and the S_3 parallel mafic dykes.

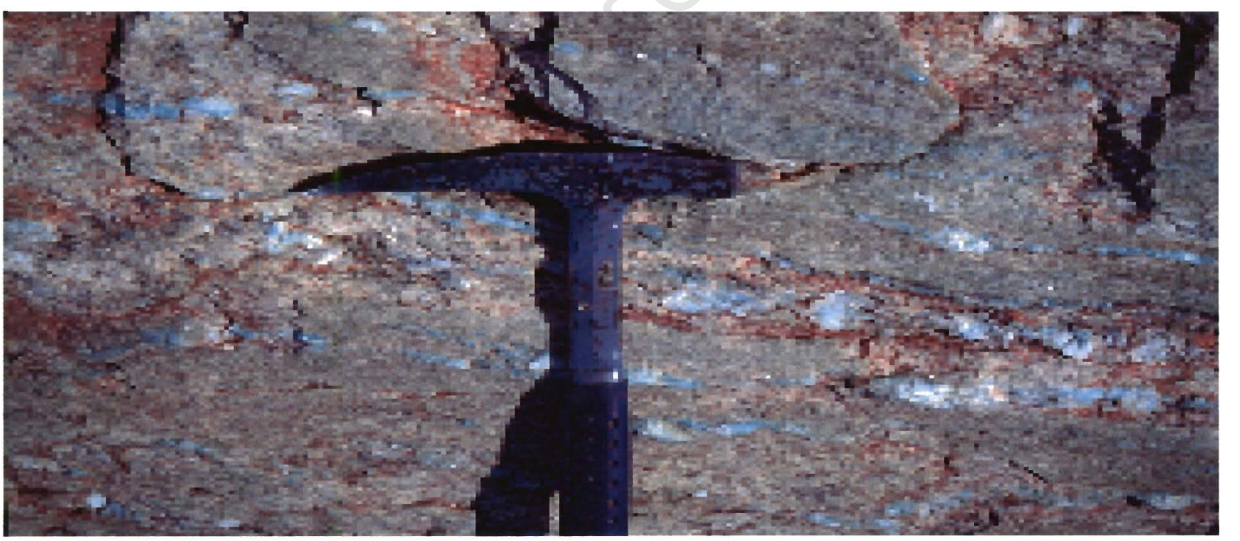

Figure 3.21 Finger-like apophyses of leucogranite intrude the host banded gneisses on the margins of the Tverreggtelen leucogranite (Locality 39). The apophysy shown here has been termed the "Turquoise Dyke" by Jackson (1997) and cross-cuts a porphyritic granite dyke at this locality. The turquoise colouration is a result of large amazonite crystals which are characteristic of these dykes.

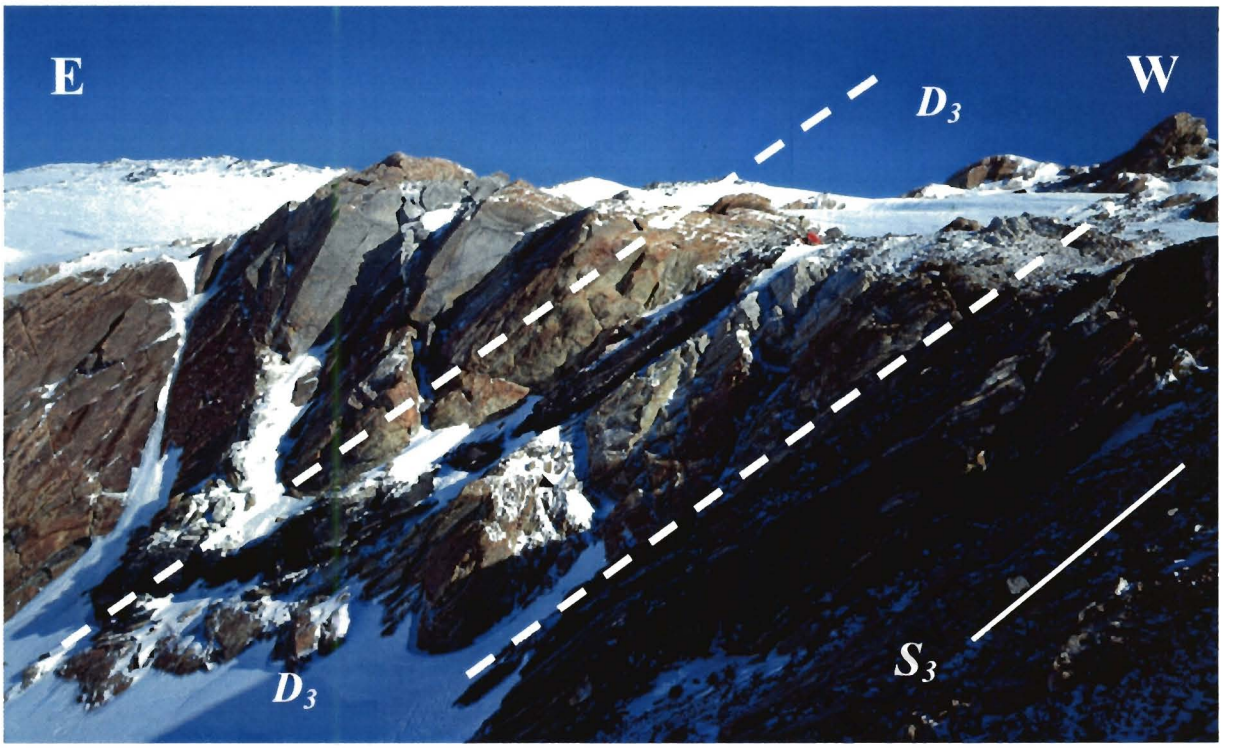

Figure 3.22 Silicic metasomatism in the Tverreggtelen Leucogranite at Tverreggtelen (Locality 44). Note the moderate to steep D_3 shear zone which affects the leucogneiss at this locality. Scale differs with perspective, but the cliff is ~ 60m high.

3.2.7 Metacarbonate

Regionally extensive units (>300m thick and 5km strike length) comprising metacarbonates with quartzofeldspathic and calc silicate gneisses are exposed in the H. U. Sverdrupfjella (Grantham *et al.* 1995*b*; Groenewald *et al.* 1995) where they collectively make up the Fuglefjellet Formation (Hjelle 1974). Although these carbonate sequences are best developed at Fuglefjellet, substantial thicknesses are also exposed at Skarsnuten further to the south where a 200m high cliff reveals a package of alternating, up to 3m thick bands of sparry calcite and quartzofeldspathic gneiss punctuated by strings of boudinaged calc silicate gneiss. The metacarbonate sequence is intruded by numerous generations of late, relatively undeformed pegmatite dykes, sills and stocks. A large stock-like pegmatite body intrudes the metacarbonate sequence at Skarsnuten (Fig. 3.23).

Carbonate-rich layers comprise ~ 90% sparry calcite and have a weak to moderately developed fabric defined by quartz, plagioclase and diopside. Reaction rims of garnet and diopside are developed within the metacarbonate on the contacts with the intrusive pegmatites. Quartzofeldspathic layers comprise medium-grained quartz – feldspar – muscovite – hornblende, are well banded and contain centimetre-thick quartz + feldspar leucosomes and zoned calc silicate boudins. The cores of the boudins are pale green and comprise diopside – quartz – plagioclase, the felsic rims surround the cores and comprise feldspar + quartz with minor garnet and hornblende (Fig. 3.24).

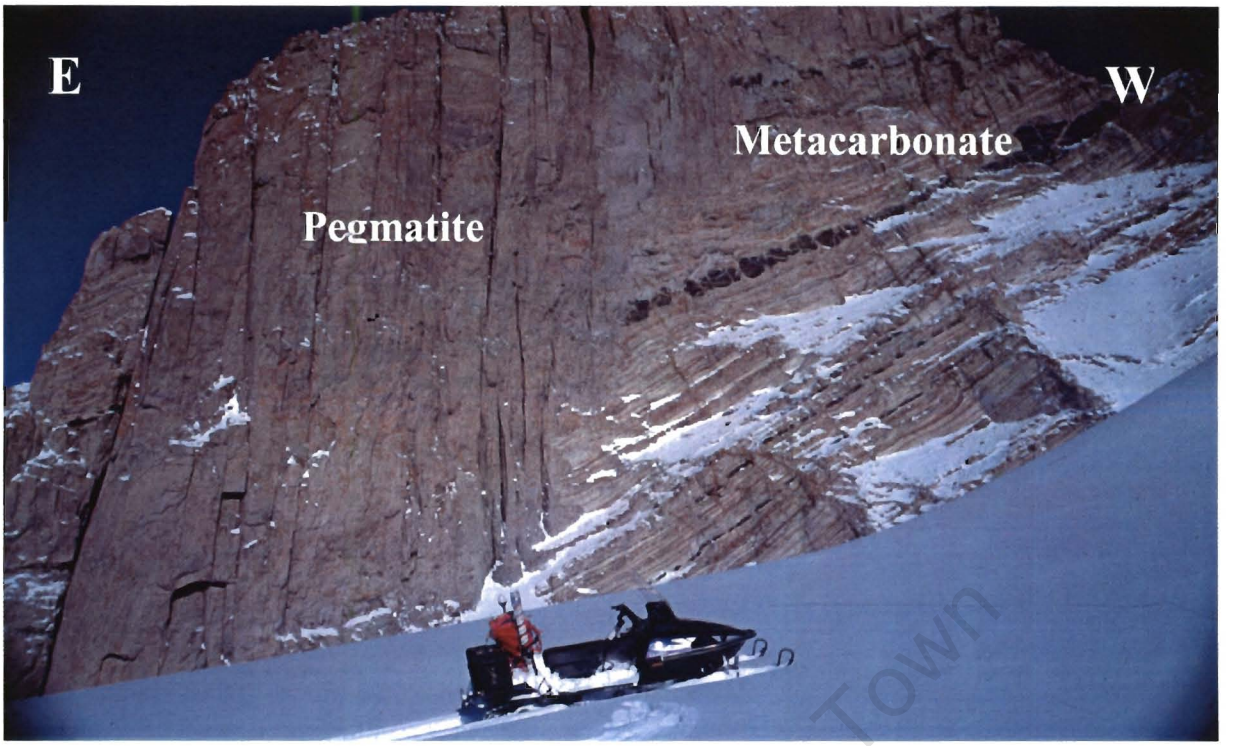

Figure 3.23 The Fuglefjellet Formation at Skarsnuten in the H. U. Sverdrupfjella. At this locality, a large body of undeformed pegmatite intrudes the layered carbonate, calc silicate and quartzofeldspathic gneiss sequence.

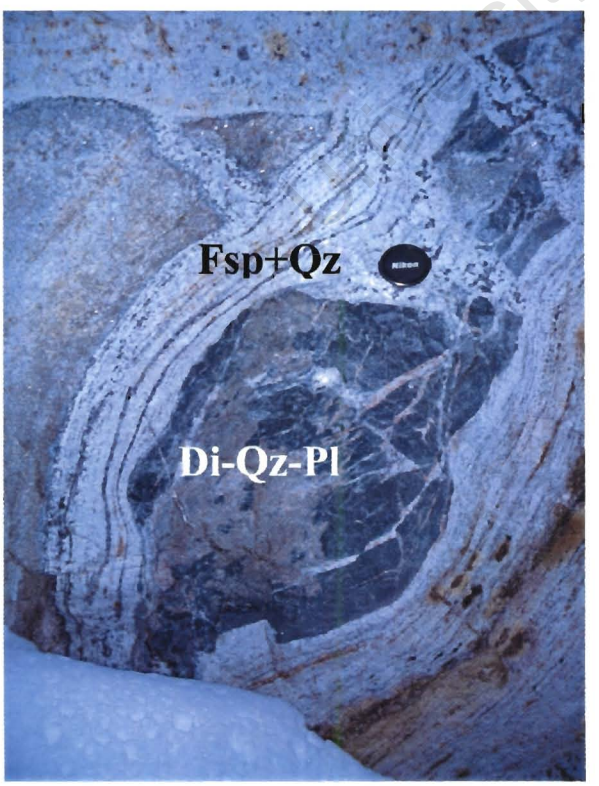

Figure 3.24 Zoned calc silicate boudin within a quartzofeldspathic gneiss host at Skarsnuten in the H. U. Sverdrupfjella. The pale green core comprises diopside - quartz - plagioclase, whereas the rims are feldspar + quartz with minor garnet and hornblende.

3.2.8 Dykes & Pegmatites

The *Swartbandufsa Mafic Dykes* are the most common mafic intrusive rocks in the central Kirwanveggen and are best exposed at Swartbandufsa where they occur as 40m wide vertical dykes cross-cutting early fabrics in the *Kvervelnatten Granite Gneiss Complex* (Fig. 3.25). At Tverregga, these thinner (~ 4m wide), more numerous and regularly spaced dykes are deflected into a wide D_3 shear zone (Fig. 3.6). Recent Ar-Ar dating by Jackson (1997) on hornblende separates from these dykes yields two ages, an older Grenvillian age and a younger age of 552 ± 5 Ma. Since the dykes cross-cut both S_1 and S_2 fabrics in the *Kvervelnatten Granite Gneiss Complex* as well as the earliest S_3 fabrics in the *Tverregga Banded Gneiss*, they provide a minimum age for these fabrics and a maximum age for final activation of D_3 shear zones. Petrographically, chlorite + hornblende define a schistose fabric overprinting a recrystallized quartz matrix. Coarse quartz + feldspar veinlets are late and contain abundant calcite. Grains of sphene are scattered throughout and some contain ilmenite cores.

Numerous buff brown coloured porphyritic granite dykes cross-cut the early S_1 and S_2 fabrics in the *Kvervelnatten Granite Gneiss Complex* and are parallel to the regional S_3 fabric within the *Kirwanveggen Megacrystic Orthogneiss Complex*. U-Pb SHRIMP dating of zircons from these dykes yielded an age of ~ 1011 ± 8 Ma (Jackson 1997). The porphyritic texture of these dykes is distinctive but is locally modified by varying degrees of mylonitization or even destroyed by fluid alteration and metasomatism. In thin section, K-feldspar grains occur as porphyroclasts in a recrystallized quartz matrix. The well developed fabric is defined by muscovite, biotite and hornblende alignment. Ilmenite grains are arranged in trails parallel to the fabric and are partially replaced by sphene. Oxides are present in high concentrations.

Felsic dykes which cross-cut the early S_1 and S_2 fabrics in the *Kvervelnatten Granite Gneiss Complex* are only found near the margins of the leucogranite at Tverreggtelen and can be traced into the main body of leucogneiss. These variably altered dykes are interpreted by Jackson (1997) to be apophyses of the *Tverreggtelen Leucogranite Suite*. Alteration of the dykes increases away from the main leucogneiss body where the dykes contain amazonite which imparts a blue-turquoise colour on the rock. At a single outcrop (Fig. 3.21), one of these felsic dykes cross-cuts a porphyritic granite dyke. This relationship confirms the young age of the leucogneiss (~ 990 Ma) relative to the ~ 1011 Ma age of the porphyritic granite dykes. In thin section, a medium-grained quartz matrix contains large (2mm) K-feldspar grains (amazonite) and smaller microcline crystals which exhibit cross-hatch twinning. Late muscovite overprints the matrix and individual grains are aligned so as to define a fabric. Apatite is a relatively abundant accessory phase.

Discordant pegmatite bodies are common within the *Kvervelnatten Granite Gneiss Complex* at Tverreggtelen (Fig. 3.4) where they cross-cut early S_1 and S_2 fabrics. These pegmatite bodies have an irregular shape, are variable in size and comprise very coarse quartz + feldspar (> 5cm) with minor hornblende, biotite and magnetite. U-Pb SHRIMP dating of these bodies by Jackson (1997) provides an age of ~ 1050 Ma suggesting a possible link to the *Kirwanveggen Megacrystic Orthogneiss Complex*.

The youngest dykes in the central Kirwanveggen are the Jurassic dolerite dykes (Fig. 3.26) which intrude the banded gneisses in the main face of Hallgrenskarvet. These dykes represent the youngest rock type exposed in the central Kirwanveggen and cross-cut all other lithologies, entities, veins and fabrics. The doleritic texture is typically hypabyssal and chill margins are well developed away from the contact with the host gneisses.

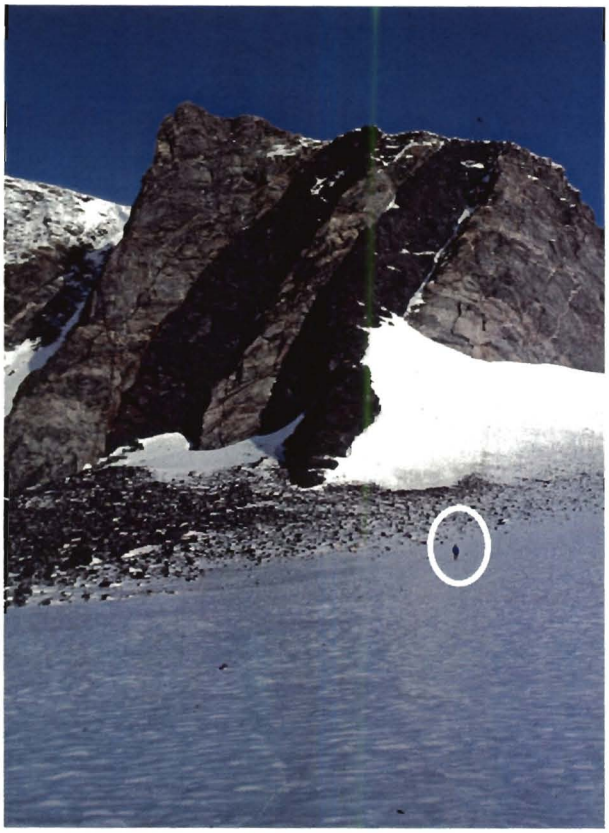

Figure 3.25 *Swartbandufsa Mafic Dykes* intruding gneisses of the *Kvervelnatten Granite Gneiss Complex* at Swartbandufsa in the central Kirwanveggen. The circle indicates a man for scale.

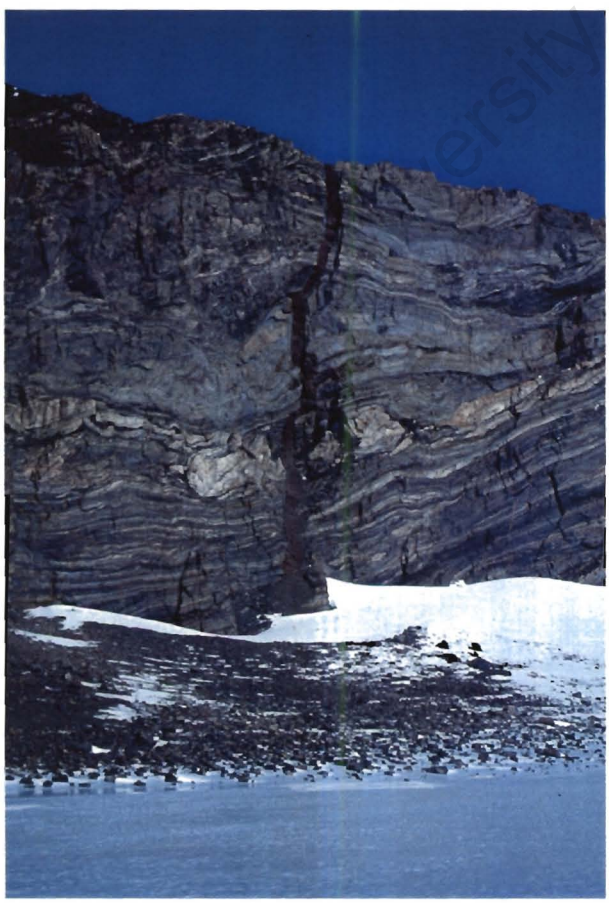

Figure 3.26 A Jurassic dolerite dyke intruding gneisses of the Sverdrupfjella Group at Hallgrenskarvet. The cliff is ~ 350m high for scale.

3.2.9 Veins

Veins are ubiquitous throughout the central Kirwanveggen and attest to the presence of fluids during the evolution of this part of the Maud Belt. The majority of the veins are mono-mineralic quartz while fewer veins contain calcite. Some of the veins show more complex parageneses, such as quartz – chlorite – calcite ± feldspar ± biotite and quartz – hornblende – feldspar ± epidote ± calcite, probably as a result of differences in host rock composition and the metamorphic grade at which the veins were precipitated (Kerrick 1983).

The veins have been classified according to their form and structural disposition in the field as synfolial, boudin-eye and discordant types (Figs. 3.27a, b and c). Synfolial veins regularly indicate a sense of shear whereas boudin-eye veins fill dilational sites within the boudinaged fabric, these two vein types are likely to have been formed by pressure solution processes during fabric development. The discordant veins show a variety of geometrical forms, including irregular vug-filling and crack-filling varieties, as well as tension gash arrays. The process by which these discordant veins form is distinct from that which is responsible for the synfolial veins because they reflect more brittle conditions. The synfolial and boudin-eye vein types precipitated from a fluid phase present during regional fabric development whereas the discordant veins are probably the result of later fluid flow at a shallower crustal level.

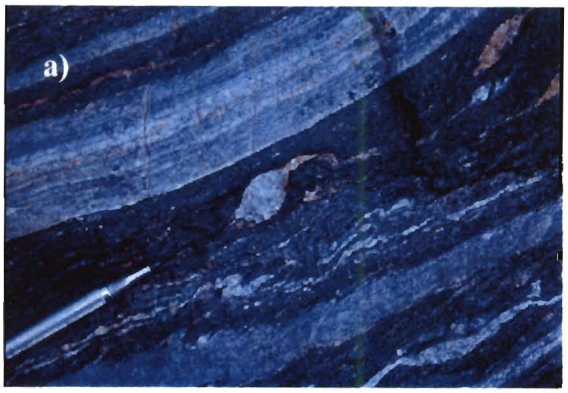

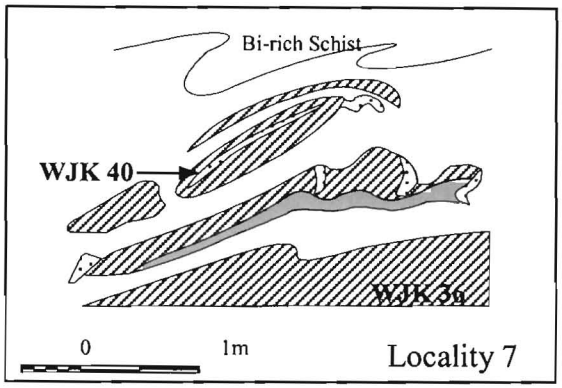

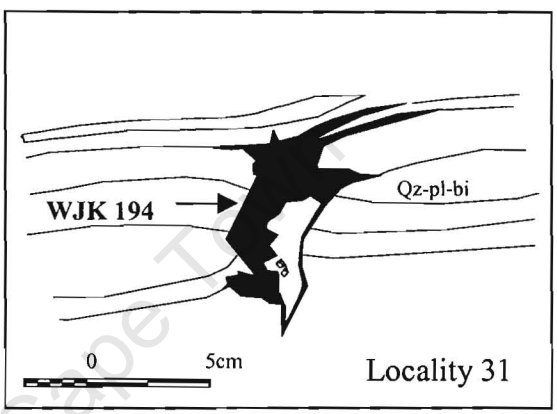

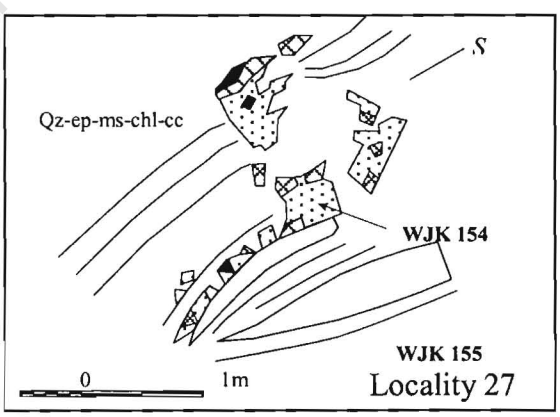

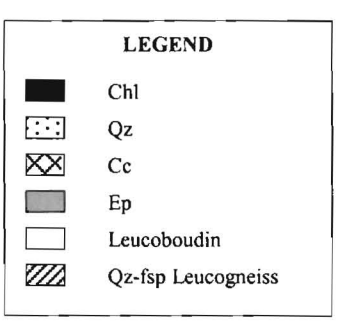

Figure 3.27 Photographs and corresponding field sketches showing the vein types of the central Kirwanveggen: a) synfolial, b) boudin-eye, and, c) discordant. Note that the sketches do not represent the exact locality of the photographs.

CHAPTER FOUR

4. ANALYTICAL METHODS

4.1 INTRODUCTION

Analytical methods typically employed in fluid studies of high-grade metamorphic rocks include: stable isotope geochemistry (especially O, C and H), whole-rock geochemistry, fluid inclusion studies, metamorphic petrology, and, isotope geochronology. The purpose of this chapter is to describe in some detail, the analytical methods employed in this study. The sample preparation procedure and specifications are first described, this is followed by a discussion of XRF and ICP-MS techniques employed for whole-rock geochemistry, finally, the procedure for extraction of O, C and H for stable isotope measurement is described.

4.1.1 Sample material and preparation

For the purposes of this section, the sample material can be broadly categorized into four components namely: felsic gneiss, mafic gneiss, metacarbonate, and, vein material. Felsic and mafic gneissic material was generally used for whole-rock analysis with only a small number of samples selected for mineral separation. Most metacarbonate samples were prepared in a similar manner to that required for whole-rock analysis, except that only the carbonate fraction was analysed. A larger number of metacarbonate samples compared to that of the gneisses, were selected for mineral separation. All vein material was processed in order to obtain the cleanest possible quartz separate for analysis.

All samples were prepared at the University of Cape Town. Hand samples were initially split and then crushed in a jaw-crusher. Special care was taken with the megacrystic augen gneiss samples to ensure that a large enough sample was split and crushed on account of the coarse grain size of this rock type. In the case of whole-rock determinations, crushed host rock material was then pulverised in a sieb mill to produce a powder (< 200#). Venneman & Smith (1990) showed that relatively coarse grain size fractions of up to 120# are acceptable for stable isotope determination using ClF_3 as reagent. In the case of quartz veins and mineral separate preparation , the crushed sample was put through 20#, 40# and 60# sieves. Sieved material was subjected to magnetic separation prior to hand picking under a binocular microscope. Magnetic separation was carried out on a Franz Magnetic Separator at a fixed angle and over a range of susceptibilities from 0.2 to 1.2amps. The pure mineral separates were then powdered to < 200# using a mortar and pestle. Some of the sieved material from quartz vein samples was treated in HF which has the effect of acid-vapour etching any feldspar grains that could not be detected under the microscope. Powdered samples were then dried in an oven at 110°C overnight to remove any excess H_2O.

4.2 WHOLE ROCK ANALYSIS

Major elements were analysed by means of X-ray fluorescence (XRF) spectrometry, whereas trace and rare earth element concentrations were determined using inductively coupled plasma mass spectrometry (ICP-MS). All analyses were performed at the University of Cape Town and analytical methods for XRF are partially described in Duncan *et al.* (1984). Powders used in ICP-MS and to prepare fusion discs for XRF analysis are identical to those used in stable isotope analysis. The sample preparation procedure is described in Section 4.1.1.

4.2.1 Major elements

At the University of Cape Town, facilities are available to prepare "Claisse" fluxy fusion discs according to the following procedure: the powdered sample is weighed in a crucible, dried at 110°C for up to 4 hours and then weighed in order to determine H_2O^-. The sample is roasted overnight at 950°C, cooled and then weighed, at which time the loss on ignition (LOI) is calculated. The sample is mixed with a flux comprising LiT-LiM and a LiBr releasing agent in the ratio of 6g flux to 0.7g sample before being fused into a disc ready for XRF analysis.

Major elements were determined on a Philips PW1480 wavelength dispersive XRF spectrometer according to the procedure and specifications described by Willis (1999). Measurements were made with the dual target Mo/Sc X-ray tube set at 50kV and 50mA. Johnson Matthey Specpure Fe_2O_3 and $CaCO_3$ fusion discs were used as blanks for Si determination, whereas Specpure SiO_2 fusion discs were used for all other major elements. Philips X40 software was used to collect intensity data and corrections were made for background, spectral overlap and matrix effects. Further details of XRF procedures and estimates of detection limits and precision are given by Duncan *et al.* (1984) and le Roex (1985).

4.2.2 Trace elements

Trace and rare earth elements were analysed by means of ICP-MS methods which are described by le Roex *et al.* (2001). A 50mg portion of sample powder was digested using HF and HNO_3 in closed teflon beakers on a hotplate. The digested samples were dissolved in ~ 5% HNO_3 and analysed on a Perkin Elmer / Sciex (Elan 6000) ICP-MS instrument using external calibration standards made from synthetic multi-element standard solutions. The internal standards are 103Rh, 115In, 187Re and 209Bi. The instrument operating conditions were as follows: nebuliser gas flow = 0.86*l*/min; main gas flow = ~ 15*l*/min; auxiliary gas flow = ~ 0.75*l*/min; ICP RF power = 1075watts; autolens settings: 9Be = 6.8V; 59Co = 7.4V; 115In = 8.2V. The instrument sensitivity was 40758cps/ppb for standard 103Rh. These conditions were optimized to minimize oxide formation (CeO/Ce = 0.029) and doubly-charged ion formation (Ba++/Ba = 0.020).

4.3 STABLE ISOTOPE DETERMINATION

Stable isotope ratios of silicates and carbonates were determined on a Finnegan MAT 252 mass spectrometer at the University of Cape Town using CO_2 gas obtained from the silicate line, laser line, carbonate line and hydrogen line. The majority of the analytical data reported in this dissertation were produced at the University of Cape Town, however a small number of the silicate $\delta^{18}O$ values were obtained at Monash University in Melbourne Australia. Stable isotope ratios are expressed in δ-notation defined by $\delta = (R_{sample}/R_{standard}-1)*1000$, where $R = {}^{18}O/{}^{16}O$ or ${}^{13}C/{}^{12}C$ or D/H and units are given in ‰.

4.3.1 Silicates

Oxygen isotope ratios of silicates were obtained by conventional methods using ClF_3 as reagent (Borthwick & Harmon 1982) and are reported in δ-notation. A quartz standard MQ (Murchison Line quartz vein), was analysed in duplicate with each run of 8 samples, the raw values of MQ were then used to recalculate the sample values relative to SMOW (Standard Mean Ocean Water). This was done assuming a value of 10.10‰ for MQ (calibrated using a value of 9.64‰ for NBS-28 as recommended by Coplen *et al.* (1983)). Precision is indicated by the average difference between MQ duplicates, which at the time of this study was 0.13‰ (n = 36; 2σ = 0.14). The extraction of CO_2 from silicates was carried out on the silicate line constructed according to the principles of Clayton & Mayeda (1963) at the University of Cape Town. An aliquot (9 - 11mg) of each sample was loaded into nickel reaction vessels and then heated to 200°C for a period of 3 hours. After cooling for 1 hour, ClF_3 was introduced into the vessels and reacted with the sample at 550°C for 5 hours. During this process, O_2 was liberated from the silicate samples according to the reaction:

$$3SiO_2 + 4\,ClF_3 \rightleftharpoons 3SiF_4 + 2Cl_2 + 3O_2 \qquad (4.1)$$

Oxygen (O_2) was then converted to CO_2 by reaction with heated graphite:

$$C + O \rightleftharpoons CO_2 \qquad (4.2)$$

The CO_2 yield was then measured and the gas trapped in glass bottles or tubes to complete the extraction process. All measured yields were higher than the 95% required for accurate stable isotope measurement (Venneman & Smith 1990). Further details of the methods used for the

extraction of oxygen from silicates at the University of Cape Town are given by Venneman & Smith (1990) and Harris & Erlank (1992). Oxygen was extracted from diopside and garnet separates using a laser microprobe attached to a flourination vacuum line built according to the principles of Sharp (1990) at the University of Cape Town. In this procedure, as many as 30 single mineral grains weighing between 1mg and 2mg are placed in a grooved sample holder made of Ni which is heated to 110°C and loaded into a reaction chamber. The laser is then focussed onto the sample which reacts in the presence of 15kPa ClF_3. Purified O_2 is converted to CO_2 and the yield measured before being stored in 'break-seal tubes". Further details of this procedure are described by Harris *et al.* (2000).

4.3.2 Carbonates

Carbon and oxygen isotope ratios of calcite were obtained by reaction with phosphoric acid according to the method of McCrea (1950). A fractionation factor of 1.01025 was used to correct the $\delta^{18}O$ value of the acid liberated CO_2 to that of calcite (Martinez *et al.* 1996). The $\delta^{18}O$ and $\delta^{13}C$ values are reported with respect to SMOW and PDB (Pee Dee Belemnite) reference standards, respectively, to which they were calibrated using an internal carbonate standard calibrated using NBS-19 ($\delta^{18}O$ = 28.64‰; $\delta^{13}C$ = 1.95‰). The extraction of CO_2 from carbonates was carried out on the carbonate line at the University of Cape Town. Approximately 1g of carbonate-bearing silicate material was reacted with 100% phosphoric acid at 25°C overnight in an acid bath:

$$3CaCO_3 + 2H_3PO_4 \rightarrow 3CO_2 + 3H_2O + Ca_3(PO_4)_2 \qquad (4.3)$$

The CO_2 generated during this process is continuously removed.

4.3.3 Hydrogen / Deuterium

Hydrogen / Deuterium isotope ratios of silicates were obtained according to the principles of Coleman *et al.* (1982). Two silicate standards (CGbi: Cape Granite biotite; δD = -59‰) were analysed with each run of 8 samples. Two water standards (CTMP: Cape Town millipore water; δD = -9‰) were also run in order to check for drift in the reference gas. The δD values were calibrated to the SMOW scale using the equations given in Coplen (1993), which incorporate the SMOW / SLAP (Standard Light Antarctic Precipitate) normalization based on the last time SMOW and SLAP were analysed. The data were then shifted so that the internal water standard (CTMP) gave the accepted value of -9‰. At the time of this study, accuracy and precision are indicated by Cgbi, which gave an average δD value of –57‰ ($n = 9$, $1\sigma = 1.7$).

The extraction of hydrogen from silicates was carried out on the hydrogen line constructed according to the principles of Venneman & O'Neil (1993) at the University of Cape Town. The 100g sample was loaded into a quartz tube, covered by pre-roasted quartz wool and then heated in a resistance furnace. The sample was heated incrementally e.g. at 300°C, then at 500°C and then at 600°C for 5 minutes each. A propanol-liquid nitrogen substance was used to separate H_2O and CO_2 in the sample which was then collected in glass tubes containing Zn shavings. The tubes were subsequently heated to 480°C and hydrogen was extracted according to the reaction:

$$H_2O + Zn \rightleftharpoons ZnO + H_2 \qquad (4.4)$$

CHAPTER FIVE

5. WHOLE ROCK COMPOSITION

5.1 INTRODUCTION

The application of whole-rock geochemistry to the study of metamorphic terranes is important in determining the protolith of metamorphosed rocks and can be used to quantify fluid alteration by establishing major element losses and gains associated with metasomatism e.g. Cartwright & Buick (1999). In the Maud Belt, Knoper (1995) suggested that the protoliths of the early gneisses such as the *Kvervelnatten Granite Gneiss Complex*, the *Tverregga Banded Gneiss* and the *Mjöllföykje Banded Gneiss*, were reworked supracrustal rocks. These gneisses are interpreted as being volcanic in origin (Krynauw 1996), and were intruded by granitic rocks such as the *Kirwanveggen Megacrystic Orthogneiss Complex* and the *Tverreggtelen Leucogranite Suite* during Mesoproterozoic orogeny (Knoper 1995).

In this study, whole-rock geochemistry has been performed on a small sub-suite of samples of the granite gneiss, retrogressed banded gneiss, banded gneiss, augen gneiss, leucogneiss and felsic dykes of the central Kirwanveggen. The principle aim of this chapter is to present the whole-rock chemistry of each rock type as an adjunct to the rock descriptions presented in Chapter Three. The whole-rock composition of the rocks is then discussed with respect to the nature of the protolith, metamorphism and fluid alteration as a lead up to Chapter Six, which investigates fluid-rock interaction by means of stable isotope geochemistry. The compositions presented here give an indication of the protolith compositions of these rocks, e.g. S or I-Type in the case of the orthogneisses, and allow an estimation of the original $\delta^{18}O$ values.

Table 5.1 Whole-rock analyses of samples of the major rock types of the Sverdrupfjella Group in the central Kirwanveggen.

Sample	WJK 224	WJK 155	WJK 156	WJK 159	WJK 160	WJK 36	WJK 3	WJK 12	WJK 21	WJK 278	CJK 146	WJK 2
Rock Type	GG	BG(R)	BG(R)	BG	BG	BG	AG	AG	LG	LG	LG	Aplite
Wt %												
SiO_2	57.97	60.88	80.08	67.52	70.60	75.43	68.90	57.52	72.14	75.73	77.34	73.73
TiO_2	0.74	0.50	0.15	0.41	0.32	0.05	0.65	1.88	0.35	0.04	0.05	0.21
Al_2O_3	17.19	10.67	9.64	13.18	14.29	13.74	14.06	13.82	13.52	12.54	13.09	13.81
Fe_2O_3T*	6.78	5.90	1.69	5.54	2.78	0.87	3.96	10.11	4.07	1.78	1.06	2.06
MnO	0.12	0.16	0.02	0.10	0.04	0.01	0.06	0.16	0.03	0.04	0.03	0.03
MgO	2.74	3.94	1.31	2.07	0.61	0.09	0.76	2.23	0.10	0.04	0.02	0.28
CaO	5.85	13.41	0.33	4.22	2.15	0.59	2.02	4.75	0.80	0.90	0.78	1.00
Na_2O	4.29	0.00	1.94	3.35	4.58	4.67	3.53	3.15	4.45	3.66	3.96	3.53
K_2O	1.82	0.09	4.08	1.96	2.50	4.23	5.18	3.82	4.55	4.54	3.85	5.70
$Na_2O+ K_2O$	6.11	0.09	6.02	5.31	7.08	8.90	8.71	6.97	9.00	8.20	7.81	9.23
P_2O_5	0.29	0.27	0.08	0.28	0.11	0.01	0.22	0.91	0.06	0.00	0.00	0.05
SO_3	0.04	0.17	0.08	0.06	0.05	0.02	0.03	0.05	0.02	0.03	0.02	0.02
H_2O-	0.02	0.07	0.08	0.63	0.03	0.09	0.09	0.10	0.06	0.02	0.01	0.07
LOI	0.71	3.49	0.86	0.78	0.41	0.31	0.22	0.53	0.23	0.66	0.66	0.16
Al-index	0.87	0.44	1.18	0.86	1.01	1.03	0.93	0.77	0.99	1.00	1.08	1.00
Total	98.56	99.54	100.34	100.09	98.46	100.09	99.66	99.01	100.36	99.99	100.88	100.64
ppm												
Li	NA	NA	NA	NA	NA	1	11	18	4	NA	12	8
Sc	13	11	2	11	3	1	7	20	5	1	2	3
V	68	198	11	52	15	8	39	99	8	1	1	15
Cr	12	49	27	11	7	11	17	18	10	6	35	16
Co	17	13	4	12	3	1	6	17	1	0	0	2
Ni	12	109	16	13	6	4	8	12	4	5	1	6
Cu	33	6	3	21	8	7	10	19	7	3	1	4
Rb	49	2	100	35	34	90	108	98	84	262	216	164
Sr	894	1162	33	397	328	69	184	279	61	15	42	85
Y	16	34	18	14	11	6	42	99	57	188	119	22
Zr	18	111	48	9	111	55	98	117	318	143	104	181
Nb	8.7	9.3	2.1	6.5	15.6	3.8	18.5	38.5	20.6	93.4	57.3	13.8
Cs	0.7	0.0	1.7	0.5	0.3	0.1	1.1	0.4	0.2	2.0	0.6	1.1
Ba	950.9	38.9	622.6	738.1	1803.3	199.3	1321.3	1241.6	808.8	48.0	142.0	538.6
La	48.0	116.5	58.2	114.0	150.1	43.8	112.6	280.6	168.2	138.1	55.2	73.7
Ce	82.2	94.2	42.8	106.6	109.2	41.1	125.5	300.4	158.3	135.7	51.2	109.8
Pr	43.6	73.4	35.5	60.9	83.1	32.5	97.9	259.8	116.6	127.5	44.1	49.5
Nd	37.5	59.0	27.9	42.6	56.5	26.2	84.2	233.3	94.7	109.6	38.9	37.2
Sm	24.9	36.8	18.0	24.6	27.7	18.0	57.8	151.2	62.9	107.2	44.8	26.2
Eu	21.1	19.9	12.2	16.7	18.1	6.0	32.1	64.1	13.4	11.3	10.6	8.9
Gd	14.9	26.0	14.5	14.9	12.9	9.4	37.5	104.2	44.3	97.1	49.4	18.0
Tb	11.9	22.8	13.5	12.5	10.2	6.3	33.8	88.2	41.0	105.4	57.0	17.3
Dy	10.2	21.0	12.7	11.0	8.9	4.8	31.0	77.6	38.5	108.4	59.8	15.9
Ho	8.7	19.4	11.3	9.7	7.7	4.1	27.2	66.6	35.7	103.2	59.3	14.0
Er	8.2	19.8	10.7	9.4	7.3	3.9	26.8	63.5	36.9	109.5	68.0	14.1
Tm	7.7	19.0	9.5	8.9	7.0	3.7	23.8	55.5	34.9	109.6	76.2	13.5
Yb	7.7	19.2	9.1	8.6	6.9	3.8	22.4	51.7	35.1	112.8	87.3	13.7
Lu	7.5	19.3	8.8	8.4	6.6	4.2	21.2	48.7	34.2	110.3	95.2	13.3
Hf	0.5	3.0	1.4	0.3	2.7	2.6	2.6	3.0	8.6	7.6	6.7	5.6
Ta	0.5	0.6	0.1	0.3	0.9	0.1	0.7	1.6	1.3	4.6	7.4	1.1
Pb	11.7	10.5	9.2	10.6	14.3	10.0	16.6	14.1	6.3	69.0	76.0	22.0
Th	2.7	8.8	3.9	8.2	7.8	26.6	2.6	2.8	7.3	40.1	20.6	24.0
U	0.7	12.1	0.5	1.0	0.6	10.6	0.9	1.0	2.4	23.5	20.9	2.1

GG granite gneiss; BG(R) banded gneiss (retrograde assemblages); BG banded gneiss; AG augen gneiss; LG leucogneiss. All major elements analysed by XRF and all trace elements analysed by ICP-MS. Rare earth element data are normalized to chondrite; data from Sun and McDonough (1989). All samples analysed to 100% loss free; Fe_2O_3T* is total Fe expressed as Fe_2O_3; NA = not analysed; LOI = loss on ignition at 1000°C. The Al-index was calculated as $(Al_2O_3 / 101.94) / ((Na_2O / 61.98) + (K_2O / 94.20) + (CaO / 56.08))$.

5.2 RESULTS

Major and trace element (including rare earth element) analyses are presented in Table 5.1. Selected major element concentrations are plotted against SiO_2 content in Figure 5.1 and against $Na_2O + K_2O$ in Figure 5.4, the compositions of relevant metamorphic minerals are also shown in these diagrams. Trace elements are plotted against Zr in Figure 5.2 and rare earth element (REE) data are presented on a chondrite normalized plot in Figure 5.3.

5.2.1 Major elements

The variation of major element oxides with SiO_2 is presented in Figure 5.1. The SiO_2 content of the central Kirwanveggen gneisses varies substantially (57.52wt.% to 80.08wt.%) and major element oxides also have a large range e.g. ~ 10wt.% for Al_2O_3, $Na_2O + K_2O$, Fe_2O_3 and CaO. In the major element variation diagrams, Fe_2O_3 and CaO show negative correlations with silica for all samples except WJK 155 which has an anomalously high CaO concentration. Both Al_2O_3 and $Na_2O + K_2O$ show no obvious correlation with silica. The $Na_2O + K_2O$ concentration shows a restricted range for all silica concentrations, again with the exception of WJK 155, similarly, the range of Al_2O_3 is restricted for all silica concentrations if granite gneiss (high Al_2O_3) and retrogressed banded gneiss (low Al_2O_3) samples are ignored. In general, the pairs of retrogressed banded gneiss and augen gneiss samples are very different whereas banded gneiss and leucogneiss samples are very similar and show good grouping for all variables plotted against silica.

A single sample from the *Kvervelnatten Granite Gneiss Complex*, WJK 224, was analysed. This rock type has been described in Section 3.2.1 and is essentially a quartzofeldspathic

gneiss with significant hornblende and biotite content. Major element analysis indicates very low SiO_2 content with anomalously high TiO_2, Al_2O_3, Fe_2O_3 and elevated MnO, MgO, CaO and Na_2O.

Two samples of retrogressed banded gneiss, WJK 155 and WJK 156 were analysed. These samples represent different types of variably retrogressed banded gneiss from the *Tverregga Banded Gneiss* at Tverregga. There is a substantial difference in SiO_2 content between the samples analysed e.g. 60.88wt.% and 80.08wt.%. Sample WJK 155 is an epidote- and chlorite-rich rock sample which has low SiO_2 and K_2O in contrast to elevated MgO, CaO and SO_3. In contrast, WJK 156 is a quartz- and K-feldspar-rich rock with extremely high SiO_2 content. This sample has slightly lower Al_2O_3 and Na_2O and is depleted in CaO relative to other banded gneisses, granite gneiss, augen gneiss and leucogneiss.

Three samples of banded gneiss, two from Tverregga and one from Hallgrenskarvet were analysed. For this rock type the major oxides Fe_2O_3 and CaO show negative correlations with silica whereas alkalis show a positive correlation with silica. The typical melanocratic and leucocratic banding of the banded gneiss is represented by WJK 159 and WJK 160 respectively. Although these samples are from the *Tverregga Banded Gneiss* at Tverregga, an area which is characterised by almost pervasive retrogression, there is little petrographic evidence for significant retrogression in WJK 159 and WJK 160 such as that observed in WJK 155 and WJK 156. These samples both have high silica (~ 70wt.%), alumina (~ 14wt.%) and Na_2O content in contrast to low K_2O. The melanocratic sample has slightly lower alumina, K_2O and Na_2O content. Sample WJK 36 represents the leucocratic component of the banded gneiss in the *Mjöllföykje Banded Gneiss* at Hallgrenskarvet. This sample has high silica and alumina, elevated K_2O and Na_2O content and low Fe_2O_3, MnO and SO_3.

Two samples of augen gneiss WJK 3 and WJK 12 were analysed. Sample WJK 12 has a very low silica content (< 60wt.%), which is similar to that of the granite gneiss and contains high concentrations of TiO_2, Fe_2O_3, MnO and P_2O_5 relative to other gneisses of the central Kirwanveggen. Sample WJK 3 has a higher silica content (~ 70wt%.) as well as elevated alumina, Na_2O and K_2O, similar to that of the leucocratic banded gneisses and the leucogneisses of the central Kirwanveggen. A single aplite dyke was analysed (WJK 2). This sample is typical of the numerous felsic dykes which cross-cut the *Kirwanveggen Megacrystic Orthogneiss Complex* throughout the central Kirwanveggen (Fig. 6.11a). In comparison to the host augen gneiss, the aplite is silica-rich with relatively low concentrations of TiO_2 and CaO. The aplite also has significantly lower Fe_2O_3 and MgO and slightly lower MnO, P_2O_5 and SO_3 concentrations than that of the augen gneiss.

Three samples of leucogneiss, two from Tverreggtelen (WJK 278 and CJK 146) and one from Hallgrenskarvet (WJK 21) were analysed. These samples have a restricted range of major element concentrations and show a negative correlation with Fe_2O_3, alkalis and CaO. The silica content of the three samples is constant (72.14wt.% to 77.34wt.%) and all leucogneiss samples are aluminous (average Al-index = 1.02), have high K_2O and low MnO, MgO, CaO, SO_3 and P_2O_5. The leucogneiss sample from Hallgrenskarvet has slightly elevated TiO_2 and Fe_2O_3 and lower MgO values than those of the Tverreggtelen samples.

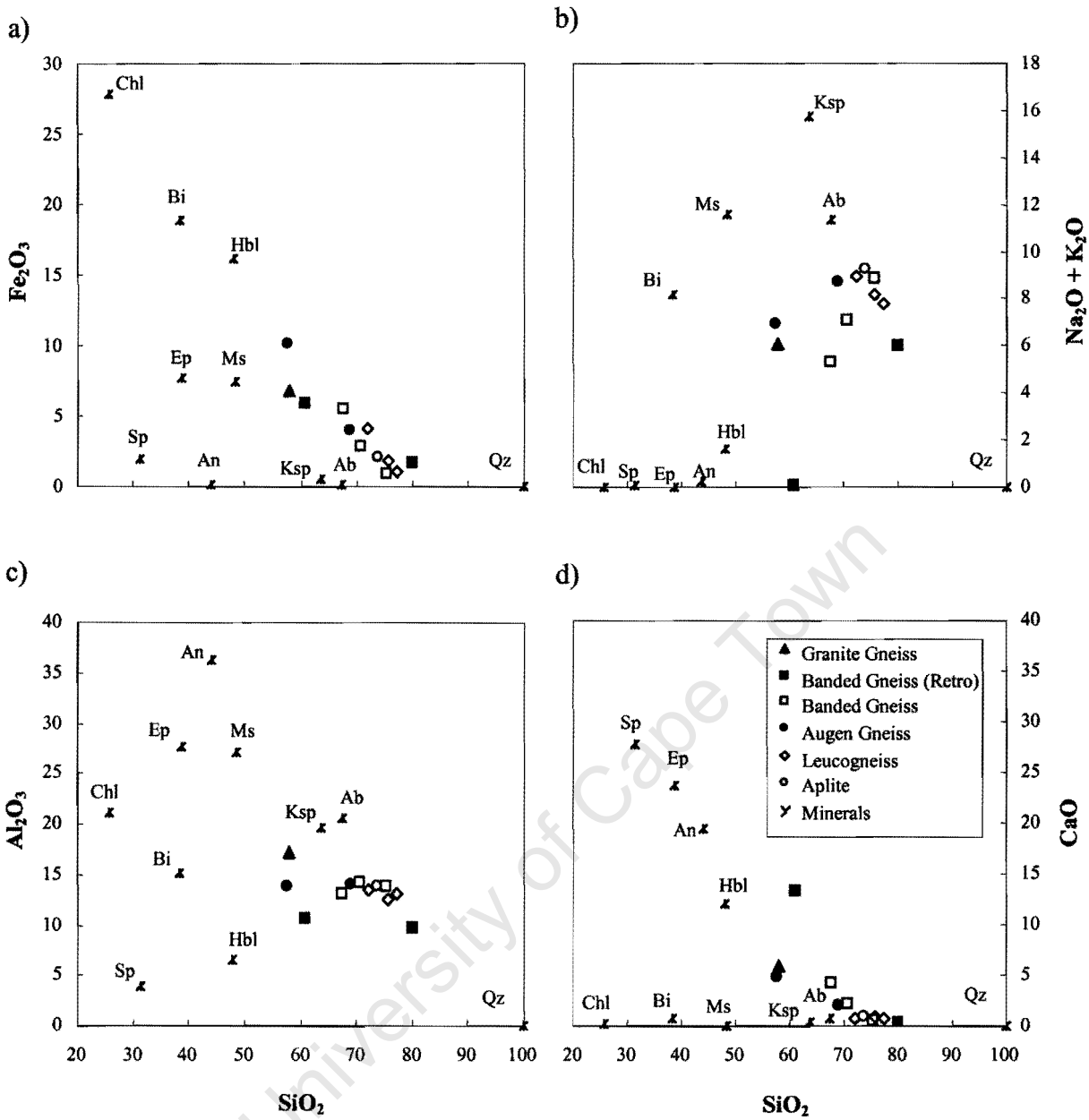

Figure 5.1 Major oxides plotted against SiO_2 for the gneisses of the central Kirwanveggen. Metamorphic mineral compositions are taken from Deer *et al.* (1992), abbreviations are described in APPENDIX C. For all minerals, total Fe is expressed as Fe_2O_3.

5.2.2 Trace elements

The variation of SiO_2 and selected trace elements with Zr for all the gneisses is shown in Figure 5.2. Trace elements are plotted against Zr because this element is one of the more abundant trace elements and shows a large variation in composition, furthermore, according to (Erlank & Kable 1976), of all the elements, Zr is the least likely to have been affected by alteration. For all rock types excluding the leucogneiss, there is no correlation between SiO_2 and Zr. For leucogneiss, the SiO_2 exhibits a weak negative correlation with Zr which has a large range from 104ppm to 318ppm, the anomalously high Zr concentration is present in WJK 21. Leucogneiss shows the same large range of Zr values for a restricted range of Sr values, but Sr shows no apparent correlation with Zr. In the case of the Y and Nb content of leucogneiss (Fig. 5.2b and c), there is a large range of Zr/Y ratios and Zr/Nb ratios. The Y and Nb concentration of the granite gneiss and the banded gneisses is very low (Y < 40ppm; Nb < 18ppm) relative to the orthogneisses e.g. augen gneiss and leucogneiss.

5.2.3 Rare earth elements

Rare earth element data of the gneisses of the central Kirwanveggen are shown on Figure 5.3. All the gneisses show weak light rare earth element (LREE) enrichment and variable negative Eu anomalies. Felsic orthogneisses, especially augen gneiss, have higher total REE content than the banded gneisses and granite gneiss. Leucogneiss samples, especially WJK 278, show distinctive negative Eu anomalies relative to the other gneisses. Most gneiss samples show different concentrations but remarkably similar patterns of heavy rare earth elements (HREE) on a chondrite normalized diagram. Sample WJK 36 shows a variable HREE concentration whereas CJK 146 shows a HREE enrichment and WJK 12 shows HREE depletion.

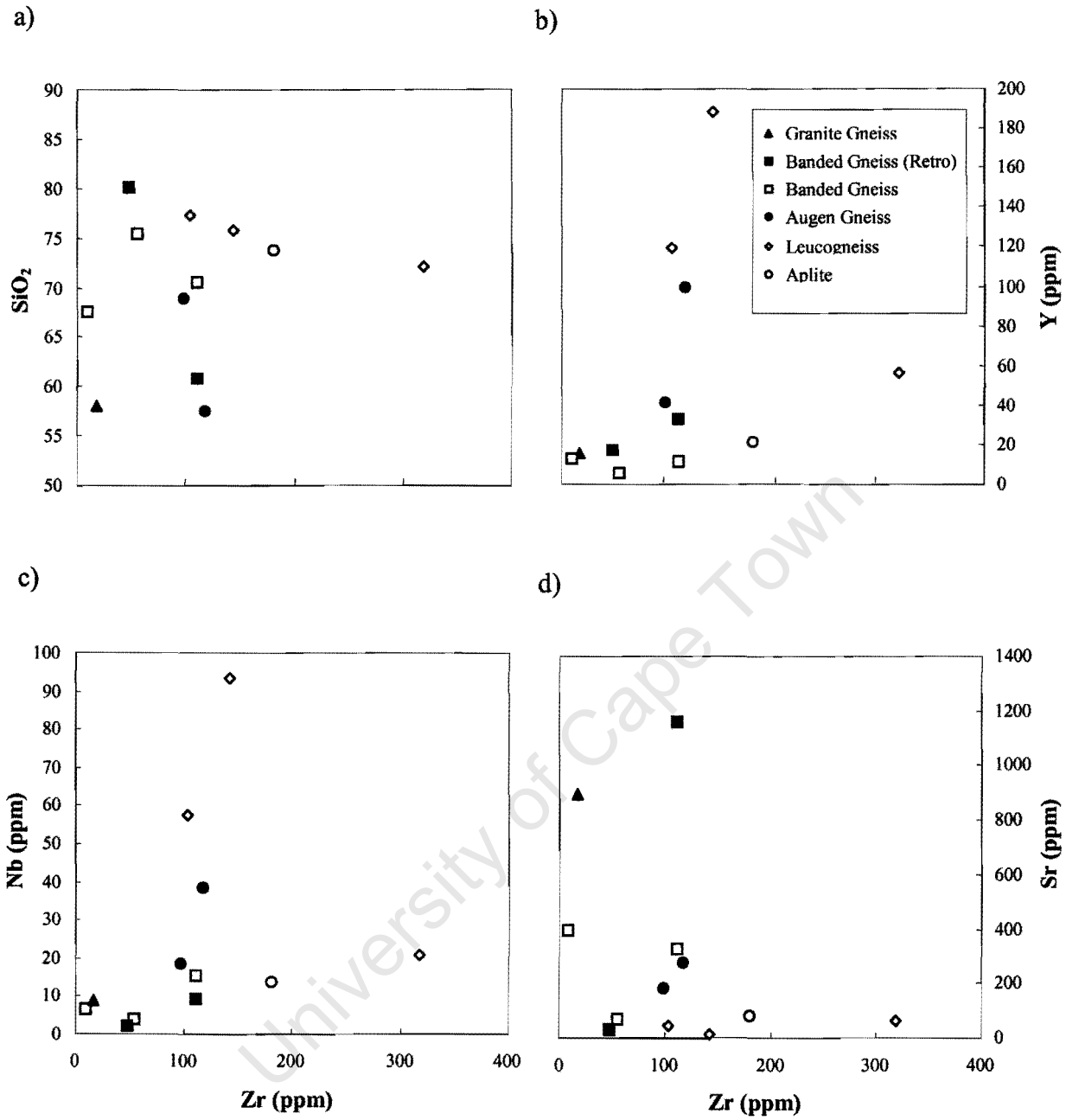

Figure 5.2 Selected trace elements and SiO_2 plotted against Zr for the gneisses of the central Kirwanveggen.

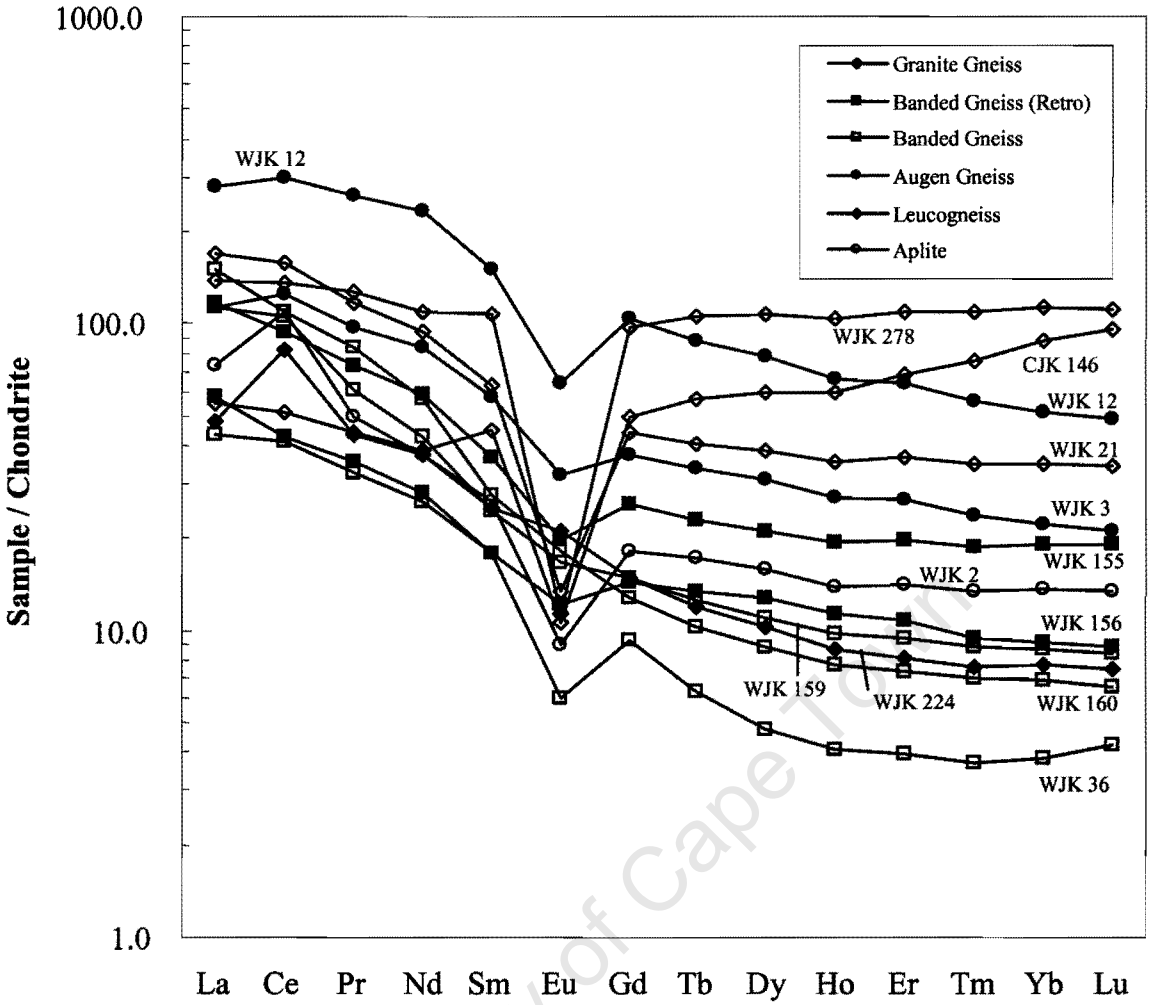

Figure 5.3 Rare earth element profiles for the gneisses of the central Kirwanveggen, data are normalized to chondrite using data from Sun & McDonough (1989).

5.3 DISCUSSION

The causes of chemical variability observed in the gneisses of the central Kirwanveggen are discussed below in terms of a) protolith composition, b) metamorphic composition and c) retrogression and fluid alteration.

5.3.1 Protolith composition

Groenewald *et al.* (1995) have conducted whole-rock geochemical studies on samples from the H. U. Sverdrupfjella in order to determine the likely precursor rocks of the Sverdrupfjella Group in that area (Section 2.2.1). These authors recognize volcanic, granitic and sedimentary protoliths for the lithostratigraphic units of the H. U. Sverdrupfjella. In the central Kirwanveggen, Knoper (1995) demonstrates that the trace element distributions of the early gneisses e.g. the granite gneisses and banded gneisses, indicate that these rocks result from the crystallization of either mantle-derived melts or melting of arc-derived crustal rocks. He also cites Nb depletion and LILE enrichment as being inherited from the source. In this study, major, trace and rare earth element data distinguishes these early gneisses from the younger orthogneisses of the central Kirwanveggen. The SiO_2 content of the granite gneiss is substantially lower than that of the felsic orthogneisses such as the augen gneiss and leucogneiss. Trace element concentration, especially Y and Nb of the granite gneiss and the banded gneisses is very low (Y < 40ppm; Nb < 18ppm) relative to the orthogneisses, the same is true for REE content. These data suggest a very different protolith composition for the *Kvervelnatten Granite Gneiss Complex*, the *Mjöllföykje Banded Gneiss* and the *Tverregga Banded Gneiss* as opposed to the *Kirwanveggen Megacrystic Orthogneiss Complex* and the *Tverreggtelen Leucogranite Suite* of the central Kirwanveggen. The volume of whole-rock data presented in Table 5.1 is not sufficient to allow classification of precursor rock types as, for example, basalt or andesite. However, this study supports previous studies which infer a volcanic origin for the early banded gneisses and an intrusive origin for the younger orthogneisses of the central Kirwanveggen (Grantham 1992; Grantham *et al.* 1995*b*; Groenewald *et al.* 1995; Krynauw 1996).

There is abundant field evidence which points to an igneous parentage for the *Kirwanveggen Megacrystic Orthogneiss Complex* and the *Tverreggtelen Leucogranite Suite* such as preserved igneous textures, mafic xenoliths and intrusive contact relationships. In the case of augen gneiss, Knoper (1995) reports Fe-enrichment similar to that observed in WJK 12 and proposes either reworked crustal rocks or thinned lithospheric mantle as possible sources for this rock type. In this study, the consistency of the silica content of the three leucogneiss samples reflects the homogenous nature of this rock type described in Section 3.2.6, and the SiO_2 values of around 75wt.% are consistent with a granitic protolith. Moreover, the relatively high Al-index (0.99 – 1.08) indicates an S-Type affinity for the *Tverreggtelen Leucogranite Suite* which is of regional significance because similar S-Type leucogranites have been identified in the H. U. Sverdrupfjella by Groenewald *et al.* (1995). One of the leucogneiss samples (WJK 21) has a very high Zr/Y and Zr/Nb ratio compared to the other leucogneisses and could indicate multiple sources for this meta-igneous rock. The negative Eu anomaly in all of the gneisses except the granite gneiss and two of the banded gneiss samples (WJK 159 and WJK 160), indicates plagioclase fractionation at some stage during the evolution of these rocks. This effect is most pronounced in the plagioclase-rich leucogneiss samples which have large negative Eu anomalies (Fig. 5.3).

5.3.2 Metamorphic composition

In the central Kirwanveggen, amphibolite facies mineral assemblages record the peak metamorphic conditions during the Mesoproterozoic Maud Orogeny at between 1200 Ma and 900 Ma. Subsequent retrogression has modified these assemblages to greenschist facies locally. The variable mineral assemblages of the central Kirwanveggen gneisses highlights the large number of different rock types which make up the Sverdrupfjella Group in this area

(Chapter Three). This feature is reflected in the wide range of SiO_2 of the 12 samples analysed in this study (Table 5.1 and Fig. 5.1). For almost all samples, silica shows a negative correlation with Fe_2O_3 and CaO (Fig. 5.1a and d), such correlations indicate that at least some of the gneisses are genetically related and that differences in whole-rock chemistry are due to differences in modal mineralogy. The following discussion considers the whole-rock geochemical data in Table 5.1 with respect to the metamorphic mineral assemblage of each rock type, the retrogressed banded gneiss samples are discussed in Section 5.3.3. Metamorphic mineral compositions are plotted on the major element diagrams (Figs. 5.1 and 5.4) in order to give an indication of the modal mineralogy of the analysed rocks. The mineral data has been sourced from Deer *et al.* (1992) and the choice of compositions is based, in each case, on the sample description which most closely resembles that of the rocks analysed in this study (Chapter Three & APPENDIX C). For the feldspars, the K-feldspar composition is of a microcline in charnokite at St Thomas' Mt Madras in India, anorthite is from a calc silicate rock in the Sittampundi complex also in India, and the albite composition is from an amphibolite containing quartz and sphene in Val Devero, Italy. For the micas, biotite composition is from a granulite facies gneiss at Warriup Hill in south Western Australia and the muscovite is from a low-grade psammitic schist at Inverness-shire in Scotland. For the mafic minerals, hornblende composition is from granodiorite of the Central Sierra Nevada Batholith in California, epidote is from anorthosite at Sittampundi in Madras, India. Sphene is grothite in pumpellyite-actinolite facies schists of the Taveyanne Formation in Valais, Switzerland, and chlorite is from a chlorite-epidote-albite schist at Limebury Point in South Devon.

The SiO_2 content of WJK 224 (57.97wt.%) is in fact too low for a granite gneiss (~70wt.%) and is more consistent with a dioritic composition (~60wt.%). The high Fe_2O_3 and elevated

MgO contents reflect the mafic mineral e.g. hornblende, biotite, epidote and chlorite content of this rock. Elevated CaO reflects both hornblende and plagioclase. High Al_2O_3 is consistent with the K-feldspar-rich nature of this rock but the SiO_2 content is surprisingly low probably on account of the biotite content. The chemical composition of WJK 224 raises an interesting question, because this sample is considered to be representative of the *Kvervelnatten Granite Gneiss Complex* at Tverreggtelen. Comparison of WJK 224 with preliminary whole-rock data of granite gneiss samples collected from the type area at Kvervelnatten itself, indicates that these are not the same rock type and that the *Kvervelnatten Granite Gneiss Complex* at Tverreggtelen includes rocks with a dioritic composition.

The leucocratic and melanocratic components of the banded gneiss (WJK 160 and WJK 159) have remarkably similar major element compositions despite their contrasting appearance in the field. Both samples have high silica (~ 70wt.%) and quartz is the dominant rock forming mineral, whereas the contrasting modal proportions of other minerals in each rock, is highlighted by the Fe_2O_3, CaO and Na_2O concentrations. The difference in major oxide concentrations is a function of the epidote and hornblende content of the melanocratic sample, and the K-feldspar and plagioclase content of the leucocratic sample. Similarly, the negative correlation of Fe_2O_3 and CaO with silica of all gneisses (Fig. 5.1), reflects the increased modal proportion of hornblende, biotite, epidote and chlorite in the melanocratic gneisses at the expense of quartz and feldspar. This argument is strengthened by the slightly lower alumina, K_2O and Na_2O content of the melanocratic sample compared to that of the leucocratic sample, as a consequence of the relative paucity of feldspar in this sample. The generally low K_2O (~ 2wt.%) content of both banded gneiss samples is surprising given the high biotite and K-feldspar content of these rocks. The high silica and alumina as well as the elevated K_2O and Na_2O content of the leucocratic banded gneiss sample from Hallgrenskarvet (WJK 36) reflects

the high proportion of K-feldspar and albite, the absence of biotite and the paucity of mafic minerals in this rock compared to the banded gneisses from Tverregga.

The major, trace and rare earth element plots (Figs. 5.1, 5.2 and 5.3) all highlight the compositional disparity between the two augen gneiss samples (WJK 3 and WJK 12) analysed in this study. The very low SiO_2 (~ 57.52wt.%) content of WJK 12 is surprising given that this sample is representative of typical quartz – K-feldspar-rich augen gneiss. Furthermore, sample WJK 12 has a distinctive REE pattern (Fig. 5.3) compared to other gneisses of the central Kirwanveggen. The low silica content of this sample is balanced out by the high concentration of Fe_2O_3 and TiO_2 and could be a function of the relatively high proportion of biotite, and to a lesser degree, sphene in the augen gneiss. Sample WJK 3 contains a high proportion of quartz + feldspar migmatitic material which is reflected in the high silica content of this sample relative to WJK 12. The elevated alumina, Na_2O and K_2O in WJK 3 is related to the presence of K-feldspar and alkali feldspar which are the dominant minerals in the augen gneiss, the K-feldspar is both primary (megacrysts) and secondary (migmatite). The disparate data of WJK 3 and WJK 12 are not consistent with the regionally homogenous character of the augen gneiss described in Chapter Three. The disparity is a result of the anomalous nature of the major and rare earth element geochemistry of WJK 12, which indicates that this sample has suffered geochemical modification through contamination or alteration. The relatively high SiO_2 content of the aplite dyke is a function of the high quartz content and low mafic mineral content of this rock compared to that of the K-feldspar dominated augen gneiss host. This is emphasized in the low Fe_2O_3 and CaO concentrations in the aplite which define negative correlations with silica if combined with the augen gneiss samples (Fig. 5.1a and d). The paucity of sphene in the aplite as compared to the high concentration of this mineral in the augen gneiss could be responsible for the relatively low concentration of TiO_2. However,

sphene is not necessarily the main TiO_2 and CaO bearing phase in the augen gneiss, and the very low CaO content, at least, could be attributed to the absence of plagioclase in the aplite.

Of all the samples analysed, the leucogneisses show the most restricted range of major element concentrations, which is in keeping with the homogenous nature of the *Tverreggtelen Leucogranite Suite*. The relatively high concentration of K_2O in the leucogneiss samples is a function of the K-feldspar, biotite and muscovite content of the leucogneiss whereas the low MgO and CaO reflect the paucity of mafic minerals such as hornblende, epidote and sphene. The low CaO content of WJK 21 is surprising because this is a plagioclase-rich rock. Minor differences in modal mineralogy between the leucogneiss sample from Hallgrenskarvet and those from Tverreggtelen are responsible for the observed differences in TiO_2, Fe_2O_3 and MgO contents. The leucogneiss at Hallgrenskarvet (WJK 21) contains hornblende, sphene and oxides as accessory phases which is evident in the slightly elevated TiO_2 and Fe_2O_3 content of this sample relative to leucogneisses at Tverreggtelen (CJK 146 and WJK 278). Similarly, the elevated level of MgO in WJK 278 could be related to accessory diopside.

5.3.3 Retrogression and fluid alteration

Metamorphism and associated fluid-rock interaction following peak conditions in the central Kirwanveggen is responsible for hydrous retrograde assemblages characterised by biotite, chlorite and epidote (Section 3.2.3). These rocks form part of the *Tverregga Banded Gneiss* package which according to Knoper (1995) were originally reworked supracrustal rocks and which are interpreted as being volcanic in origin (Krynauw 1996). The compositional variation of such a protolith is likely to have been large, and subsequent metamorphism with associated retrogression and alteration would have had the effect of increasing the

geochemical variability. Studies of metasomatism typically make use of whole-rock geochemical analyses to establish the losses and gains of major elements during fluid alteration (Grant 1986; Ferry & Dipple 1991; Cartwright & Buick 1999). This approach requires comparison of the altered rock with a least-altered equivalent and the choice of a best fit line or isocon corresponding to a zero change in concentration (Grant 1986). The small number of samples analysed in this study does not allow for such a calculation, but similar conclusions can be drawn from a simple comparison of the major element composition of altered rocks versus their unaltered equivalent. The following discussion considers whole-rock geochemical data of the two retrogressed banded gneiss samples WJK 155 and WJK 156, both of which show petrographic evidence for late fluid alteration (APPENDIX C). The altered samples are then compared against less altered components of the banded gneiss package at Tverregga, e.g. WJK 160 and WJK 159.

The marked difference in the major element content of the two retrogressed banded gneiss samples, highlights the heterogeneity of this rock type in the central Kirwanveggen (Table 5.2). The paucity of quartz and absence of feldspar in WJK 155 is indicated by the low SiO_2 and K_2O content respectively, the elevated oxide concentrations e.g. MgO and CaO, probably reflect the plagioclase, epidote, chlorite and calcite content of this sample. In the case of WJK 156, the extremely high SiO_2 content (80.08wt.%) highlights the siliceous nature of this rock and the low Al_2O_3 reflects the paucity of feldspar in this sample.

Table 5.2 Comparison of the major element compositions of WJK 155 and WJK 156.

Sample	Rock Type	Wt%	**SiO_2**	TiO_2	Al_2O3	Fe_2O_3	MnO	MgO	**CaO**	Na_2O	K_2O	**Na_2O + K_2O**	P_2O5	SO_3	NiO	Cr_2O_3	H_2O^-
WJK 155	BG(R)		**60.88**	0.50	10.67	5.90	0.16	3.94	**13.41**	0.00	0.09	**0.09**	0.27	0.17	0.01	0.01	0.07
WJK 156	BG(R)		**80.08**	0.15	9.64	1.69	0.02	1.31	**0.33**	1.94	4.08	**6.02**	0.08	0.08	0.00	0.01	0.08

When the two retrogressed banded gneiss samples are compared with relatively unaltered components of the *Tverregga Banded Gneiss*, there is evidence for significant changes in whole-rock geochemistry (Table 5.3). The major element composition of samples WJK 159 and WJK 160 have already been described in Section 5.3.2. The altered melanocratic gneiss (WJK 155) records an increase in Ca and Mg and a decrease in Si, Al, K and Na. In contrast, the altered leucocratic gneiss (WJK 156) records an increase in Si, Mg and K, and a decrease in Al, Fe, Ca and Na. These changes suggest that the nature of the fluid flow responsible for the alteration of the melanocratic gneisses is different to that responsible for the alteration of the leucocratic gneisses. In general, an increase in Si and K such as that observed in altered leucocratic gneiss indicates down-temperature fluid flow, and a decrease in Si such as that observed in melanocratic gneiss indicates up-temperature fluid flow (Dipple & Ferry 1992).

Table 5.3 Comparison of the major element compositions of altered samples, WJK 155 and WJK 156 with corresponding unaltered samples, WJK 159 and WJK 160.

Sample	Rock Type	Wt%	SiO_2	TiO_2	Al_2O3	Fe_2O_3	MnO	MgO	CaO	Na_2O	K_2O	$Na_2O + K_2O$	P_2O5	SO_3	NiO	Cr_2O_3	H_2O^-
Melanocratic																	
WJK 155	BG(R)		**60.88**	0.50	10.67	5.90	0.16	3.94	**13.41**	0.00	0.09	**0.09**	0.27	0.17	0.01	0.01	0.07
WJK 159	BG		**67.52**	0.41	13.18	5.54	0.10	2.07	**4.22**	3.35	1.96	**5.31**	0.28	0.06	-	-	0.63
Leucocratic																	
WJK 156	BG(R)		**80.08**	0.15	9.64	1.69	0.02	1.31	**0.33**	1.94	4.08	**6.02**	0.08	0.08	0.00	0.01	0.08
WJK 160	BG		**70.60**	0.32	14.29	2.78	0.04	0.61	**2.15**	4.58	2.50	**7.08**	0.11	0.05	-	-	0.03

The compositional variability of all the metamorphic rocks in this area is best demonstrated by the retrogressed banded gneiss sample WJK 155, which has an anomalously high CaO content and an extremely low alkali content compared to that of the other Kirwanveggen gneisses (Fig. 5.1). This could simply reflect a different protolith composition to that of WJK 156 and the other gneisses. However the very low K_2O composition and absence of Na_2O in this rock indicates a loss of alkalis presumably as a result of fluid alteration. This

interpretation is strengthened by field observations which indicate that the heterogeneity of the banded gneisses has been exacerbated by variable degrees of superimposed fluid alteration.

More evidence for loss of alkalis is revealed when the alkali versus major element content of all the central Kirwanveggen gneisses are compared in Figure 5.4. Well developed trends for banded gneiss and leucogneiss indicate the relationship of samples of each of these rock types with differences being the result of the modal proportions of constituent minerals. However, closer inspection shows that all gneiss samples have $Na_2O + K_2O < 9.3$wt.% which is lower than the alkali content of the major rock forming minerals in these rocks e.g. K-feldspar, albite, and muscovite, but not biotite and quartz. This means that changes in the proportions of the major minerals, especially feldspar and muscovite, cannot necessarily explain the observed Na and K concentrations. As mentioned above, the retrogressed banded gneiss samples, especially WJK 155, are depleted in $Na_2O + K_2O$ and have almost certainly suffered a loss of alkalis.

The compositional variation observed in this study is likely to represent a combination of the very different protolith compositions as well as metamorphic and metasomatic assemblages which make up the metamorphic rocks of the central Kirwanveggen. In particular, the retrogressed banded gneisses appear to have had very different starting compositions to those recorded in Table 5.2, which were subsequently modified as a result of retrogression and metasomatism. The concept of fluid-rock interaction affecting the chemistry of the central Kirwanveggen gneisses is investigated further in the next chapter (Chapter Six) by considering the stable isotope geochemistry of these rocks.

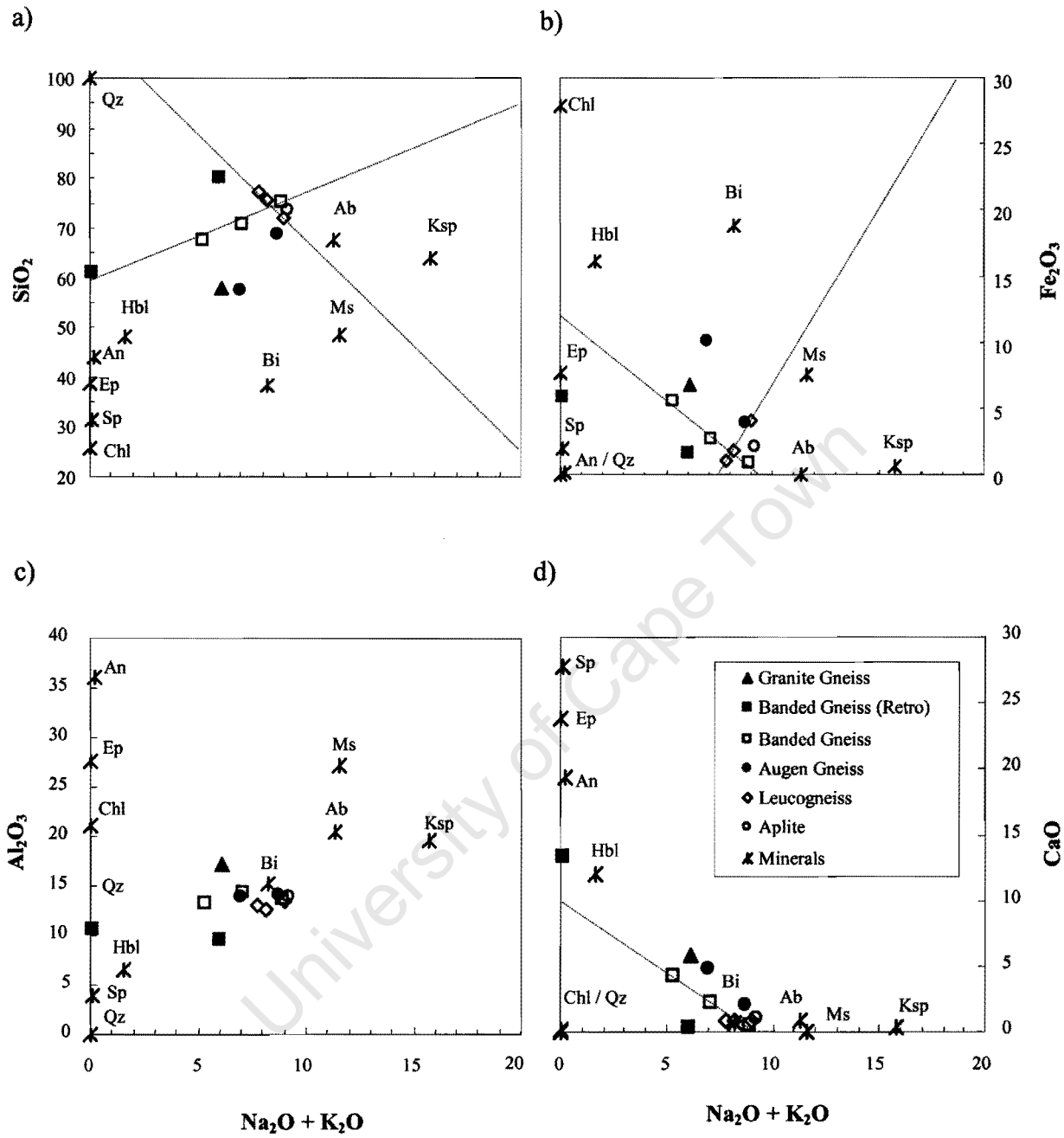

Figure 5.4 Major oxides plotted against $Na_2O + K_2O$ for the gneisses of the central Kirwanveggen. Metamorphic mineral compositions are taken from Deer *et al.* (1992). The lines indicate discernible trends in the data, in a) and b) the trends are for banded gneiss and leucogneiss, in d) the trend is for banded gneiss.

CHAPTER SIX

6. STABLE ISOTOPE INVESTIGATION

6.1 INTRODUCTION

Stable isotope geochemistry is well suited to fluid-rock interaction studies because oxygen isotope ratios are resistant to change as a result of closed-system metamorphism but are susceptible to processes involving external fluids. Such processes include metasomatism, and provided the fluid:rock ratio and or temperature is sufficiently high, partial melting and hydrous retrogression. The principal aims of this study are to identify, elucidate and interpret fluid-rock interaction in the high-grade metamorphic rocks of the Sverdrupfjella Group. Fluid-rock interaction in the Sistenup lavas is highlighted by extremely low $\delta^{18}O$ values and is considered of major importance, despite the fact that these rocks do not form part of the Sverdrupfjella Group. This chapter presents and discusses oxygen, carbon and hydrogen isotope data, which forms the core of this study.

6.1.1 Stable isotope geochemistry

Some of the basic principles of stable isotope geochemistry are discussed below. These include the factors affecting equilibrium isotope fractionation such as temperature and mineral composition, as well as isotopic disequilibrium and fluid-rock interaction. The range in the oxygen and carbon isotope composition of common geological materials is also presented and serves as a reference against which the results of this study can be compared.

Equilibrium isotope fractionation

Isotopes of a given element e.g. O or C partition between phases with different isotope ratios which is known as isotope fractionation. Isotope fractionation can be divided into a) equilibrium isotope exchange processes, b) evaporation / condensation processes, and, c) kinetic processes (Hoefs 1997). In the case of equilibrium fractionation of oxygen between two phases e.g. quartz and calcite, the fractionation factor:

$$\alpha_{qz\text{-}cc} = R_{qz} / R_{cc} \qquad (6.1)$$

where R = $^{18}O/^{16}O$ of quartz and calcite. Isotope compositions are conventionally expressed in δ-notation which is a measure of the enrichment of the heavy isotope relative to a standard. For any isotope:

$$\delta = (R_{sample}/R_{standard}-1)*1000 \qquad (6.2)$$

where R = $^{18}O/^{16}O$ or $^{13}C/^{12}C$ or D/H and units are given in ‰ (per mil or parts per thousand). The relationship between δ and the fractionation factor α for two phases e.g. quartz and calcite is given by:

$$\delta_{qz} - \delta_{cc} = \Delta_{qz\text{-}cc} \approx 10^3 \ln \alpha_{qz\text{-}cc} \qquad (6.3)$$

Note that this only holds where $\delta_{qz} - \delta_{cc} < 10‰$. Equilibrium fractionation is strongly temperature dependent where the fractionation factor α is proportional to $1/T^2$ and temperature is given in K (Fig. 6.1). For equilibrium mineral (X) – mineral (Y) fractionation:

$$\delta_X - \delta_Y = \Delta_{X-Y} = A \cdot 10^6 T^{-2} + K \quad (6.4)$$

where A = 0.38 for quartz – calcite fractionation ; A = 0.94 for quartz – albite fractionation and A = 1.99 for quartz - anorthite fractionation as determined by Clayton *et al.* (1989) and Chiba *et al.* (1989) using calcite as the oxygen isotope exchange medium. For these equations, K = 0 which is not the case for all fractionations.

Rayleigh fractionation is important during metamorphic devolatilization. Isotopic fractionation during evaporation and condensation of water is the result of differences in vapour pressure of isotopic compounds and occurs when one phase is continuously lost from the system during heating or cooling. This will lead to a systematic change in the isotopic composition of the residual phase with respect to the phase being lost from the system and is controlled by the fractionation factor α between the two phases. Rayleigh decarbonation is described by Valley (1986), is illustrated in Figure 6.2 and is responsible for the distinctive ^{18}O and ^{13}C trends observed in many metacarbonate and calc silicate rocks.

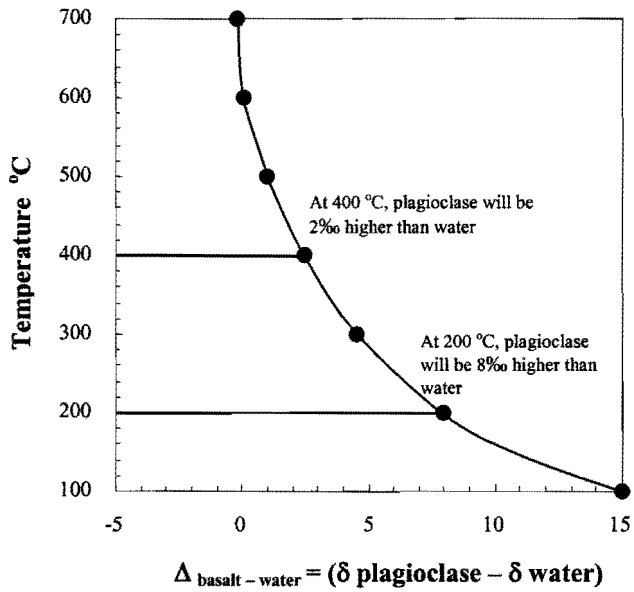

Figure 6.1 Plot of temperature vs fractionation between basalt and water for theoretical data illustrating the temperature dependent nature of equilibrium fractionation between two phases e.g. plagioclase and water (after O'Neil & Taylor 1967).

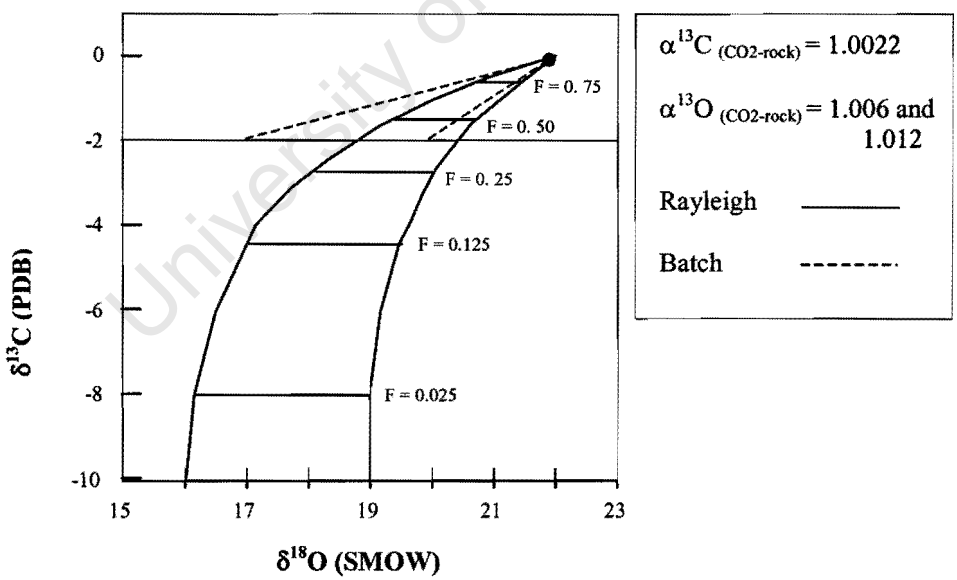

Figure 6.2 Theoretical oxygen vs carbon trends as a result of Rayleigh decarbonation in marble. The starting composition is that of unaltered limestone and F is the mole fraction of C remaining in the rock (after Valley 1986).

Mineral composition also influences equilibrium fractionation, this effect depends on bond strength where bonds between highly charged ions with a small atomic mass e.g. Si^{4+}, C^{4+} and oxygen tend to concentrate the heavy isotope. For this reason, quartz and calcite are enriched in ^{18}O, and minerals such as magnetite which contains the relatively large Fe^{2+} ion, is ^{18}O deficient (Hoefs 1997). In the case of oxygen, the $\delta^{18}O$ value of whole-rock samples depends on the $\delta^{18}O$ values of constituent minerals, the concentration of oxygen in each mineral and the mineral proportions.

Kinetic processes are a further cause of isotope fractionation and are geologically important when considering volume diffusion. Minerals with low diffusion coefficients and high closure temperatures are likely to preserve isotope fractionations through cooling and yield high isotope equilibrium temperatures. Mineral pairs with as large as possible a fraction difference such as quartz and magnetite are best for isotope thermometry.

Fluid-rock interaction

Isotope disequilibrium occurs as a result of fluid-rock interaction when one phase exchanges with a fluid at a different rate to a co-existing phase and the relationship in equation (6.4) is not honoured. Stable isotope data can provide evidence for isotope disequilibrium as illustrated using theoretical data in Fig. 6.3. Interaction between fluid and rock will reset the oxygen or hydrogen isotope composition of the fluid and / or the rock if, a) the $\delta^{18}O$ or δD value of the fluid and rock is very different and b) the volume of fluid is sufficiently large. Isotopic resetting is also dependant on temperature and kinetic processes. According to Taylor (1977), hydrogen is more readily reset than oxygen during fluid-rock interaction because rocks generally have lower concentrations of H (typically only 2 – 3wt%). The fluid:rock ratio is based on mass balance and is defined by Taylor (1974) as:

$$F/R_{closed} = \delta_{rock_f} - \delta_{rock_i} / \delta_{fluid_i} - (\delta_{rock_f} - \Delta) \quad (6.5)$$

where Δ is the isotope fractionation between water and rock ($\delta_{rock_f} - \delta_{fluid_f}$), δ_{rock_i} is the initial and δ_{rock_f} the final isotopic compositions of the rock in a closed-system. The limitations of fluid:rock ratios calculated in this way are: a) the unrealistic assumption of complete equilibration between fluid and rock, b) the units are not consistent with hydrogeological models which use fluid fluxes, and, c) that they do not provide flow path or flow direction information (Ferry & Dipple 1991; Buick 1998). More advanced modelling of fluid flow takes into account continuum-type dispersion-advection equations which better describe the movement of fluid through metamorphic rocks (Baumgartner & Rumble 1988, Ferry & Dipple 1991; Dipple & Ferry 1992; Buick 1998). Time-integrated fluid fluxes take into account the total volume of fluid passing across a unit area of rock for the time duration of a fluid flow event, they are given by $q_v = v \cdot t$ and have units of m^3/m^2 where v is the Darcy fluid flux. Time-integrated fluid fluxes can be calculated if the chemical composition of the rock and fluid are known by:

$$q_v = K_e \cdot z_a \quad (6.6)$$

where z_a is the distance that the isotopic front has moved and K_e is the fluid / rock partition coefficient for a given element e.g. O and is defined as $\rho_s/\rho_f \cdot K_d$, with ρ_s and ρ_f being the densities of the solid and fluid respectively. The solid-fluid distribution coefficient K_d is defined as C_s/C_f. In a high-grade metamorphic rock, K_e values for O are typically 1.6 to 1.8 (Buick 1998). For pervasive fluid flow during regional metamorphism, time-integrated fluid fluxes are typically $10^4 - 10^6$ cm^3/cm^2 (Ferry & Dipple 1991).

a) $\delta^{18}O_A > \delta^{18}O_B$ b) $\delta^{18}O_A > \delta^{18}O_B$

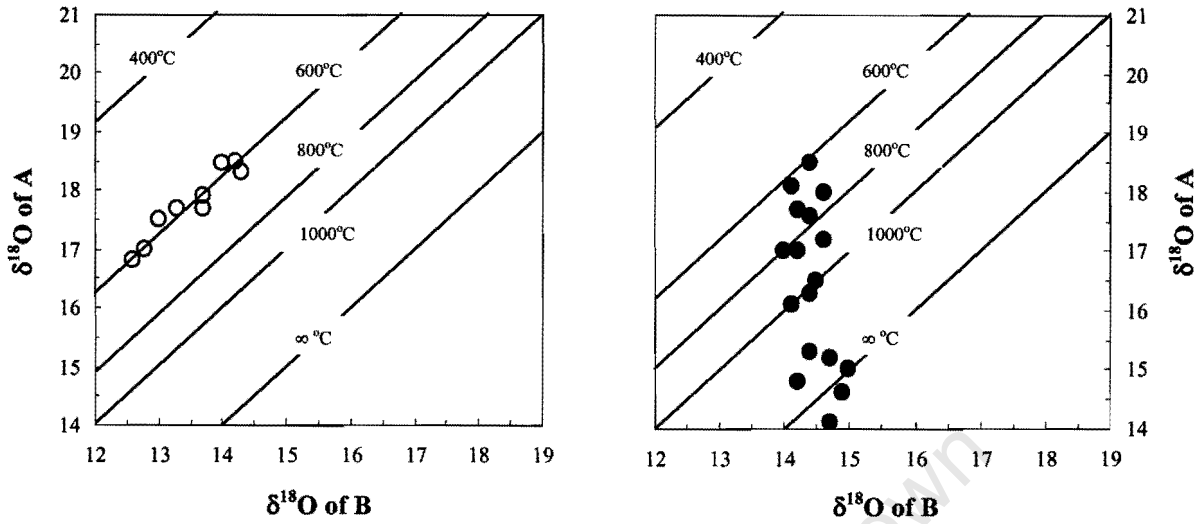

Figure 6.3 Theoretical $\delta^{18}O_A$ vs $\delta^{18}O_B$ plots for a) equilibrium and b) disequilibrium fractionations (after Buick 1998). Diagonal lines are isotherms for equilibrium fractionation between mineral phases A and B.

Stable isotope composition of rocks

The whole-rock isotope composition of a rock containing *n* minerals is given by:

$$\delta_{WR} = \sum X_i \delta_i \qquad (6.7)$$

where $i = 1$ to n, X_i is the atomic fraction and δ_i the isotopic composition of each component mineral. The range of $\delta^{18}O$ and $\delta^{13}C$ whole-rock values of common geological materials are presented in Fig. 6.4a and b. Unaltered mantle magmas e.g. MORB have $\delta^{18}O$ values of 5.7 ± 0.3‰ (Taylor & Sheppard 1986). In general sedimentary rocks are enriched in ^{18}O, this is especially true for limestone ($\delta^{18}O$ of 20‰ - 30‰). Granitic rocks have a large range of $\delta^{18}O$

values generally between 6‰ and 14‰, with values as low as 0‰ in hydrothermally altered granites (Taylor & Sheppard 1986). Metamorphic rocks have generally lower $\delta^{18}O$ values than their igneous and sedimentary precursors (0‰ to just over 20‰) because of fractionation during devolatilization. Most fluids have considerably lower $\delta^{18}O$ values than crustal rocks because the isotope fractionation between mineral and H_2O is positive.

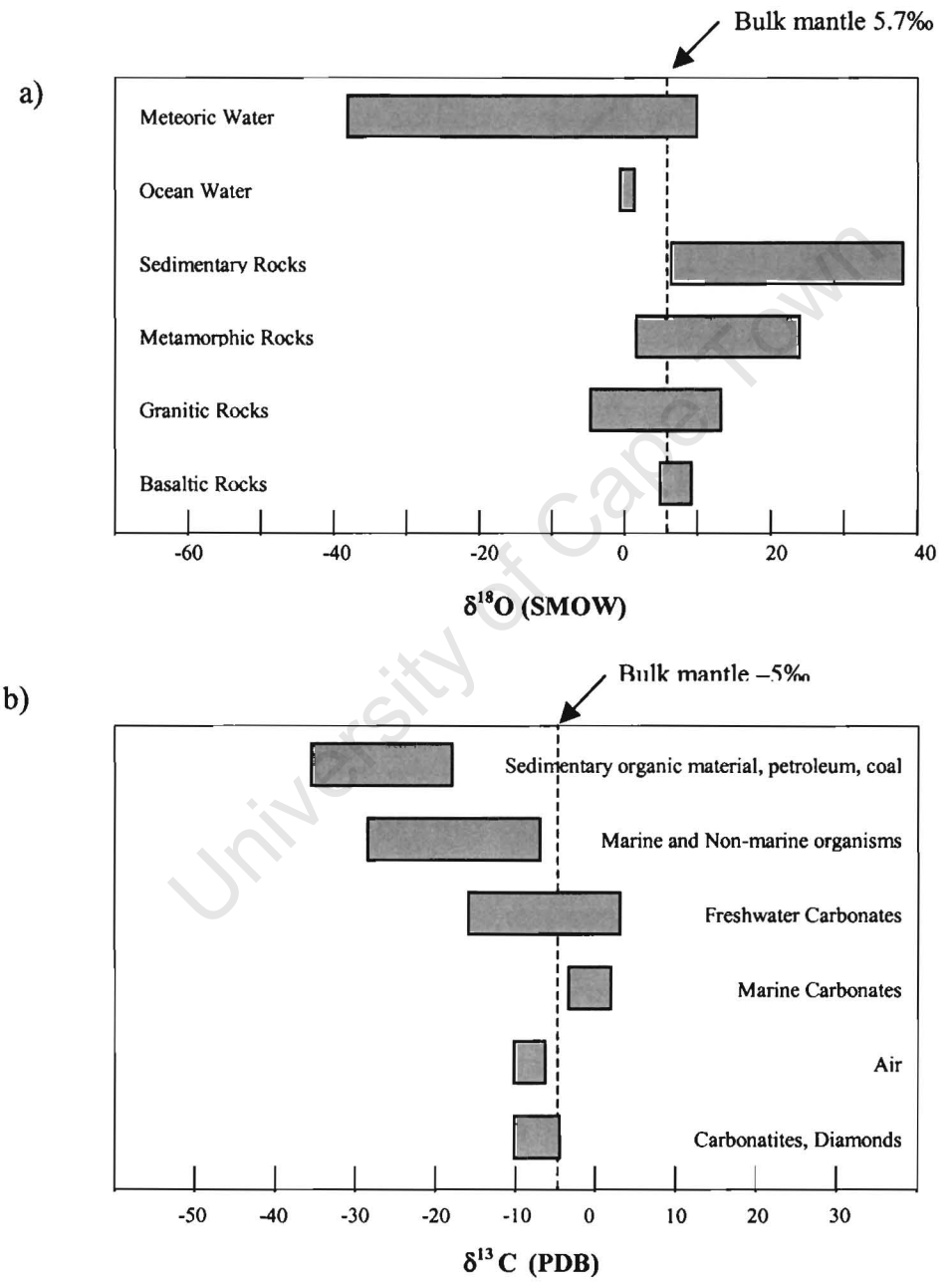

Figure 6.4 Stable isotope ratios for common geological materials, a) oxygen isotope values and b) carbon isotope values (after Hoefs 1997).

6.2 RESULTS

The full range of metamorphic rock types which comprise the Sverdrupfjella Group in the central Kirwanveggen and which are described in Chapter Three have been analysed for their oxygen isotope ratio. A selection of these samples have also been analysed for their carbon and oxygen isotope ratio of carbonate. Samples of rocks which do not form part of the Sverdrupfjella Group, such as the basalts from Sistenup, were also analysed during the course of this project. Oxygen, carbon and hydrogen isotope results from 150 samples are presented in Tables 6.1 – 6.8. The results of analyses performed on samples from the Sverdrupfjella Group and the Sistenup area are presented here according to rock type. Figure 6.5 illustrates the $\delta^{18}O$ differences between, and the range within, all the rock types considered in this study, the total range of $\delta^{18}O$ values is from -1.8‰ in the Sistenup lavas to 26.8‰ in a metacarbonate from Skarsnuten. Whole-rock geochemical data of some of the metamorphic rock types in the central Kirwanveggen was presented and discussed in Chapter Five. Figure 6.6 compares the content of major elements in selected samples to the whole-rock $\delta^{18}O$ value of these rocks and indicates that, in general, whole-rock composition does not exert an obvious control on oxygen isotope composition. These data are discussed further in Section 6.3. Stable isotope data for banded gneisses of the *Mjöllföykje Banded Gneiss* and retrogressed banded gneisses of the *Tverregga Banded Gneiss*, which are treated as separate lithological packages in Chapter Three, are presented together in Section 6.2.3. This is considered necessary because, even though the banded gneisses have been assigned separate stratigraphic names by Grantham *et al.* (1995*b*), the high degree of localized retrogression present within the *Mjöllföykje Banded Gneiss* at Hallgrenskarvet make most of the samples indistinguishable from those collected from the *Tverregga Banded Gneiss* at Tverregga. Thus all retrogressed rocks are treated as one group in this section.

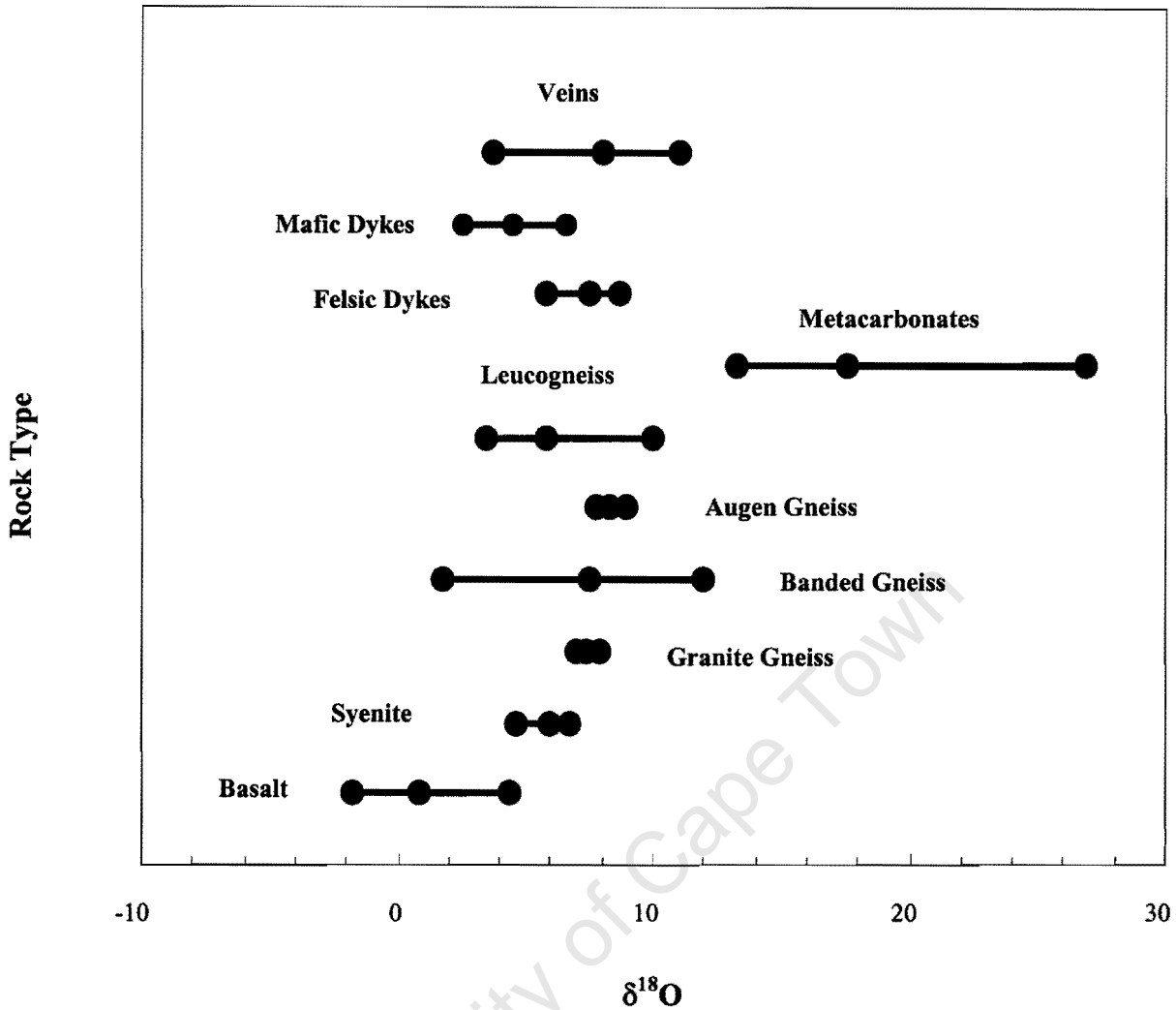

Figure 6.5 Plot of $\delta^{18}O$ vs Rock Type showing the range of $\delta^{18}O$ values for the metamorphic rock types of the Sverdrupfjella Group as well as syenite from the Sistefjell Complex and the Sistenup basalts. All $\delta^{18}O$ values are whole-rock determinations except for the metacarbonate samples, which indicate $\delta^{18}O$ values of calcite. The minimum, maximum and mean $\delta^{18}O$ value for each rock type is indicated by the 3 dots on each line.

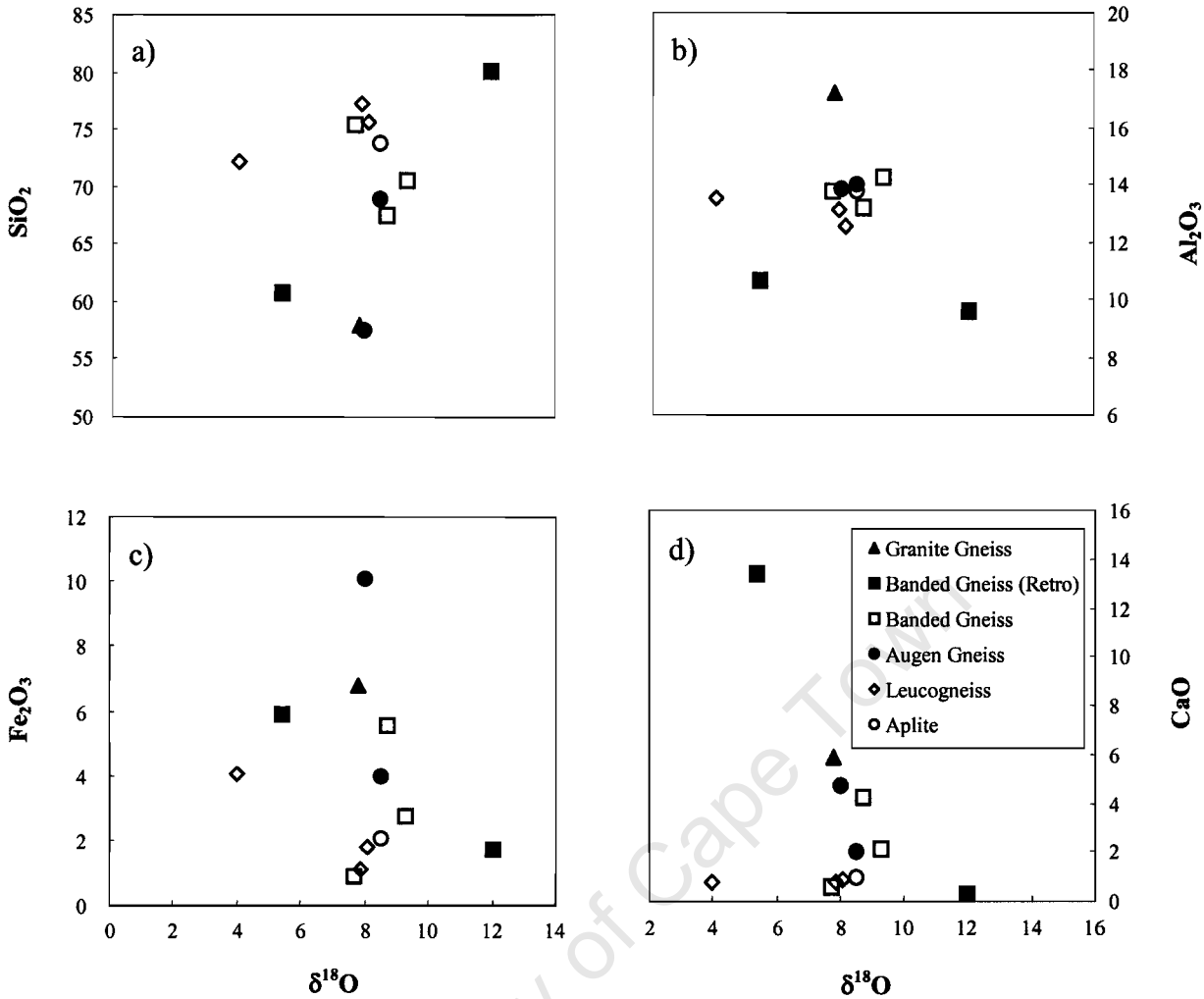

Figure 6.6 Plot of whole-rock $\delta^{18}O$ vs the content of selected major elements: a) SiO_2, b) Al_2O_3, c) Fe_2O_3, and, d) CaO for the major metamorphic rock types of the Sverdrupfjella Group.

6.2.1 Basalt & Syenite

The best evidence for fluid-rock interaction which is possibly associated with regional metamorphism in the Sverdrupfjella Group occurs at Sistenup in the north eastern Kirwanveggen. The very low oxygen isotope ratios in the Sistenup lavas (WJK 337 = -0.6‰ and SIS 5 = -1.8‰) are the lowest recorded for any rock type in western Dronning Maud

Land. A summary of mineral and whole-rock oxygen and hydrogen isotope data from Sistenup and Sistefjell is presented in Table 6.1. The basalts have $\delta^{18}O$ values ranging from -1.8‰ to +4.4‰ with very low oxygen isotope ratios recorded in both aphyric and plagioclase-phyric varieties. Plagioclase separates have $\delta^{18}O$ values of +4.7‰ and –0.1‰ corresponding to host rock $\delta^{18}O$ values of +4.4‰ and –0.6‰ respectively. Hydrogen isotope analyses of the basalt and associated rocks show a range of δD from -167‰ to -141‰ (Fig. 6.7).

Intrusive syenite of the Sistefjell complex has very low $\delta^{18}O$ values from 4.2‰ to 5.6‰, whole-rock $\delta^{18}O$ values calculated from feldspar and biotite mineral δ values and modal proportions are higher at 6.7‰ but still low for an alkaline intrusion. These data are similar to data from the Straumsvola nepheline syenite complex (Harris & Grantham 1993) situated over 100km to the north north east of Sistefjell. A single hydrogen isotope analysis of the syenite returns a δD value of -133‰. Whole-rock oxygen isotope ratios have been calculated for felsic intrusive material from δ values and modal proportions of the constituent minerals, the range of calculated values is 5.3‰ to 6.7‰. Measured whole-rock $\delta^{18}O$ values of felsic material which intrudes the lavas at Sistenup are also low and range from 3.5‰ to 4.0‰. Oxygen isotope ratios of the porphyry are similarly low with values of 0.6‰ to 1.8‰, a single hydrogen isotope analysis of this material has a δD value of -167‰.

6.2.2 Granite Gneiss

Two samples of granite gneiss were analysed during this project, one sample was collected in the type area of the *Kvervelnatten Granite Gneiss Complex* at Kvervelnatten itself (WJK 296) and the other was collected at Tverreggtelen in the study area of this project (WJK 224). Sample WJK 296 has a whole-rock $\delta^{18}O$ value of 7.1‰ and a quartz separate $\delta^{18}O$ value of

9.4‰ whereas WJK 224 has a whole-rock $\delta^{18}O$ value of 7.8‰. An additional sample (CJK 153), collected at Tverreggtelen by Chris Jackson during a previous sampling survey in the central Kirwanveggen, has an identical oxygen isotope ratio to that of WJK 224 (Harris & Johnstone 1997). The $\delta^{18}O$ value for these samples compares very well with granite gneiss samples collected in the H. U. Sverdrupfjella by Geoff Grantham which have $\delta^{18}O$ values ranging from 7.0‰ to 7.9‰ with a mean of 7.4‰ (Harris & Johnstone 1998). Hydrogen isotope ratios of the latter samples show a range from –127‰ to –59‰. A summary of stable isotope data compiled from the three sampling surveys is presented in Table 6.2, those samples which were also analysed for hydrogen are plotted in Figure 6.7.

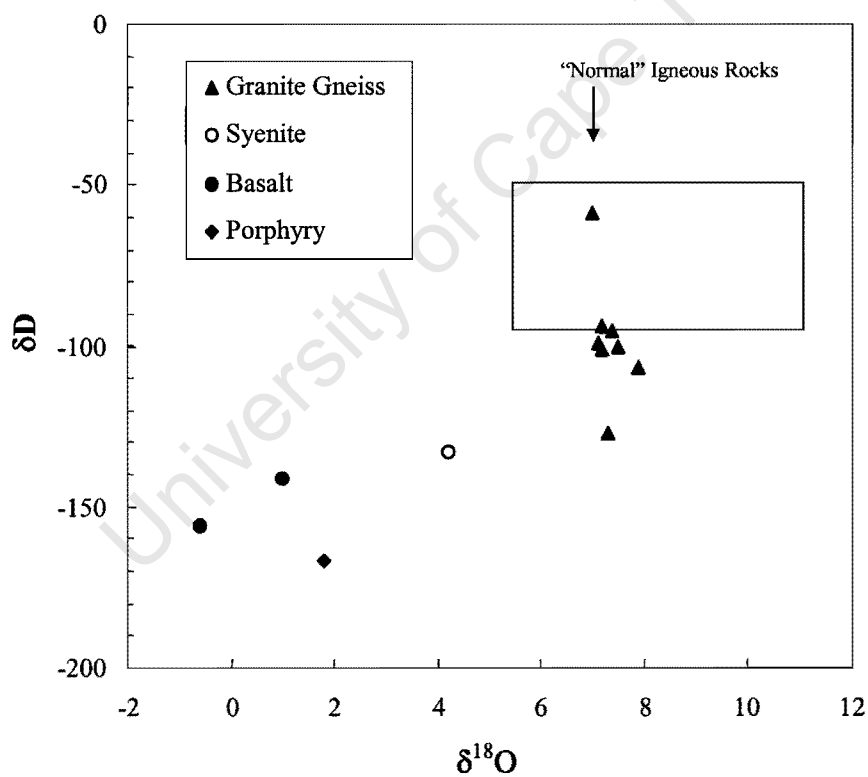

Figure 6.7 Plot of $\delta^{18}O$ vs δD for the basalts at Sistenup and granite gneisses from the central Kirwanveggen. The range of values for "normal" igneous rocks (after Taylor & Sheppard 1986) is also shown.

Table 6.1 A summary of mineral and whole-rock oxygen and hydrogen isotope data from Sistenup and Sistefjell.

Sample	$\delta^{18}O_{quartz}$	$\delta^{18}O_{feldspar}$	$\delta^{18}O_{mafic}$	$\delta^{18}O_{WR}$	$\delta^{18}O_{WR}$ (calc)	δD_{WR}
Syenite						
SIS 2*	8.1 (0.05)	7.0	5.4		6.7	
SIS 34*	8.0 (0.15)	5.5	5.5		6.7	
WJK 332				4.2		-133
WJK 333		5.4		4.6		
WJK 334		6.2		5.6		
Felsic Intrusions						
Sistefjell						
SIS 12*	7.4 (0.08)		4.7 (0.05)		6.0	
SIS 29*	7.1 (0.24)#				6.1	
SIS 31*	7.7 (0.06)#				6.7	
SIS 32*	6.3 (0.20)#				5.3	
Sistenup						
WJK 330				3.5		
WJK 335				4.0		
Sistenup lavas						
Plagioclase-phyric						
SIS 8*		4.7		4.4		
WJK 337		-0.1		-0.6		-156
Aphyric						
SIS 5*				-1.8		
SIS 48*				1.5		
SIS 49*				0.7		
WJK 336				1.0		-141
Sistenup porphyry						
SIS 51*				0.6		
WJK 329				1.8		-167

Figures in paretheses are deviations from the mean for duplicate analyses. Quartz marked # were analysed 6 times; associated figures in paretheses represent the standard deviations. WR (calc) = whole-rock δ value calculated from mineral δ values and modal proportions for SIS 2, SIS 34, SIS 12 or assuming $\Delta_{qz\text{-}melt} = 1.0‰$ for SIS 29, SIS 31, SIS 32 (Taylor & Sheppard 1986).

* Samples collected by C Harris

Table 6.2 Summary of whole-rock oxygen isotope ratios determined for granite gneisses from the *Kvervelnatten Granite Gneiss Complex* in the central Kirwanveggen and the "Grey Gneisses" in the H. U. Sverdrupfjella.

	Rocktype	$\delta^{18}O_{quartz}$	$\delta^{18}O_{WR}$	$\Delta_{quartz\text{-}WR}$	δD_{WR}
Tverreggtelen					
WJK 224	Qz-Ksp-Pl-Hbl-Bi-ep-chl Gneiss		7.8		
CJK 153*	Qz-Ksp-Pl-Hbl-Bi-ep-chl Gneiss		7.8		
Kvervelnatten					
WJK 296	Qz-Ksp-Pl-Hbl-Bi-ep-chl Gneiss	9.4	7.1	2.3	
WJK 298	Qz-Ksp-Pl-Hbl-Bi-ep-chl Gneiss		7.0		
WJK 299	Ep-Qz-Pl Ultramylonite		7.0		
H. U. Sverdrupfjella					
H 2**	Granite Gneiss		7.1		-99
H 12**	Granite Gneiss		7.2		-101
JE 18**	Granite Gneiss		7.9		-107
JE 43**	Granite Gneiss		7.5		-100
RK 22**	Granite Gneiss		7.2		-94
RK 25**	Granite Gneiss		7.3		-127
MDB 52**	Granite Gneiss		7.0		-59
MDB 53**	Granite Gneiss		7.4		-95
Average			7.4		

* Samples collected by C Jackson
** Samples collected by G Grantham

6.2.3 Banded Gneiss

Oxygen and carbon isotope data determined for the numerous lithological components of the banded gneiss sequence in the central Kirwanveggen are summarised in Tables 6.3 and 6.4. More than 25 samples collected from the *Tverregga Banded Gneiss* at Tverregga have been analysed, and almost all of these rocks comprise retrogressed mineral assemblages such as those described in Section 3.2.3. Approximately 20 banded gneiss samples collected from the *Mjöllföykje Banded Gneiss* at both Hallgrenskarvet and Tverreggtelen were also analysed. Many of the later samples show signs of retrogression, despite the fact that the *Mjöllföykje Banded Gneiss* is considered to be less retrogressed than the *Tverregga Banded Gneiss* hence the separate stratigraphic names for banded gneisses exposed in the central Kirwanveggen (See Sections 3.2.3 and 3.2.4).

The range of $\delta^{18}O$ values for all banded gneiss samples at Tverregga, is 4.9‰ to 12.0‰. Samples of the three distinctive lithological components of the *Tverregga Banded Gneiss*: a) quartz – chlorite - epidote – biotite schist, b) quartz – K-feldspar – plagioclase – sericite – chlorite schist, and, c) quartz – epidote – muscovite – chlorite – calcite – sphene schist have whole-rock $\delta^{18}O$ values of 8.7‰, 12.0‰ and 5.4‰ respectively. Similarly large ranges of $\delta^{18}O$ values are observed in banded gneisses from other parts of the central Kirwanveggen (*Mjöllföykje Banded Gneiss*), e.g. a $\delta^{18}O$ range of 4.3‰ to 7.1‰ for Tverreggtelen and 1.7‰ to 10.5‰ for Hallgrenskarvet. Invariably, the low $\delta^{18}O$ values occur in retrogressed components of the banded gneiss, for example, at Tverreggtelen, $\delta^{18}O$ values are as low as 4.3‰ in a hornblende – biotite gneiss and at Hallgrenskarvet, $\delta^{18}O$ values are as low as 1.7‰ in a quartz – biotite – chlorite schist. Oxygen and carbon isotope data for calc silicate boudins, and metasomatic calc silicates are presented below.

Table 6.3 Summary of whole-rock oxygen isotope ratios determined for banded gneisses from the *Tverregga Banded Gneiss* and the *Mjöllföykje Banded Gneiss* sequences in the central Kirwanveggen.

	Mineralogy / Rock Type	$\delta^{18}O_{WR}$
Hallgrenskarvet		
WJK 36	Qz-pl-ksp Gneiss	7.7
WJK 37	Qz-bi-ep Schist	6.8
WJK 68	Qz-fsp-bi Gneiss	10.5
WJK 74	Qz-fsp-bi Schist	4.2
WJK 80	Qz-ksp-pl-ms Gneiss	9.3
WJK 82	Qz-fsp-hbl-bi Schist	6.3
WJK 85	Qz-fsp-bi Schist	4.6
WJK 95	Qz-pl-bi Schist	6.1
WJK 97	Qz-pl-bi Schist	8.0
WJK 99	Qz-pl-bi-ep Schist	2.9
WJK 103	Bi-qz-hbl-chlt Schist	3.6
WJK 113	Qz-bi-chl Schist	1.7
WJK 121	Qz-fsp-bi Pegmatite	9.6
WJK 123	Qz-pl-bi Gneiss	9.5
Average		6.5
Tverregga		
WJK 155	Qz-ep-chl-ms Schist	5.4
WJK 156	Qz-fsp-ser-chl Schist	12.0
WJK 159	Qz-ep-bi Gneiss	8.7
WJK 160	Qz-ksp-bi-ms Gneiss	9.3
WJK 180	Qz-ksp-ep leucosome	10.4
WJK 193	Qz-pl-bi-ep Gneiss	4.9
WJK 196	Qz-pl-bi Gneiss	7.8
WJK 199	Qz-Fsp Pegmatite	8.8
WJK 200	Qz-pl-bi Gneiss	7.9
WJK 201	Qz-ksp-bi-ep Agmatite	7.5
WJK 202	Qz-fsp-bi Gneiss	10.2
WJK 203	Qz Ultramylonite	7.0
WJK 204	Qz-Bi Schist	7.9
WJK 205	Qz-ksp-bi Gneiss	7.8
WJK 207	Qz-ksp-bi-ep Agmatite	8.2
WJK 208	Qz-fsp-bi Gneiss	8.2
WJK 209	Qz Ultramylonite	9.7
WJK 210	Qz-fsp-bi Gneiss	9.1
WJK 211	Qz-fsp-bi Gneiss	7.7
WJK 212	Qz-fsp-bi Gneiss	8.9
WJK 213	Qz-fsp-bi Gneiss	9.0

WJK 214	Qz-fsp-bi Gneiss	9.0
WJK 215	QZ-fsp-bi Schist	8.1
WJK 216	Qz Ultramylonite	8.4
WJK 220	Qz-pl-bi Gneiss	7.9
Average		8.4

Tverreggtelen

WJK 254	Amphibolite	4.3
WJK 255	Qz-Bi-fsp Gneiss	5.2
WJK 260	Qz-bi-hbl-ep Schist	4.7
WJK 268	Qz-fsp-bi Gneiss	7.1
Average		5.3

Calc silicate boudins

Calcite from the early boudins which form part of the retrograde zones of the *Tverregga Banded Gneiss* (Grantham *et al.* 1995*b*) shows a range in $\delta^{18}O$ and $\delta^{13}C$ of 9.0‰ to 12.8‰ and –11.1‰ to –6.0‰ respectively (Table 6.4, Fig. 6.8a and b). One of the zoned boudins (WJK 145) was divided into three components, A: whole boudin, B: core – periphery, and, C: core (Fig. 6.9). The calcite-rich core has a $\delta^{18}O$ value of 12.8‰ compared to the silicate-rich core - periphery sample which has a $\delta^{18}O$ value of 10.4‰. The whole boudin sample has a $\delta^{18}O$ value of 11.2‰. Carbon isotope ratios of calcite from this sample are around –7.0‰.

Metasomatic calc silicates

Calcite oxygen and carbon isotope data for metasomatic calc silicates which constitute part of the *Mjöllföykje Banded Gneiss* sequence of the central Kirwanveggen are summarised in Table 6.4 and presented in Figures 6.8a and b. Calcite from the zoned metasomatic calc silicate body (Fig. 3.15) shows a range in $\delta^{18}O$ and $\delta^{13}C$ of 10.2‰ to 14.9‰ and –1.7‰ to +2.6‰ respectively. Samples from the central zone have $\delta^{18}O$ values greater than 12.0‰ whereas samples from the peripheral zone have $\delta^{18}O$ values of less than 12.0‰. The five components of sample WJK 274 (A-F) illustrate the heterogeneity of the central zone (Fig. 6.10). This sample was collected from a single locality and includes, A: host calcite – amphibole – talc, B: a coarse mafic layer of amphibole – talc, C: a calcite – amphibole – biotite layer, D: a calcite boudin, E: a coarse calcite pod, and, F: an amphibole porphyroblast. The $\delta^{18}O$ value of the host (component A) is 13.4‰, whereas the range of all the components combined (A – F) is just over 1.0‰. Carbon isotope ratios of all the components (A – F) have a $\delta^{13}C$ range of 0.6‰ to 2.6‰.

Table 6.4 Oxygen and carbon isotope ratios of calcite from calc silicate rocks in the central Kirwanveggen. The boudins constitute part of the retrogressed banded gneiss sequence at Tverregga (*Tverregga Banded Gneiss*) and the metasomatic calc silicate material constitutes part of the banded gneiss sequence at Tverreggtelen and Hallgrenskarvet (*Mjöllföykje Banded Gneiss*).

	Mineralogy	$\delta^{18}O_{calcite}$	$\delta^{13}C_{calcite}$	Wt.% Cc	$\delta^{18}O_{quartz}$	$\delta^{18}O_{diopside}$	$\delta^{18}O_{garnet}$
Boudins							
WJK 81	Qz-Fsp-Di-Hbl-Sp	10.0	-11.1	0.4			
WJK 83	Qz-Pl-Ksp-Di-Act-Cc	9.6	-9.1	0.6			
WJK 145 A	Qz-Fsp-hbl-bi + Cc-Di-act-ep	11.2	-6.0				
WJK 145 B	Qz-Fsp + Cc-Di-act-ep	10.4	-7.6	3.6			
WJK 145 C	Cc-Di-act-ep	12.8	-7.4	51			
WJK 148	Ksp-Qz-Pl-Di-Act-Tr	9.0	-8.6	4.3			
Average		10.5	-8.3				
Metasomatic							
WJK 269	Cc-Tr-Di-chl	11.0	1.5	58			
WJK 270	Cc-Di-Tr-qz-chl-serp-sp	10.6	1.2	45			
WJK 271	Cc-Di-Serp-Amph	11.4	1.7	54			
WJK 273 A	Cc-Di-Tr-qz-chl-serp-sp	12.6	-1.7	98			
WJK 273 B	Cc-Di-Tr-qz-chl-serp-sp	10.2	0.6	2.2			
WJK 274 A	Cc-Amph-Tc	13.4	0.9	20			
WJK 274 B	Amph-Tc	14.4	0.6	11			
WJK 274 C	Cc-Amph-Bi	13.5	0.9	32			
WJK 274 D	Cc	13.9	1.3	19			
WJK 274 E	Cc	14.9	2.6	83			
WJK 274 F	Amph	14.5	1.3	15			
Average		12.8	1.0				
Metacarbonates							
WJS 1	Cc-fsp-di-gt	15.8	0.9	36			
WJS 2	Cc-fsp-di-gt	13.3	-2.4	6.1	11.7		7.4
WJS 3	Di-qz-pl				13.0	9.9	
WJS 4	Fsp-qz-cc	14.6	0.1	12	13.6		
WJS 5	Qz-Fsp-Ms-hbl				11.9		
WJS 6	Cc	26.8	2.8	81			
Average		17.6	0.4				

All metacarbonates are from Skarsnuten. The wt.% Cc was obtained from CO_2 yield and calibrated using pure Cc standards.

a)

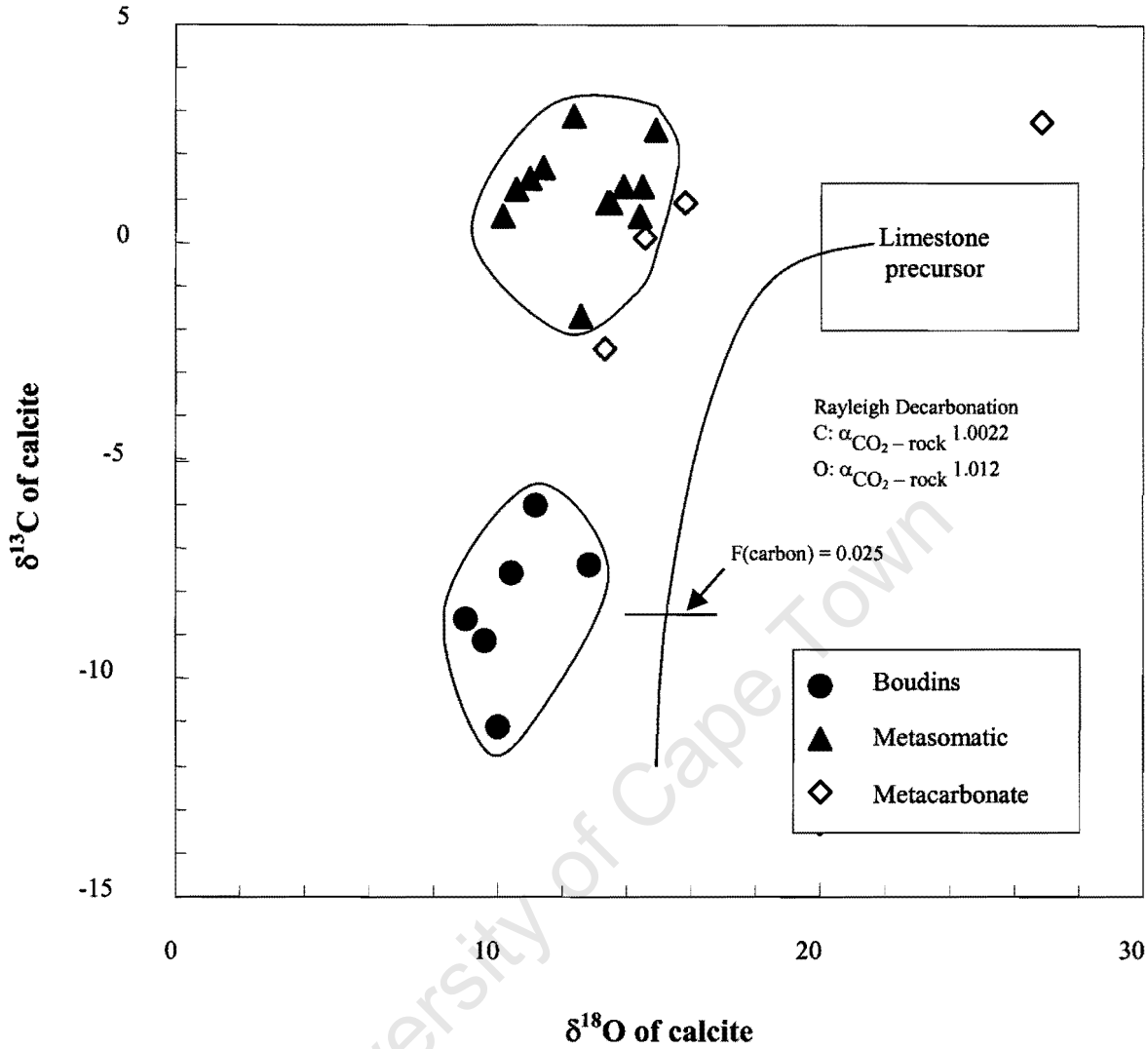

Figure 6.8 Stable isotope plots for calc silicate rocks from the central Kirwanveggen. Metacarbonate samples collected from Skarsnuten in the H. U. Sverdrupfjella are also plotted. Figure 6.8a is a plot of $\delta^{18}O$ vs $\delta^{13}C$, the field for unaltered limestone (Viezer & Hoefs 1976) is shown along with the theoretical curve for a precursor limestone undergoing Rayleigh decarbonation with a $\alpha_{CO_2\text{-rock}}$ for C of 1.002 and for O of 1.012.

b)

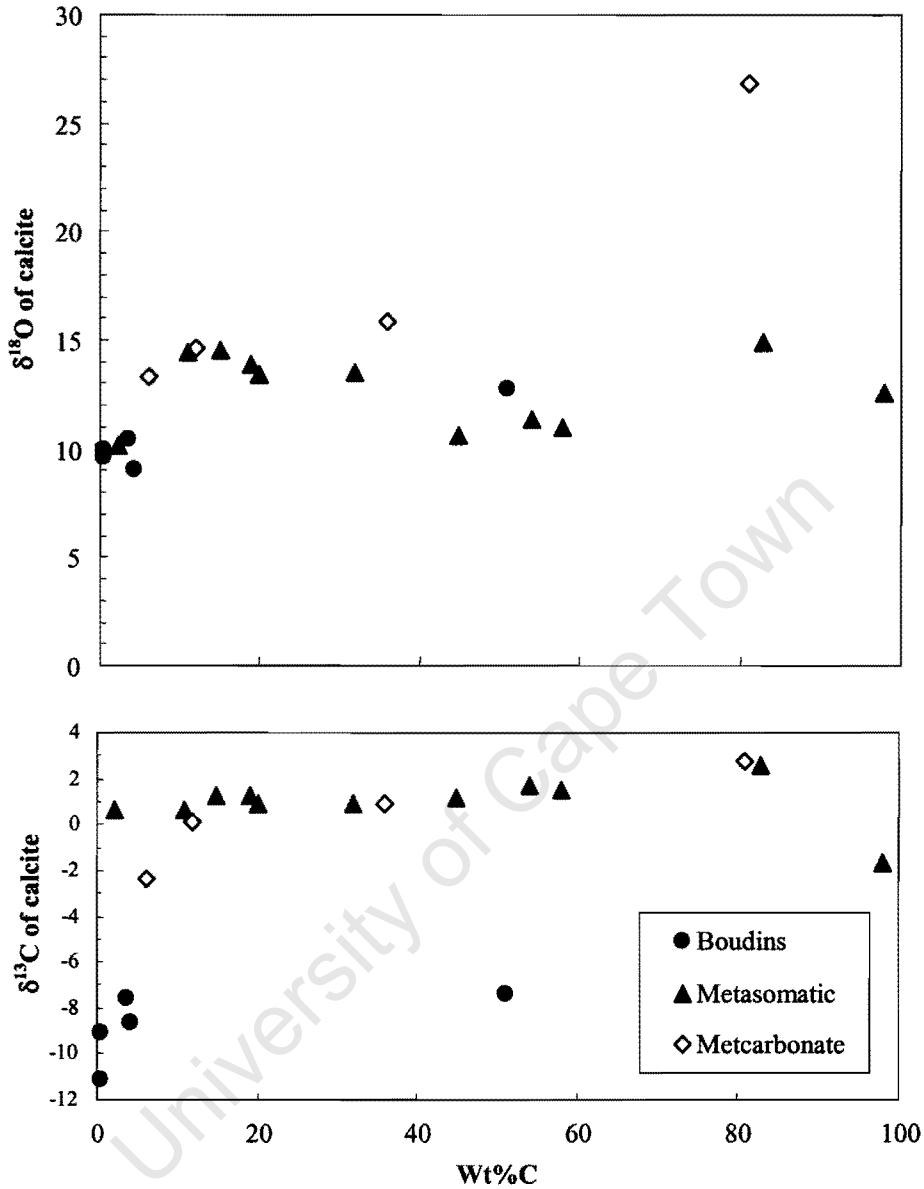

Figure 6.8 Stable isotope plots for calc silicate rocks from the central Kirwanveggen. Metacarbonate samples collected from Skarsnuten in the H. U. Sverdrupfjella are also plotted. Figure 6.8b is a plot of $\delta^{18}O$ and $\delta^{13}C$ vs Wt%Cc.

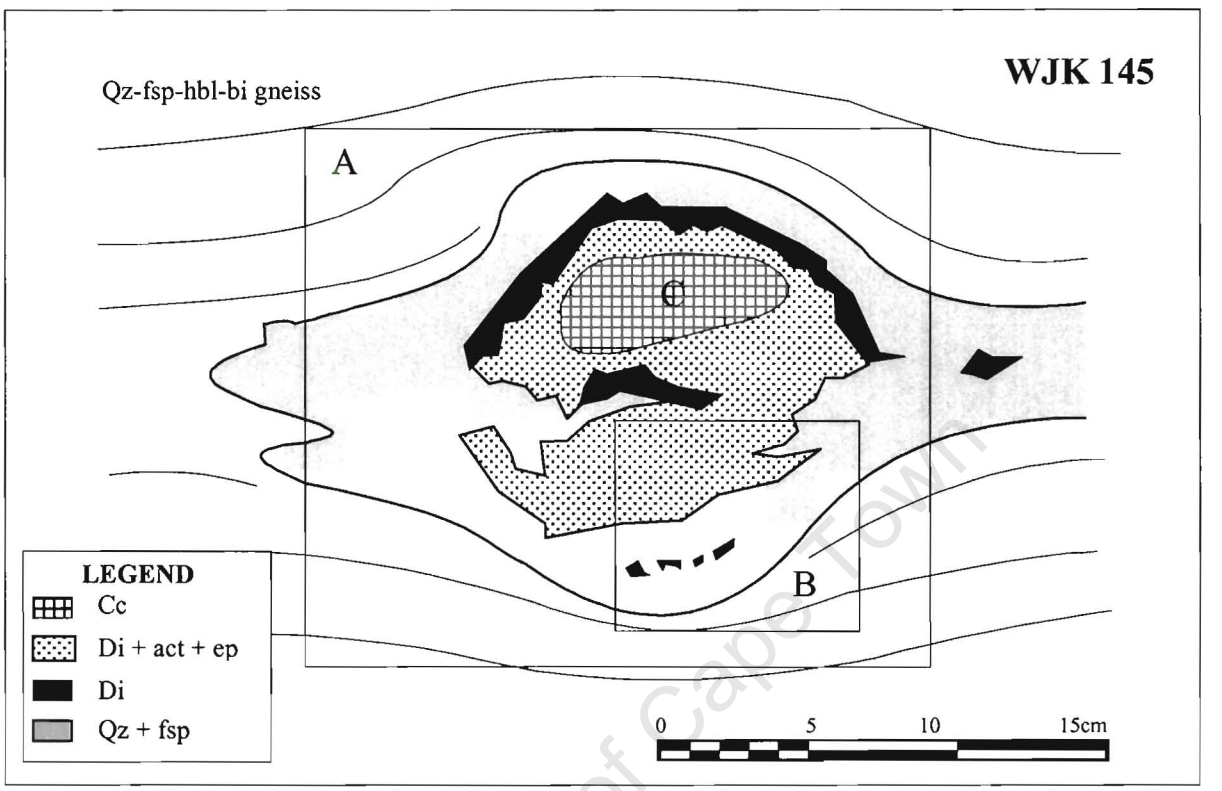

Figure 6.9 Sampling diagram of WJK 145 at locality 26 with components, A: whole boudin ($\delta^{18}O$ = 11.2‰), B: core – periphery ($\delta^{18}O$ = 10.4‰), and, C: core ($\delta^{18}O$ = 12.8‰). A photograph of this boudin has been presented in Figure 3.10.

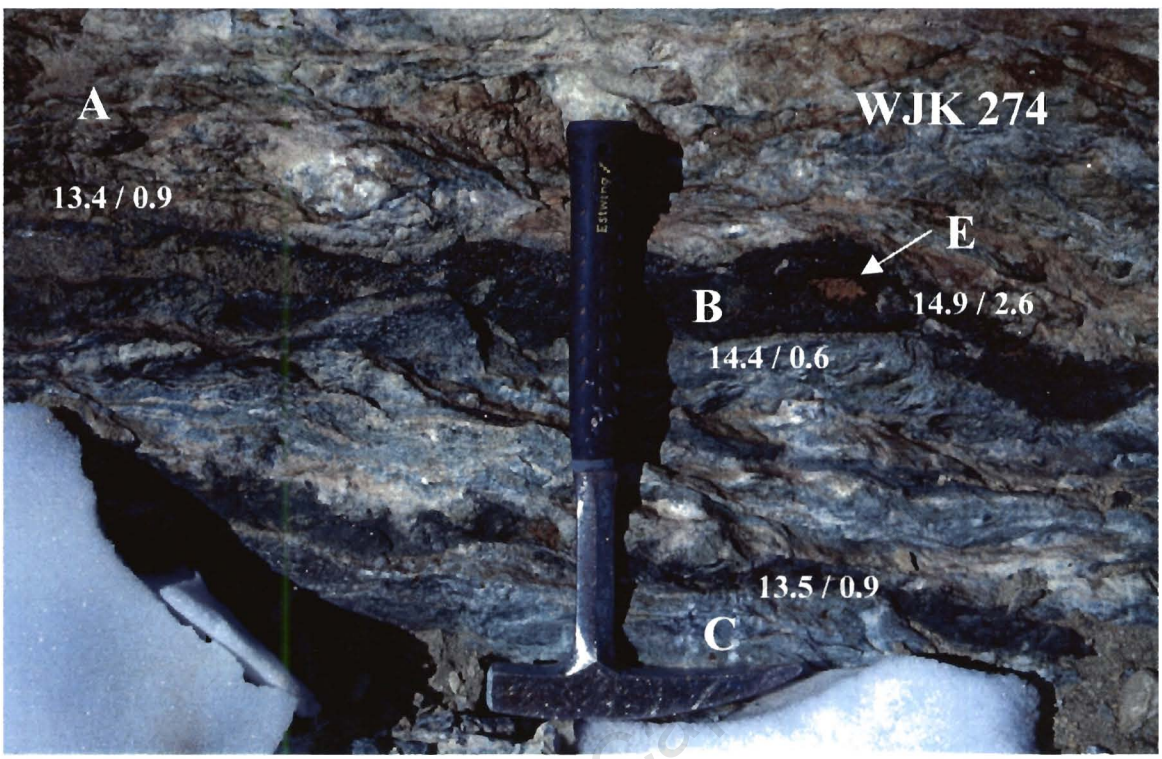

Figure 6.10 Photograph of the metasomatic calc silicate body at Tverreggtelen showing the heterogeneity of the calc silicate material reflected in sample WJK 274 at locality 41. A: host calcite – amphibole – talc ($\delta^{18}O$ = 13.4‰; $\delta^{13}C$ = 0.9‰), B: a coarse mafic layer of amphibole – talc ($\delta^{18}O$ = 14.4‰; $\delta^{13}C$ = 0.6‰), C: a calcite – amphibole – biotite layer ($\delta^{18}O$ = 13.5‰; $\delta^{13}C$ = 0.9‰), D: a calcite boudin ($\delta^{18}O$ = 13.9‰; $\delta^{13}C$ = 1.3‰), E: a coarse calcite pod ($\delta^{18}O$ = 14.9‰; $\delta^{13}C$ = 2.6‰), and, F: an amphibole porphyroblast ($\delta^{18}O$ = 14.5‰; $\delta^{13}C$ = 1.3‰). Note that components D and F are not shown in this photograph.

6.2.4 Augen Gneiss

Whole-rock and mineral separate oxygen isotope data for augen gneiss samples and associated rocks are summarised in Table 6.5. Augen gneiss samples were collected in two separate areas, the Stignabben nunatak, which is located 12 km north east of Hallgrenskarvet and, the eastern buttress of Hallgrenskarvet itself. All 11 augen gneiss samples have been analysed along with associated rocks such as amphibolite xenoliths, cross-cutting aplite dykes and quartz veins. At Stignabben, the augen gneiss samples were collected along a traverse crossing a discrete high angle D_5 shear zone (Fig. 6.11a) and show a variable degree of mylonitization ranging from a weakly developed S_3 foliation to intense S_5 ultramylonitization and quartz recrystallization.

The range of whole-rock $\delta^{18}O$ values for all augen gneiss samples from both areas is less than 1.0‰ if the ultramylonite sample (WJK 5) is excluded, with a minimum value of 7.8‰ and a maximum value of 8.7‰. The lower $\delta^{18}O$ values; 7.8‰ and 8.2‰ occur in mylonitized samples which tend to be finer-grained and are biotite-rich. In contrast the recrystallized ultramylonite sample has a high $\delta^{18}O$ value of 9.0‰. At Stignabben, samples show a slight increase in $\delta^{18}O$ value away from the shear zone for a distance of 2m, however from 2m up to and beyond 30m away from the shear zone, the $\delta^{18}O$ values are at a minimum (Fig. 6.11b). For WJK 1, WJK 3 and WJK 6, $\Delta_{quartz\text{-}feldspar}$ is 0‰, 1.4‰ and 1.8‰ respectively. Analyses of the felsic aplite dykes and mafic xenoliths which are hosted in augen gneiss, are presented in Section 6.2.7.

Table 6.5 Oxygen isotope data for whole-rock samples as well as for quartz and feldspar mineral separates of augen gneisses and associated rocks from the *Kirwanveggen Megacrystic Orthogneiss Complex.*

	Mineralogy / Rocktype	$\delta^{18}O_{quartz}$	$\delta^{18}O_{feldspar}$	$\delta^{18}O_{WR}$	$\Delta_{qz\text{-}fsp}$
Stignabben					
WJK 1	Qz-Ksp-bi	10.0	10.0	7.8	0.0
WJK 3	Ksp-Pl-Qz-bi-sp	9.8	8.4	8.5	1.4
WJK 5	Qz-Ksp-bi-sp Ultramylonite			9.0	
WJK 6	Ksp-Pl-Qz-Bi-sp	10.1	8.3	8.2	1.8
WJK 9	Ksp-Pl-Qz-Bi-sp			7.8	
WJK 10	Qz-Ksp-bi			8.6	
minimum				7.8	
maximum				9.0	
average				8.3	
East Hallgrenskarvet					
WJK 12	Qz-Ksp-bi			8.0	
WJK 13	Qz-Ksp-bi			8.3	
WJK 14	Qz-Ksp-bi			8.0	
WJK 15	Qz-Ksp-bi			8.3	
WJK 16	Qz-Ksp-bi			8.7	
minimum				8.0	
maximum				8.7	
average				8.3	

a)

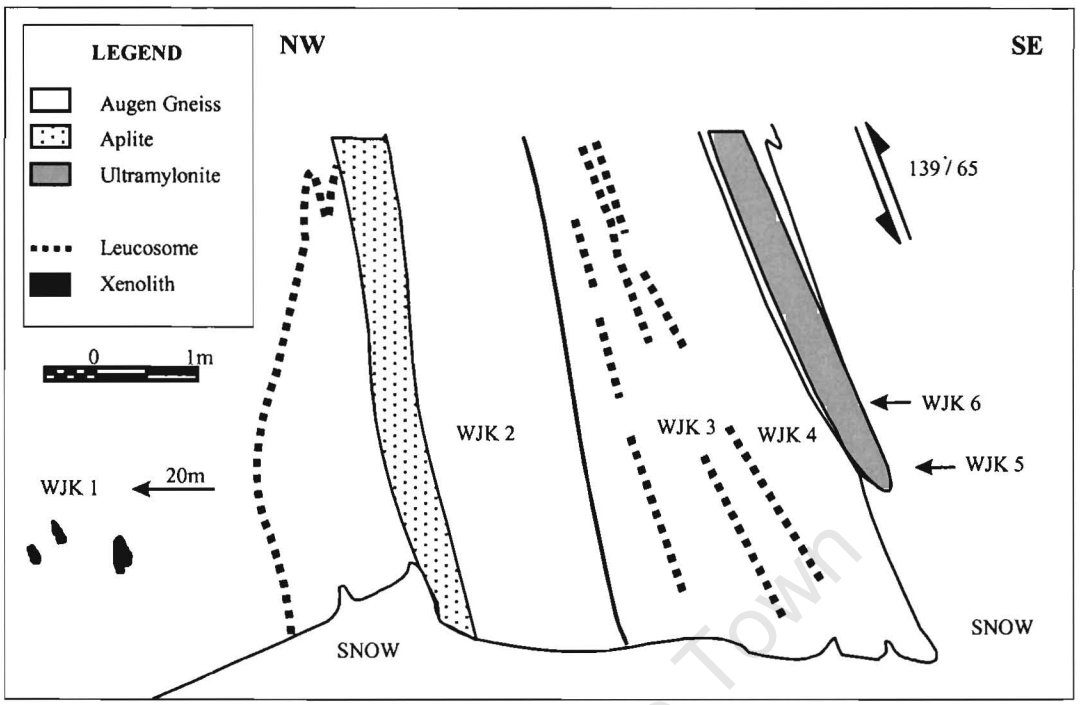

b)

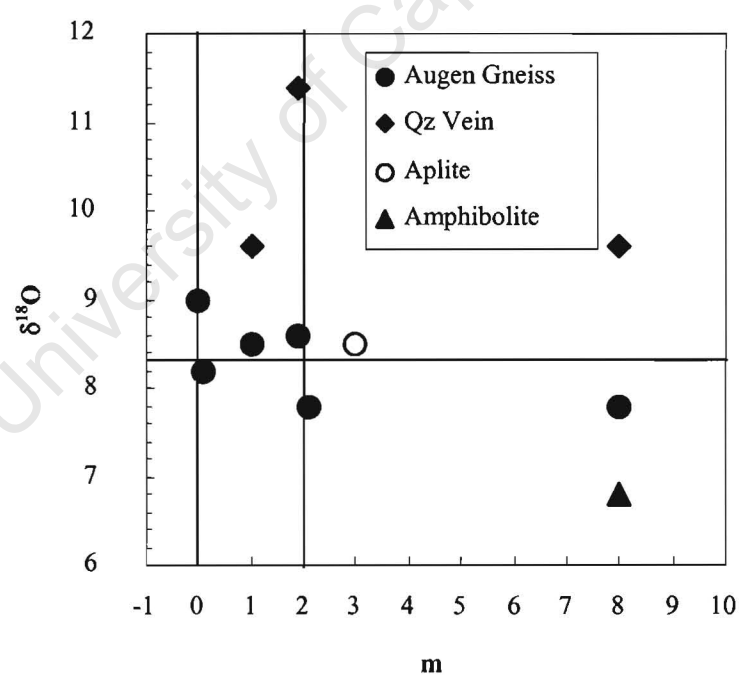

Figure 6.11 Augen gneiss at Stignabben a) field sketch of sampling locality 1 showing the sample traverse WJK 1 – WJK 6 across the D_5 shear zone, b) plot of $\delta^{18}O$ variation with distance from the shear zone.

6.2.5 Leucogneiss

Whole-rock oxygen isotope data for leucogneiss samples collected from Hallgrenskarvet and Tverreggtelen are summarised in Table 6.6. The range in $\delta^{18}O$ values of all the leucogneisses is 3.5‰ to 10.0‰. Leucogneisses from Hallgrenskarvet have generally lower $\delta^{18}O$ values (average $\delta^{18}O$ = 4.9‰) than those from Tverreggtelen (average $\delta^{18}O$ = 7.0‰) and show a large variation in $\delta^{18}O$ values of up to 1.8‰ over a distance of only 2m within the same layer or horizon (Fig. 6.12). Leucogneiss samples from Tverreggtelen can be separated into those collected from the main leucogranite body and those collected from leucogranite apophyses around the margins of the main intrusive body. Figure 6.13 shows that sampling of the main leucogranite body at Tverreggtelen was conducted in such a way as to include the silicified D_3 shear zone described in Section 3.2.5. Leucogneiss samples in close proximity to the shear zone have $\delta^{18}O$ values of 5.6‰ and 7.0‰ whereas those collected several hundred metres from the shear zone have $\delta^{18}O$ values of 8.1‰ and 10.0‰. A quartz separate from one of the latter samples (WJK 278, whole-rock $\delta^{18}O$ = 8.1‰) has a $\delta^{18}O$ value of 8.9‰. The siliceous material in the centre of the shear zone has a $\delta^{18}O$ value of 4.5‰. Oxygen isotope results of leucogranite apophyses are presented in Section 6.2.7.

Table 6.6 Oxygen isotope data for whole-rock samples as well as for quartz mineral separates of leucogneisses from the *Tverreggtelen Leucogranite Suite* at Hallgrenskarvet and Tverreggtelen.

	Mineralogy / Rocktype	$\delta^{18}O_{quartz}$	$\delta^{18}O_{WR}$	$\Delta_{quartz\text{-}WR}$	Distance from SZ (m)
Hallgrenskarvet					
WJK 20	Qz-fsp-ms-bi Gneiss		3.5		
WJK 21	Qz-fsp-ms-bi Gneiss		4.0		
WJK 22	Qz-fsp-ms-bi Gneiss		5.3		
WJK 23	Qz-fsp-ms-bi Gneiss		4.1		
WJK 24	Qz-fsp-ms-bi Gneiss		6.3		
WJK 50	Qz-fsp-ms-bi Gneiss		6.3		
Average			4.9		
Tverreggtelen					
WJK 278	Qz-ksp-ms-bi-pl-fl Gneiss	8.9	8.1	0.8	>100
WJK 282	Qz-ksp-ms-bi-pl-fl Gneiss		5.6		<10
WJK 283	Qz Mylonite		4.5		0
WJK 285	Qz-ksp-ms-bi-pl-fl Gneiss		7.0		<10
WJK 292	Qz-ksp-ms-bi-pl-fl Gneiss		10.0		>100
Average			7.0		